Power production from radioactively contaminated biomass and forest litter in Belarus - Phase 1b

Roed, Jørn; Andersson, Kasper Grann; Fogh, C.L.; Olsen, S.K.; Prip, H.; Junker, H.; Kirkegaard, N.; Jensen, J.-M.; Grebenkov, A.J.; Solovjev, V.N.; Kolchanov, G.G.; Bida, L.A.; Klepatzky, P.M.; Pleshchenkov, I.G.; Gvozdev, A.A.; Baxter, L.

Publication date:
2000

Document Version
Publisher's PDF, also known as Version of record

Risø-R-1146(EN)

Power Production from Radioactively Contaminated Biomass and Forest Litter in Belarus - Phase 1b

Jørn Roed, Kasper G. Andersson, Christian L. Fogh, Svend K. Olsen and Henrik Prip
Risø National Laboratory, Denmark

Helle Junker, Niels Kirkegaard and Jens-Martin Jensen
ELSAMPROJEKT, Denmark

Alexandre J. Grebenkov, Vitalij N. Solovjev, Gregory G. Kolchanov, Leonid A. Bida, Peter M. Klepatzky, Igor G. Pleshchenkov, Arnold A. Gvozdev
IPEP, Belarus

Larry Baxter
Sandia National Laboratories, USA

Risø National Laboratory, Roskilde
March 2000

Abstract The Chernobyl accident has led to radioactive contamination of vast Belarussian forest areas. A total scheme for remediation of contaminated forest areas and utilisation of the removed biomass in safe energy production is being investigated in a Belarussian-American-Danish collaborative project. Here the total radiological impact of the scheme is considered. This means that not only the dose reductive effect of the forest decontamination is taken into account, but also the possible adverse health effects in connection with the much needed bio-energy production. This report presents the results of an in-country, commercial-scale investigation of the effect of a baghouse filter in retaining contaminants so that they are not released to the atmosphere in the biomass energy production process. Approximately 99.5% of the activity of a commercially representative, dust-laden boiler flue gas was removed from the stream by using a combination of a cyclone and a baghouse filter.

ISBN 87-550-2619-2
ISBN 87-550-2620-6 (Internet)
ISSN 0106-2840

Information Service Department, Risø, 2000

Summary

The Chernobyl Bio-energy Project focuses on remediation of the forest areas contaminated by the 1986 Chernobyl power plant disaster. The combustion of biomass in an electric-power-producing boiler plays a central role in this strategy. A primary concern in connection with this combustion is the fate of the radionuclides. Experiments under carefully controlled laboratory conditions and under larger-scale commercial conditions typical of western technology were conducted earlier in separate programs. However, boiler design and operation differ significantly between the West and the Former Soviet Union. This report documents results obtained from commercially operating facilities of a design and operating style typical of the region of Belarus considered in this project.

The facility selected is a boiler at a sawmill that uses mildly contaminated wood as a feedstock. A slipstream from the flue gas of one boiler from this stream was redirected to a baghouse equipped with filters manufactured in the Former Soviet Union (but of western specification and design). The baghouse design and construction were completed under the direction of the Institute of Power Engineering Problems with funding and technical collaboration by Sandia National Laboratories. This document reports on the results of tests conducted at this facility that were supervised by Risø National Laboratory and in which all of the principal institutions played a role.

In comparison with western systems, boilers in the Former Soviet Union lack sophisticated control or particle cleanup systems. The selected boiler is typical in both regards. The boiler is hand fed and has a stationary grate. These features lead to large fluctuations in combustion conditions, particle loading, etc. It was anticipated that such fluctuations would compromise the quality of the data obtained from this investigation, and this anticipation proved well founded. High quality equipment and a careful experimental plan were both deployed during this investigation. In most cases, the features of the equipment and technique were compromised by boiler operation. However, the system was operated as carefully as possible and the results obtained are probably as high of quality as can be expected from such equipment.

Analyses of the samples have shown that sufficient information was obtained to characterise the filter performance. The filter efficiency was found to be around 99.5 % for ^{137}Cs. This means that about 0.5 % of the caesium that is entrained in the flue gas prior to the filter passed through the filter and would be emitted from the stack. This is a significantly higher fraction of the material than would be released in similar western boilers with baghouse filters, but it is also significantly below the level that would pose a significant risk to surrounding individuals.

Calculations show that under the conditions given in the final report on Phase 1a of the project, the number of expected fatal cancers due to stack releases would be reduced from less than 2 per decade to less than one per century if furnaces were equipped with this type of particle collection system.

As the mentioned calculation was done considering highly contaminated wood fuel, the conclusion can be made that by applying a filter system and maintaining it, the radiation risk from the exhaust from the chimney is so low that it does not constitute a problem.

In addition to this, previous studies within the project have shown that:

1. The radiological risk to personnel operating the suggested type of biomass-fired power plant must be considered very low and below the recommended limit.
2. Harvesting and transporting processes in connection with fuel and ash handling can be planned in a way that would keep the doses below the limits.
3. The radioactive waste deposited in the recommended type of repositories will constitute a negligible risk to the population.

The goal of the project has been achieved, despite the problems with the stability. The results obtained were in agreement with the results expected, namely that it was possible to greatly reduce the exhaust of radiocaesium from the stack by applying a filter system based on baghouse technology.

The results of the whole project showed that it is possible to environmentally safely use forestry waste, forest litter and unclaimed biomass from radioactively contaminated forest for producing heat / power. This will enable a new production of significantly less contaminated wood at the harvested field.

Harvesting the contaminated forest and deep ploughing will reduce the dose to the population living in or near contaminated forest areas in two ways: external dose (from direct radiation) and internal dose (from intake of radioactive substances). Another environmental benefit in this context is that restricted forest areas can again be taken into use.

In Belarus, as much as 623 wood-fired boilers are currently operated in contaminated regions. These boilers utilise the woody waste from a number of local sawmills and have the total capacity of 25 MW. None of these are equipped with flue gas filtration systems, and consequently, their operation result in an annual release of about 1.5 thousand tonnes of airborne dust with an average activity of 30,000 Bq/kg. The project has shown that if these existing boilers were mounted with a filter of the tested type, the emission to the atmosphere of radioactive dust would be greatly reduced.

The project is linked to several projects previously accomplished under the auspices of programs of both the European Commission and the USA Department of Energy. A new TACIS program on addressing the clean-up and secondary medical effects of the Chernobyl disaster will disseminate the results of our project through a pilot information project in the CIS countries, which all have contaminated forests.

Contents

Preface

This report presents the results of a field test hosted at the Rechitza Drew Joint-Stock Sawmill in Rechitza, Belarus. This test is one of a series of experiments designed to determine the potential release of caesium from combustors designed as part of an environmental restoration project for forests contaminated by fallout from the Chernobyl accident. Previously, pilot-scale tests with fuels from Belarus were conducted under highly controlled laboratory conditions. Commercial-scale field tests with surrogate fuels were conducted in an operating boiler in the US, and models of combustion processes were completed. This field test was the first to include commercial-scale operation with contaminated fuels within Belarus.

The choice of a capture system type and its design is one of the most important tasks for future construction and operation of an industrial scale boiler that would safely utilise contaminated woody waste. Therefore, as a part of the pilot plant being built at IPEP to investigate all tasks related to combustion of radioactively contaminated wood fuel, the installation that includes a cyclone and a baghouse was constructed and then tested at the site of an existing boiler routinely fired with contaminated biomass. This boiler is at the site of the Rechitza Drew Joint Stock Sawmill. The management of the sawmill co-operated in providing access to the boiler and its operational parameters to allow this project to be completed. The boiler was inspected by members of the investigating team prior to the test. However, the boiler was shutdown for the weekend during the inspection.

The report serves as the final report from the project partners to the Danish Energy Agency of the Phase 1b in the Chernobyl Bio-energy project. RISØ carried out this phase in close collaboration with Institute of Power Engineering Problems, Sandia National Laboratories, and ELSAMPROJEKT. The Danish Energy Agency, the US Department of Energy (DOE), Wheelabrator Environmental System, Inc. (USA), and Belarus National Academy of Sciences, supported the work reported in this report.

1 Introduction

Vast areas of forestland in Belarus were severely contaminated by the Chernobyl accident. Many settlements, villages and towns are surrounded by the contaminated forests, which will often have a significant bearing on the external doses received by people living here. Further, it is generally popular, also for city people, to spend time in the forests, for instance for holidays, walks or collecting forest fruit (mushrooms and berries). Particularly the mushrooms accumulate relatively high levels of contaminants and the consumption of these is currently responsible for about one-fourth of the total radiation dose in the severely contaminated areas.

By removal of the contamination (i.e. vegetation and organic top soil) from the forest significant external and consumption doses can be averted. At the same time, the removed biomass may be applied to redress the Belarussian energy resource problem. By far, most of the energy consumed in Belarus is currently imported, and the option of applying biomass, which the country is very rich on, in energy production, is therefore highly attractive.

Firing with contaminated biomass removed in decontamination operations, however, demands careful analyses ensuring its radiological safety. In Phase 1a of the current project a number of studies were made of the general feasibility of the biomass power production scheme, focusing on factors such as radiological consequences, power plant design, biomass harvesting technologies and safe treatment and storage of the generated ash. These factors were addressed in a general sense on the basis of available data, and it was stressed that many influencing factors should be examined carefully in connection with analyses to evaluate the feasibility of the scheme in relation to specific sites and conditions.

Analyses of the radiological safety of the power plant are highly sensitive to the magnitude of contaminant stack releases. It was therefore deemed necessary to set up a series of tests to improve the estimate of the fraction of the contaminants in the biomass fuel that would be retained through the introduction of a baghouse filter. It was decided to carry out this test in Belarus, using contaminated biomass from the Belarussian forests, so as to make the test conditions as realistic as possible. The purpose of the test was not only to examine the filter efficiency, but also to measure the amount of radiocaesium per unit of mass in the slag and fly-ash relative to that in the fuel. Although the latter figures would be highly sensitive towards the actual firing conditions, the test would improve the understanding of the waste problem as well as the calculations of worker doses at the power plant. It is this test, which constitutes Phase 1b of the Chernobyl Bio-energy Project that is described in this report.

The main objective of the test was to investigate the capture and operational efficiency of the designed baghouse filter system under realistic operational conditions of an industrial boiler, the wood fuel of which being contaminated with ^{137}Cs and ^{90}Sr due to the Chernobyl Accident.

Further, the test is to be focused on full characterisation of wood fuel as well as boiler parameters, ashes, and flue gas before and after the filter system during the regular operation of the boiler. These data will help to quantify the extent of release of radioactive materials from the facility, and thus, to evaluate the actual radiological doses from an industrial boiler to its personnel and to the general public.

1.1 Description of the Rechitza Test Facility

The boiler selected for the tests is located at Rechitza Drew Sawmill, Rechitza City, ca. 260 km Southeast of Minsk and ca. 100 km North of Chernobyl. The boiler house was not equipped with any flue gas treatment system. It was therefore possible to introduce baghouse filter technology, as recommended for the actual energy generating power plant. Although the sawmill lies in a zone with a relatively low contamination level (40-200 kBq m^{-2}), the wood that is treated here comes from a large area, which includes much more severely contaminated spots. Within the closest 50 km there are areas with a contamination level of several MBq m^{-2}. For comparison the limit for relocation of people has been set at 1.5 MBq m^{-2}. According to the radiological survey carried out by the BelLesBumProm Concern each year, raw wood materials supplied to the Mill on average have a specific activity

of 120 Bq kg^{-1}. In 1998, additional measurements were carried out by IPEP. The maximum content of ^{137}Cs detected in wood chips and bottom slag was 162.8 Bq kg^{-1} and 4703 Bq kg^{-1}, respectively.

Description of the Boiler and its Operation

The boiler was built more than 50 years ago by TAMPELLA in Finland. The boiler is a 9 tonnes hr^{-1} steam boiler, producing steam at 230 °C and 10 bar. The combustion chamber is brick-built (i.e. non-cooled), and the wood is fired on a fixed grate. The boiler is intermittently fired with wood-residues from the sawmill. The combustion on the grate is seen on Figures 1.1 and 1.2 in situations when fuel has just been added and when all the fuel is burning, respectively. As can be seen on the photos the two combustion conditions are very different. Some key data is given in Table 1.1 below.

In modern boilers the combustion chamber is usually built using membrane wall construction. Such construction is essentially non-existent in Belarus but it provides for more compact and generally cooler combustors.

The specific objectives of the boiler investigation include:

- Characterise transient combustion conditions. Combustion conditions strongly impact data interpretation.
- Determine the potential impact of combustion conditions on Cs emissions.
- Measure the flue gas velocities and O_2.
- Compare the particulate flow in the flue gas channel to the particulate flow in the filter pilot plant to determine if the sampling to the filter plant is (at least by the mass) representative for the duct.
- Measure the fuel consumption and boiler efficiency indirectly by measuring steam and flue gas parameters

The largest share of air for the combustion comes from primary air (under fired air). Secondary air is provided near the fuel injection to support the flame.

Table 1.1 Main parameters of boiler (as given by the sawmill staff)

Type	TAMPELLA (Finland)
Wood fuel moisture content	60%
Wood fuel consumption (bulk volume)	11 m^3/h
Size of fuel fractions	>30 mm (1-2%); 20-30 mm (10%) 10-20 mm (60%); <10 mm (30%)
Temperature in furnace	1150^oC
Excess air coefficient	3.5*
Boiler heat area total	300 m^2
Steam pressure	10 bar
Steam productivity	9 ton/h
Steam temperature	230^oC
Economiser heat area	511 m^2
Economiser outlet water	188^oC
Economiser inlet water	100^oC
Flue gas temperature after economiser	140^oC
Bottom slag flow	65-70 kg/h
Fly ash flow	30-35 kg/h
Main design features	Fixed grate furnace of 13.5 m^2 -grate with 342 bars; Vertical water-tubes boiler; 4 circulation tubes of 83 mm of diameter each; 176 boiling tubes of 83 mm in diameter each; Boiler steam collector of 230 mm in diameter; 110 economiser tubes of 115 mm in diameter; 858 air-heater tubes of 70 mm in diameter; Main centrifugal air fan of 20,100 m^3/hr; Additional centrifugal air fan of 5,220 m^3/hr; No flue gas treatment system

** It should be noted that the Excess Air Coefficient, as given by the sawmill staff, is at variance with other related parameters.*

The fuel handling system consists of fuel receipt and transportation to fuel bunker near the boiler. Preplanning for this test included provisions to ensure that the fuel prepared from this test was not mixed with other fuel in the feed system, that the fuel could be accurately sampled, and that the fuel feed rate was as consistent and controlled as possible. The following observations and provisions were made:

1. The fuel received the latest is on the top of the cone of the fuel dropped in the fuel storage. When fuel is taken from the storage for transportation to the boiler, it is taken from the bottom of the cone. This limits the mixing with ”left over” fuel in the storage. However, some mixing is inevitable.
2. We considered to take the fuel samples at the conveyer belt, as this is usually where the most representative samples are taken. However, in this case it would not be easy both because the belt was constantly moving and the distance for transportation of the fuel between the storage and the boiler was very long. This would cause a long time delay. Therefore it was decided to take the fuel samples from the chute, immediately before the fuel is fed into the boiler.
3. There was significant concern regarding constant fuel feeding. The two primary concerns were manually operated, intermittently feeding onto the grate and no constant ash removal process. Both of these features create variations in combustion conditions. Plant personnel committed to devise means of providing fuel feeding conditions as uniform as possible.

The feeding system consisted of a chute filled with fuel, see Figure 1.3. When more fuel was needed the chute was opened, the moving/flowing of the chips and wood stickers was helped by manually pushing the fuel further, so it fell from the sludge to the grate, which was positioned approximately

1,5 metres below the exit of the chute. The combustion air was supposed to be closed off when feeding of the fuel took place, as a safety issue, but we did not notice that it took place.

Figure 1.1 Wood chips on the grate right after fuel addition.

Figure 1.2 Burning wood chips on the grate.

The pyrometer measurement positions in the boiler at the tests were approximately 2 and 5 metres above the grate, respectively. The lowest position is referred to as the ground level and the highest position is referred to as the 1st floor, because this was where we were working in the building to make the measurements.

Concerning the operation of the boiler there was a lack of control equipment apart from measurements of the steam pressure and steam flow. However as to the Rechitza plant, the purpose of the boiler was to get rid of the woody by-product from the sawmill, and to produce steam. The purpose has never been to produce flue gas at dedicated conditions for scientists. Therefore optimisation of the combustion has not been an issue in the boiler operation e.g. monitored by an O_2 measurement in the

flue gas, and therefore it took some time before the operation staff fully understood our needs/demands and how to satisfy these the best.

During the test more than three different fuels were used, as there were not sufficient amounts of one type purchased for the test available. The change between the different fuels caused operational problems for the operators, as the fuels had different combustion characteristics.

Figure 1.3 The photo shows the chute where the fuel is stored right before feeding into the boiler.

Baghouse Design

To secure low emission values a baghouse fitted with filter bags working according to the surface filtration principle.

The 2-stage aerosol capture system includes one inert-type cyclone filter coupled with two bag filters. The baghouse filter installation was designed and produced by "GIPRO-GasoOchistka" Public Corporation in co-operation with IPEP and Minsk Research & Design Institute of Thermal/Energy Facility Adjustment. A cyclone was installed before the baghouse in order to reduce the dust mass load to the last stage and eliminate possible access of sparkles to bag material. The system is designed to treat 2800-3000 Nm^3 of flue gas per hour.

This system is mounted in a by-pass circuit incorporated into the boiler flue gas outlet duct, thus treating about 15% of the total flue gas flow. The system is equipped with one induced fan with a productivity of 6000 $Nm^3\ h^{-1}$ and a pressure head of 5kPa. The baghouse has a filter regeneration system with pulse cleaning by air pressure jets. A warning alarm system was also installed. This was activated when the temperature and pressure drops in the baghouse exceed 200^oC and 3 kPa respectively. The overall view of the installation is shown in Figure 1.4.

Figure 1.4 Baghouse built over the underground flue gas duct. The boiler building to the left and the stack to the right.

The functional scheme of the system is shown in Figure 1.5 and 1.6. Approximately 15% of exhaust gas are iso-kinetically taken from the flue gas outlet duct and directed to the by-pass circuit where the capture system is installed, first entering the cyclone.

The gas then leaves the cyclone and enters the filtration section and is evenly distributed among two separate modules assembled in parallel. A module has a number of filter bags each made in the form of cage (cartridge) which is fixed to a cell plate on the top of module. In each module the flue gas crosses the bags from outside to inside, and the aerosols deposit on the external surface of the bags.

Then the cleaned flue gas leaves the filtration section, returning back downstream of the boiler flue gas outlet duct, and ejects from the boiler stack. The flue gas flow along the by-pass circuit is controlled by the baghouse induced fan and gate-type slide valve (SG4, see Fig. 1.5).

The design of a baghouse filter includes the counter flow compressed air injection from the top cells through injection nozzles to clean the bags. The compressed air is provided from a manifold placed between the cell plate and top platform. This rapidly pulsing counter flow air injected into each bag, escapes it through the outer side thus shaking off the filter cake and blowing off the dust retained in pores of filter material. The cleaning cycle is provided without withholding filtering process. The frequency of cleaning cycles is governed for both modules by the relevant control device, setting up the time interval between the compressed air injections and the pressure drop.

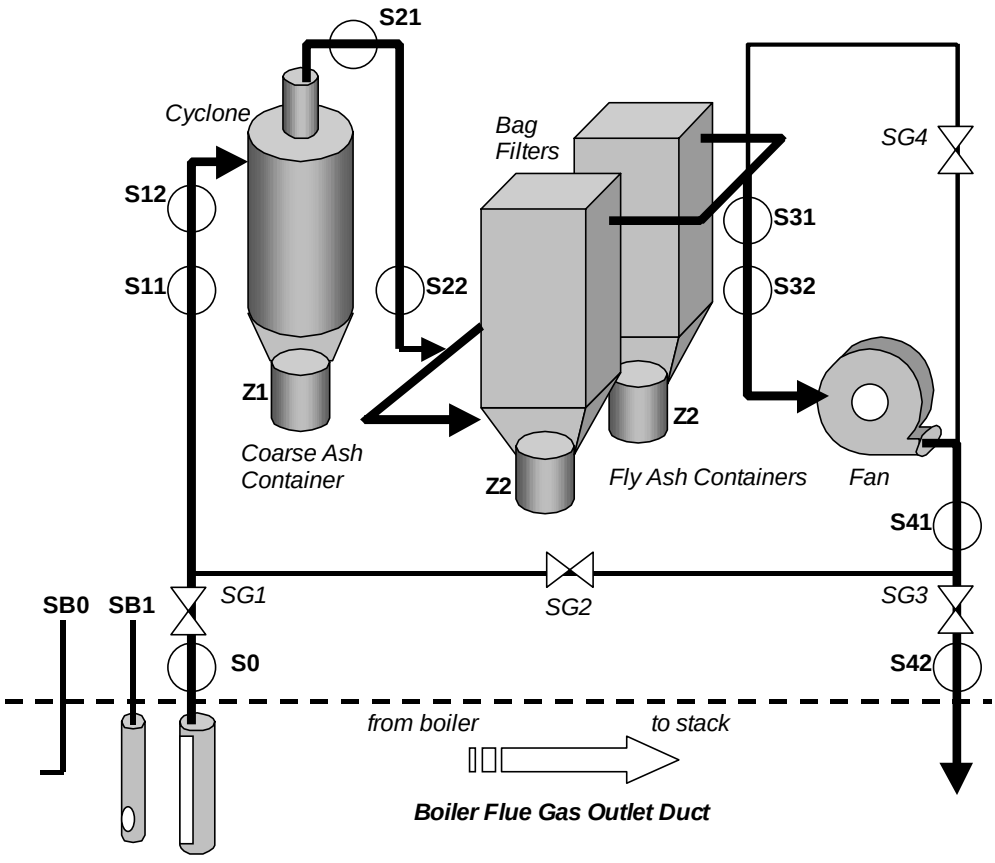

Figure 1.5 Functional scheme of the by-pass circuit with test facility and sampling positions SB/S0/S1/S2/S3/S4:

- **SB0, SB1** – Sampling probes positioned in the underground duct, see also Figure 1.6.
- **S**i – Sampling ports in the piping sections of the baghouse filter for extraction of total dust and size fractionated samples.
- **Z**i – Sampling ports for sampling of cyclone ashes (Z1) and filter ashes (Z2)
- **SG**i **–** Sliding gates for control of main flow and by-pass flow.

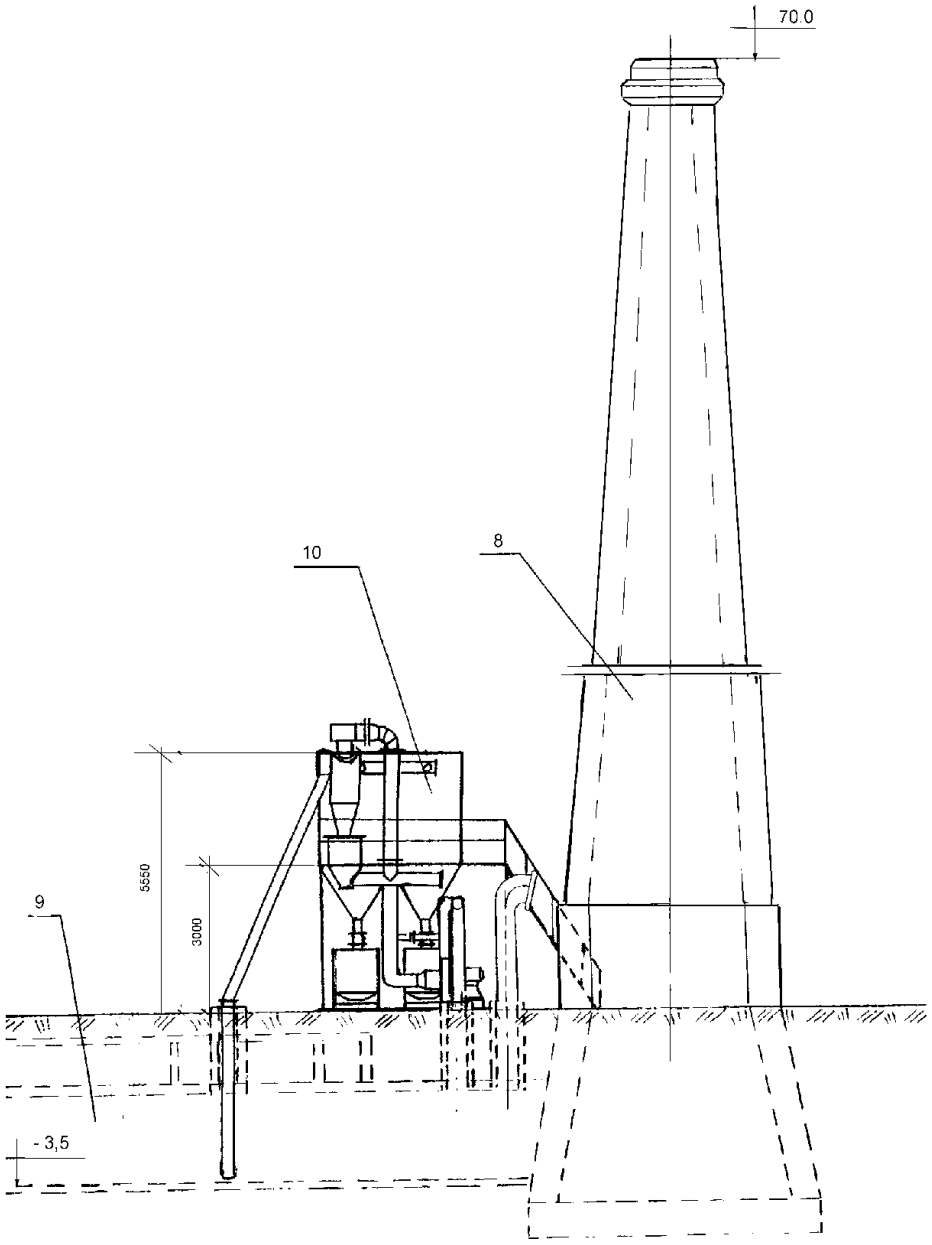

Figure 1.6 Diagram of the filter test facility constructed at the Rechitza Drew sawmill. The main duct leading the flue gas to the stack is positioned underground. In the left side the inlet pipe from the underground duct leads the flue gas in to the cyclone. The cyclone can be seen in front of the two baghouses.

2 Boiler Characteristics

2.1 Methods Applied

Peak combustor temperatures were determined using a suction pyrometer equipped with a type R thermocouple (Figure 2.1). A suction pyrometer is designed to measure gas temperatures with minimal heat radiation losses. Continuous temperature measurements were recorded over two intervals of about one hour each during the test. These temperatures were measured at two points above the combustor bed, as near to the flame as was possible given the limited access.

Combustor gas composition measurements were planned for the facility but could not be completed due to an instrument failure early in the test. However, IPEP recorded flue gas compositions from which some inferences can be made regarding combustor gas compositions.

The measurements in the duct (Figure 2.2) included (1) gas velocity, (2) oxygen content, and (3) fly ash loading. All measurements were made between the boiler and the bag house slipstream (position SB1, Figure 1.5). These measurements were made at several locations across the duct to determine spatial variations.

The velocities were determined using a calibrated Pitot tube. Gas samples were extracted to determine gas composition. Particle loading was determined by extractive sampling of particles on a ceramic fibre filter. All measurements were made at four horizontal and six vertical positions across the duct, for a total of 24 sampling locations. The gas velocity and composition measurements were made once during the three-day test. The particle loading measurements were made twice.

Steam temperature, pressure and flow rate and feed water temperature and pressure were determined three times during the last two days of the three-day test. In addition, the combustion air temperature and flue gas temperature and flow rate were determined. These measurements form the basis of the boiler efficiency and fuel feed rate determinations. Each of the three measurement campaigns lasted for more than 2 hours.

2.2 Results Achieved

The results are discussed in the following order

- Results from measurements in the boiler
- Results from measurements in the duct
- Indirect estimation of the boiler efficiency and the fuel consumption

Figure 2.1 Measurement of the combustion temperature in the boiler using a suction pyrometer.

Figure 2.2 Measurement of the flow field and oxygen distribution in the duct. A similar method is used for sampling fly ash from the duct

Results from Measurements in the Boiler

The following figures (Figures 2.3 and 2.4) show the temperature in the boiler measured at two different positions.

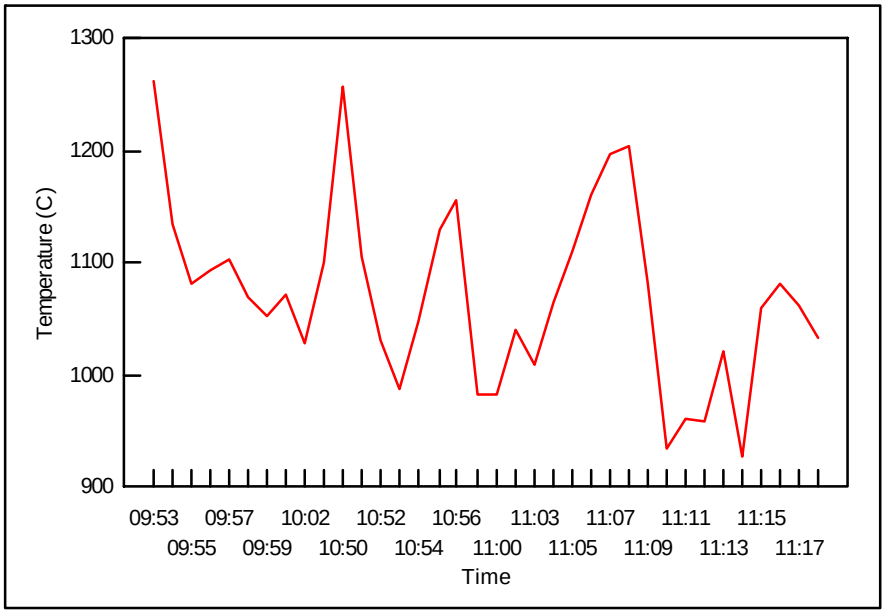

Figure 2.3 Pyrometer measurement ground level, date 1999.06.18.

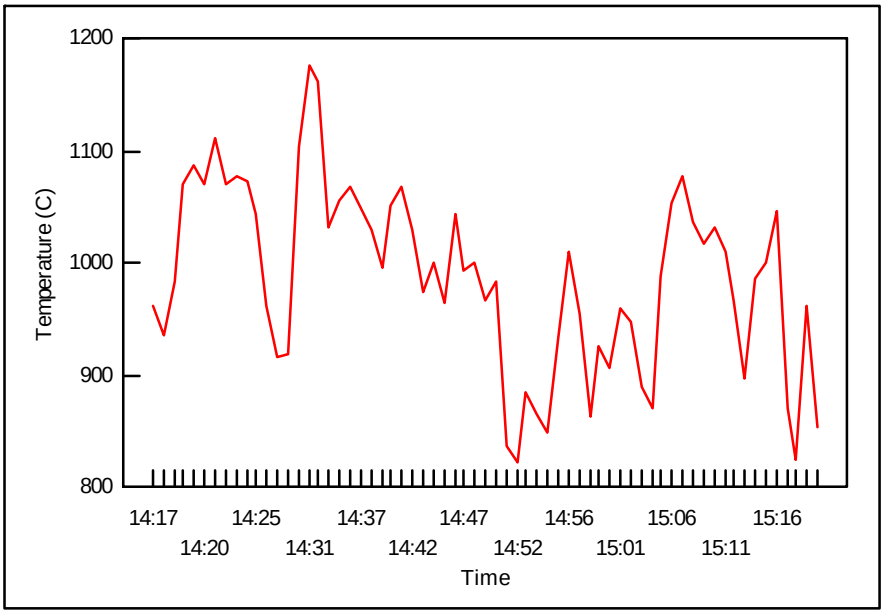

Figure 2.4 Pyrometer measurement 1. floor, date 1999.06.18.

Results from Measurements in the Duct

The parameters measured in the ducts were (1) the oxygen content, (2) the flow field, and (3) a representative sampling of fly ash. The results achieved are presented in the following, Figures 2.5 - 2.7 and Table 2.1.

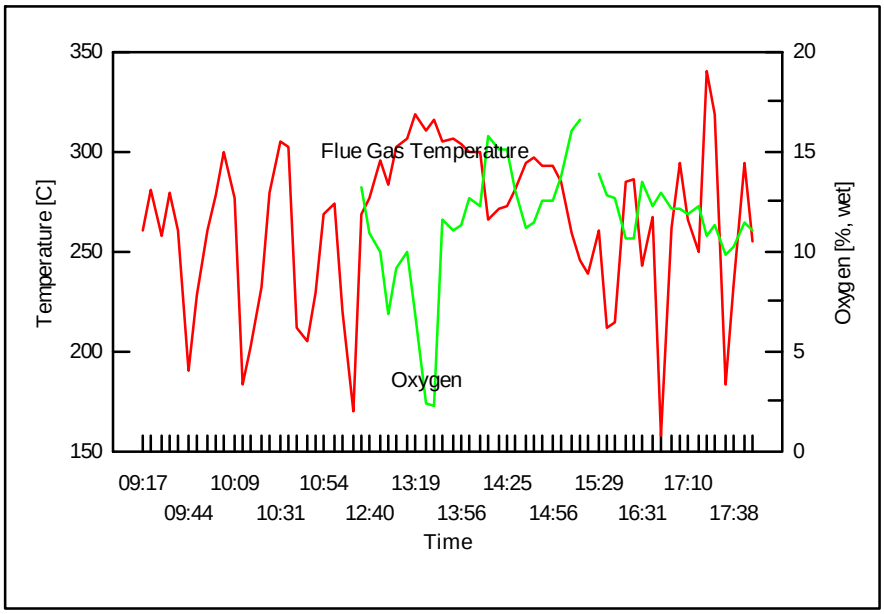

Figure 2.5 Flue Gas temperature and Flue Gas oxygen content, date 1999.06.17

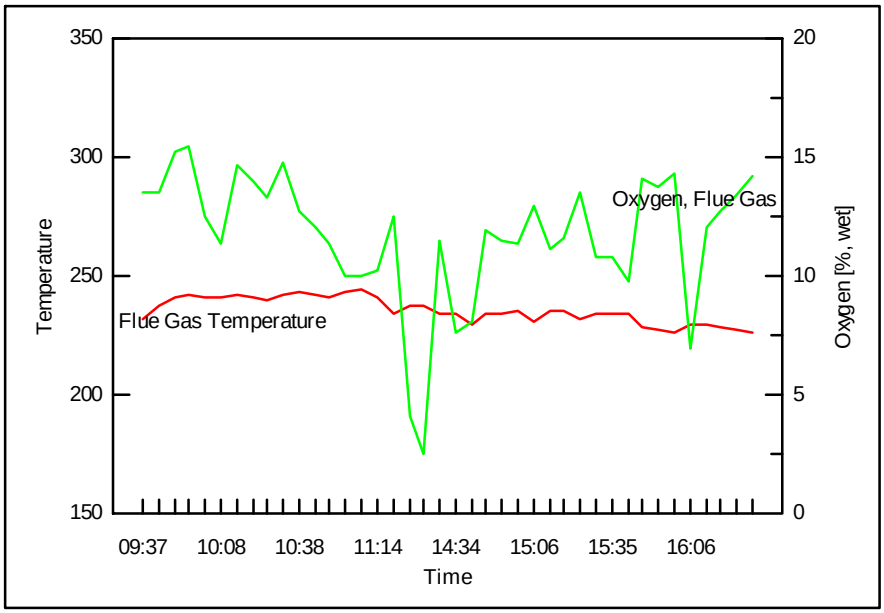

Figure 2.6 Flue Gas temperature and Flue Gas oxygen content, date 1999.06.18

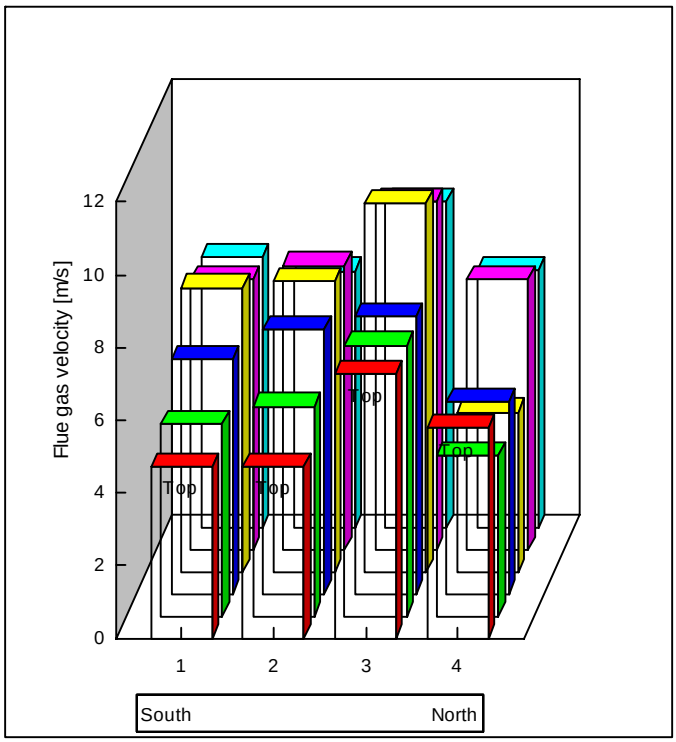

Figure 2.7 Flue Gas velocity distribution in underground duct. diagrams.

Table 2.1 Result of dust measurement in underground duct.

Dust Measurement in underground duct.			
Date		1999.06.17	1999.06.17
Time		09.17 – 11.07	16.30 – 17.40
Flue Gas velocity, avg	[m/s]	7,32	7,33
Flue Gas flow, wet	[Nm^3/h]	30663	30080
Flue Gas flow, dry	[Nm^3/h]	24266	25311
Dust collected	[g]	1,073	0,4761
Dust concentration, wet	[mg/Nm^3]	365	658
Dust concentration, dry	[mg/Nm^3]	461	783
Dust flow in duct	[kg/h]	11	20
Isokinetic ratio	[%]	14,3	10,9

Indirect Estimation of the Boiler Efficiency and the Fuel Consumption

The boiler efficiency is the ratio of energy in the steam to energy in the fuel and is a fundamental measure of boiler performance. The boiler efficiency may be determined either directly (based on fuel flow rate and steam flow rate) or indirectly. Since measurement of the solid fuel flow is often not very precise, the boiler efficiency is often most accurately determined by the indirect method. With this method the losses from the boiler are found and the efficiency is determined by difference. The largest losses from a boiler are generally, in order of decreasing importance, sensible heat in the flue gases, heat losses from the boiler, unburned carbon, and sensible heat losses associated with ash removal.

To determine the boiler efficiency by the indirect method, the following measurements are required: Flue gas flow rate, temperature and composition (O_2 and CO); combustion air temperature; fly ash carbon content; and parasitic losses from the boiler and ancillary equipment. Heat losses from the boiler were not directly measured but were determined using standard values for boiler of this size, type and fuel type.

Having found the boiler efficiency, the fuel flow may be calculated based on the known rate of steam production (Fig. 2.8 – 2.10). The results of evaluation of boiler efficiency are presented in Tables 2.2 – 2.4).

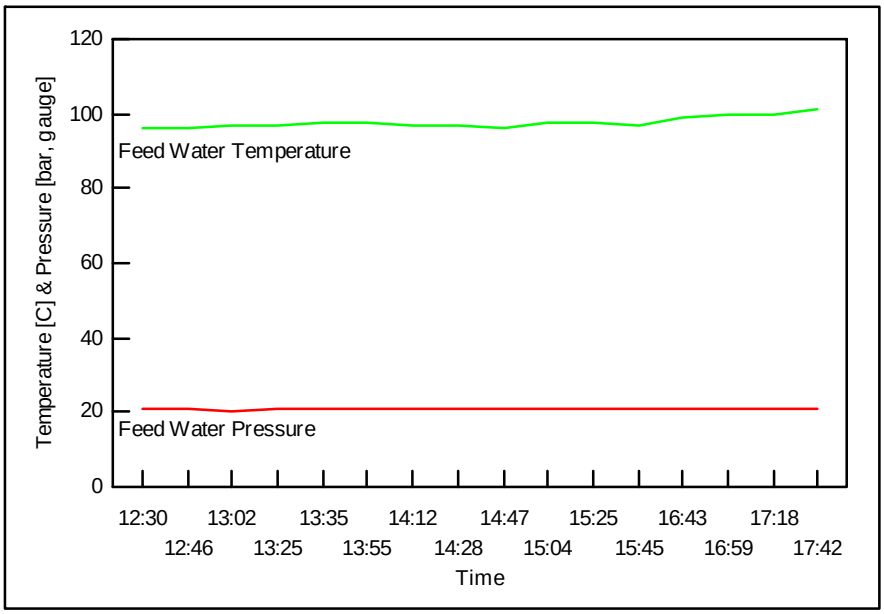

Figure 2.8 Steam data from 1999.06.17.

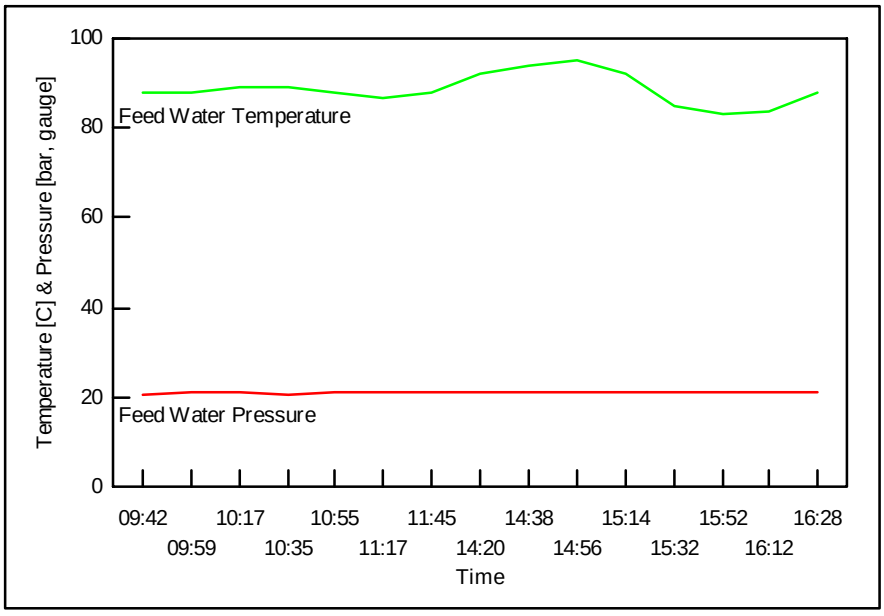

Figure 2.9 Feed Water temperature and Feed Water pressure, date 1999.06.18.

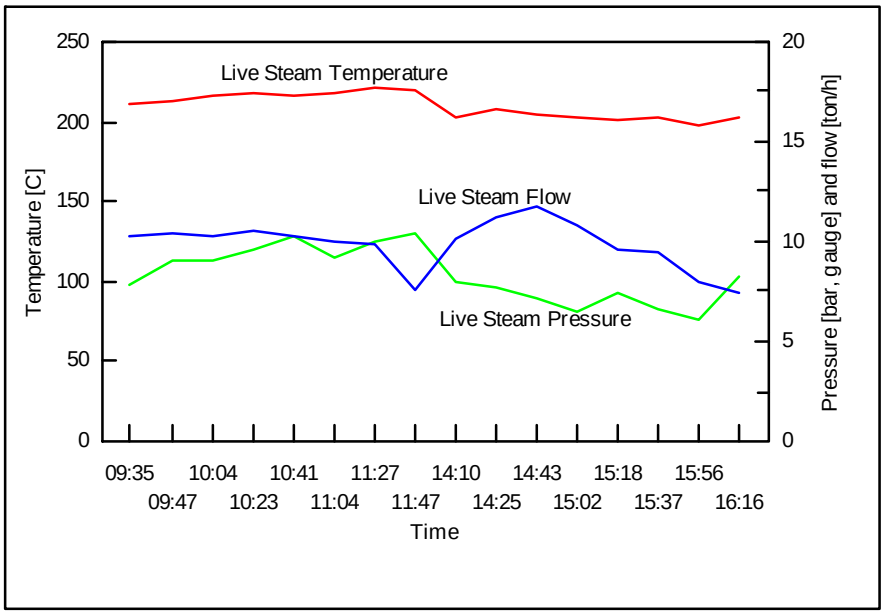

Figure 2.10 Steam data from 1999.06.18.

Table 2.2 Results of boiler efficiency measurements on 1999.06.17 during the time interval 12.25-17.50.

Fuel analysis			**Specific air / flue gas quantity**				
Hu	MJ/kg	10,21	Air, lhamda = 1	kg/kg	3,51	Nm³/kg	2,71
C		29,3%	Air, lhamda > 1	kg/kg	9,56	Nm³/kg	7,40
S		-0,0%	Flue gas, dry, lhamda = 1	kg/kg	3,78	Nm³/kg	2,70
H		3,1%	Flue gas, lhamda > 1	kg/kg	9,83	Nm³/kg	7,38
N		0,6%	**Flue gas analysis**				
O		22,2%		**O2**	**CO2**	**H2O**	**N2**
W		43,1%	% Mass, wet	13,1	10,0	8,5	67,2
A		1,7%	% Mass, dry	14,3	10,9	0,0	73,4
Cl		0,0%	%Volume, wet	11,5	6,4	13,3	68,7
Total		100,0%	%Volume, dry	13,3	7,4	0,0	79,2

Flue Gas / Air data:					
Flue gas temperature	°C	275,3	Enthalpy flue gas	kJ/kg	273,4
Reference temperature	°C	25	Air temperature	°C	35
Lhamda		2,73	Enthalpy Air	kJ/kg	10,2
Density, flue gas, wet	kg/Nm³	1,262	Water content, Air	kg/kg dry air	0,0207

Energy Balance						
Boiler effency		67,9%		O2-% Air Preheater inlet		11,5%
Steam production	MJ/s	7,0		O2-% Air Preheater outlet		11,5%
Energy, supplied	MJ/s	10,3		Air Preheater leak		-0,0%
Energy supplied (fuel)	MJ/s	10,3		Air flow	kg/s	9,6
Energy supplied (other)	MJ/s	0		Air flow	Nm³/s	7,5
Flue gas loss	MJ/s	2,882	28,0%	Flue gas, wet	kg/s	10,5
Radiation	MJ/s	0,086	0,8%	Flue gas, wet	Nm³/s	8,4
Slag	MJ/s	0,228	2,2%	Flue gas, wet	m³/s	16,8
Fly ash	MJ/s	0,108	1,0%	Fuel, gasified	kg/s	0,981
Total loss	MJ/s	3,304	32,1%	Fuel, supplied	kg/s	0,999
Difference		0,000				

Ash Balance:					
Fly ash share		5,0%	Slag, water		0,0%
Slag share		95,0%	Slag, dry	kg/s	0,022
Unburnt, fly ash		80,0%	Slag, wet	kg/s	0,022
Unburnt slag		30,0%	Fly ash	kg/s	0,004
Slag temperature	°C	500			

Table 2.3 Results of boiler efficiency measurements on 1999.06.18 during the time interval 09.30-11.45.

Fuel analysis			**Specific air / flue gas quantity**				
Hu	MJ/kg	9,90	Air, lhamda = 1	kg/kg	3,42	Nm³/kg	2,64
C		28,6%	Air, lhamda > 1	kg/kg	11,15	Nm³/kg	8,62
S		-0,0%	Flue gas, dry, lhamda = 1	kg/kg	3,68	Nm³/kg	2,63
H		3,1%	Flue gas, lhamda > 1	kg/kg	11,41	Nm³/kg	8,61
N		0,5%	**Flue gas analysis**				
O		21,6%		**O2**	**CO2**	**H2O**	**N2**
W		44,5%	% Mass, wet	14,5	8,5	7,7	68,1
A		1,7%	% Mass, dry	15,7	9,2	0,0	73,7
Cl		0,0%	%Volume, wet	12,8	5,4	12,1	69,6
Total		100,0%	%Volume, dry	14,6	6,2	0,0	79,2

Flue Gas / Air data:						
Flue gas temperature	°C	240,9	Enthalpy flue gas		kJ/kg	233,6
Reference temperature	°C	25	Air temperature		°C	35
Lhamda		3,26	Enthalpy Air		kJ/kg	10,2
Density, flue gas, wet	kg/Nm³	1,263	Water content, Air		kg/kg dry air	0,0207
Energy Balance						
Boiler effency		67,6%	O2-% Air Preheater inlet			12,8%
Steam production	MJ/s	7,0	O2-% Air Preheater outlet			12,8%
Energy, supplied	MJ/s	10,4	Air Preheater leak			-0,0%
Energy supplied (fuel)	MJ/s	10,4	Air flow		kg/s	11,6
Energy supplied (other)	MJ/s	0	Air flow		Nm³/s	9,1
Flue gas loss	MJ/s	2,956 28,3%	Flue gas, wet		kg/s	12,7
Radiation	MJ/s	0,086 0,8%	Flue gas, wet		Nm³/s	10,0
Slag	MJ/s	0,232 2,2%	Flue gas, wet		m³/s	18,9
Fly ash	MJ/s	0,110 1,1%	Fuel, gasified		kg/s	1,023
Total loss	MJ/s	3,384 32,4%	Fuel, supplied		kg/s	1,042
Difference		0,000				
Ash Balance:						
Fly ash share		5,0%	Slag, water		0,0%	
Slag share		95,0%	Slag, dry	kg/s	0,022	
Unburnt, fly ash		80,0%	Slag, wet	kg/s	0,022	
Unburnt slag		30,0%	Fly ash	kg/s	0,004	
Slag temperature	°C	500				

Table 2.4 Results of boiler efficiency measurements on 1999.06.18 during the time interval 14.10-16.15.

Fuel analysis			**Specific air / flue gas quantity**					
Hu	MJ/kg	10,39	Air, lhamda = 1	kg/kg	3,56	Nm³/kg	2,75
C		29,7%	Air, lhamda > 1	kg/kg	9,03	Nm³/kg	6,98
S		-0,0%	Flue gas, dry, lhamda = 1	kg/kg	3,83	Nm³/kg	2,73
H		3,2%	Flue gas, lhamda > 1	kg/kg	9,31	Nm³/kg	6,97
N		0,6%	**Flue gas analysis**				
O		22,5%		**O2**	**CO2**	**H2O**	**N2**
W		42,3%	% Mass, wet	12,5	10,7	8,8	66,8
A		1,7%	% Mass, dry	13,7	11,7	0,0	73,3
Cl		0,0%	%Volume, wet	11,0	6,9	13,8	68,3
Total		100,0%	%Volume, dry	12,7	8,0	0,0	79,2

Flue Gas / Air data:						
Flue gas temperature	°C	232,2	Enthalpy flue gas		kJ/kg	225,8
Reference temperature	°C	25	Air temperature		°C	35
Lhamda		2,54	Enthalpy Air		kJ/kg	10,2
Density, flue gas, wet	kg/Nm³	1,262	Water content, Air		kg/kg dry air	0,0207

Energy Balance							
Boiler effency		74,2%		O2-% Air Preheater inlet			11,0%
Steam production	MJ/s	6,9		O2-% Air Preheater outlet			11,0%
Energy, supplied	MJ/s	9,3		Air Preheater leak			-0,0%
Energy supplied (fuel)	MJ/s	9,3		Air flow		kg/s	8,1
Energy supplied (other)	MJ/s	0		Air flow		Nm³/s	6,3
Flue gas loss	MJ/s	2,009	21,6%	Flue gas, wet		kg/s	8,9
Radiation	MJ/s	0,085	0,9%	Flue gas, wet		Nm³/s	7,0
Slag	MJ/s	0,206	2,2%	Flue gas, wet		m³/s	13,0
Fly ash	MJ/s	0,097	1,0%	Fuel, gasified		kg/s	0,872
Total loss	MJ/s	2,396	25,8%	Fuel, supplied		kg/s	0,888
Difference		0,000					

Ash Balance:					
Fly ash share		5,0%	Slag, water		0,0%
Slag share		95,0%	Slag, dry	kg/s	0,020
Unburnt, fly ash		80,0%	Slag, wet	kg/s	0,020
Unburnt slag		30,0%	Fly ash	kg/s	0,004
Slag temperature	°C	500			

Discussion

Concerning the characterisation of the combustion conditions it is clear, that the combustion conditions were very unsteady, which is probably impossible to avoid when batch firing. The visual impression, that the smoke emitted were frequently very dark (black), suggests that there were frequently at least locally and probably globally reducing conditions in the boiler. During the investigation, the O_2 concentrations in the duct varied from 2% to 19%. During periods of relatively steady operation the O_2 was 12-14%. There is significant air leakage in this furnace (as is common with this style of furnace), making the estimation of furnace oxygen content difficult. However, stack opacity became high due to a sooty plume whenever the duct oxygen content dropped below 6-8 percent. The stack opacity was high every 10-25 minutes and remained high for 3-15 minutes or longer. Such heavy soothing is almost certainly associated with nearly globally reducing conditions in the furnace.

The varying stoichiometry of the furnace complicates data analysis for several reasons. First, the total concentration of particulate and especially of small particulate is heavily impacted by soot. The amount of soot produced from the transient reducing conditions almost certainly exceeds the amount of inorganic aerosol by orders of magnitude. Since we are interested in the caesium activity in the fly ash and especially in the aerosol, the varying amounts of soot have a large impact on the measurements. This can be partially corrected by correcting the aerosol activity measurements to a carbon-free basis.

A second impact of the varying stoichiometry is the impact on caesium chemistry. Reducing conditions generally promote the formation of volatile forms of alkali (caesium, potassium, and sodium). Therefore, the amount of caesium found in the aerosol was varying quite widely during the test, making data interpretation difficult. This is best corrected by limiting data evaluation to periods of time during which the combustion conditions were relatively constant and known. However, none of the samples sampled after the baghouse and few of those sampled before it were collected during periods of sufficiently constant operating conditions.

Finally, the varying conditions lead to significant changes in temperature and flow patterns in the boiler. Volatilisation of caesium is highly temperature dependent and formation of aerosol from vapour condenses depends on time. Therefore, the amount and size of the aerosol formed during the test could be expected to vary with combustion conditions. These trends will be difficult to unambiguously sort out of the data.

The measurements in the duct showed that the flue gas flow velocity was relatively constant, despite the variations in combustion conditions. The flue gas velocity in this boiler is determined almost entirely by the size of the stack and the temperature of the gases in it. Combustion conditions are relatively unimportant. Since the stack height is constant and the gas temperature is nearly constant, the velocities are also nearly constant.

The particulate flow in the flue gas duct was measured by the mass of the collected fly ash. The fly ash in the flue gas before the filter was measured in two separate tests to be 461 mg Nm^{-3} (dry) and 783 mg Nm^{-3} (dry). We do not have a quantitative measure of fly ash carbon content, but the visual indication is that it was very high. The fly ash was dark black, whereas fly ash from non-soothing boilers is grey. Comparisons of fly ash concentrations measured in the duct with those measured in the bag house inlet are not yet complete.

The boiler efficiency and fuel consumption were determined at three points during the test. The boiler thermal efficiencies (percentage of fuel energy absorbed by the steam) were 67,9%, 67,6% and 74,2%. These values are relatively constant, but significantly lower than commonly measured for western boilers, the latter varying from 85-92%. All efficiencies are determined on a lower heating value basis (as is the custom in Europe but not in the US). The lower efficiencies are associated with the older boiler design, significant air in leakage, high stack oxygen concentrations, and carbon losses in the form of unburned carbon in the fly ash. They are not particularly surprising for this style of boiler under these operating conditions. The average fuel consumptions during the three measurements were 0,999 kg/s, 1,042 kg/s and 0,888 kg/s, although these numbers are not particularly meaningful since the boiler was intermittently fed.

2.3 Evaluation of Stability Regimes

In order identify main sources of error and to find the time spans were the boiler was operating under reasonably stable conditions, suitable for data analysis, the main parameters of the boiler operation have been studied. The goal was to find time spans where different measurements could be compared.

The composition of flue gas (e.g. O_2 and CO content) was changing in a wide range that was caused by inconstancy of fuel load. Elsamprojekt and IPEP separately measured the oxygen concentration in different positions. Figure 2.11 compares the two data sets measured in the neighbouring ports SB0 and SB1. There is a good agreement between the data, especially during the more stable period on the 18/6, and both sets show considerable scatter.

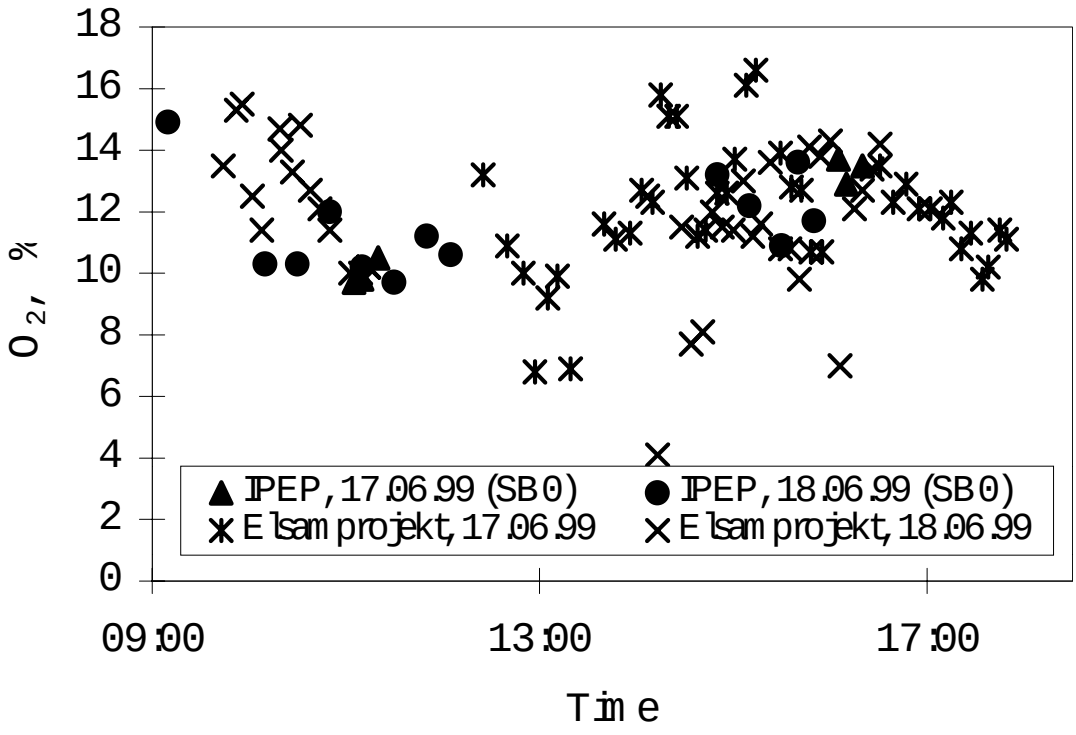

Figure 2.11 O_2 measurements in the ports SB0 (IPEP) and SB1 (Elsamprojekt)

It can be seen in Figure 2.12 that the oxygen concentration in flue gas at the point SB0 in the main duct right after furnace is lower than that at the capture system leaving point S42 located downstream. The difference is a factor of 1.3 - 1.4 that hardly belongs to measurement errors since the data obtained with different methods by Elsamprojekt and IPEP from close sampling points are in a good agreement (see Figure 2.11 above). This deviation is probably caused by a significant inflow of ambient air due to leaks in the furnace and underground flue gas duct. Some leaking would also occur during exchange of sampling probes in the pilot facility at the sampling port before S41. This is another error source and it clearly indicates that the dust samples obtained in the baghouse filter plant are not quantitatively correct for the exhaust conditions.

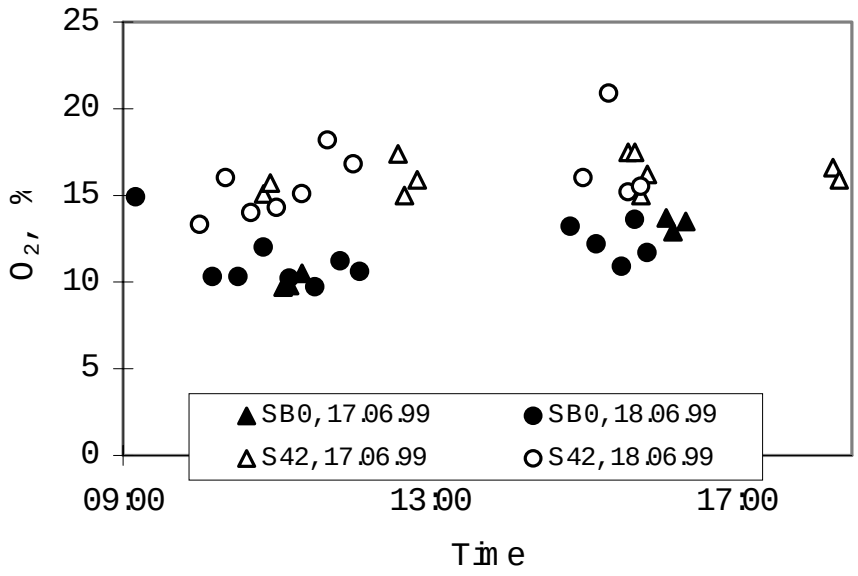

Figure 2.12 O_2 Concentration in Different Sampling Ports measured by IPEP.

The ratio between O_2 and CO illustrates the effect of the bulk firing together with the lack of control with the combustion air supply. The under-burning conditions lead to the complete oxidizing illustrated by the inverse relationship between the two gases seen in Figure 2.13.

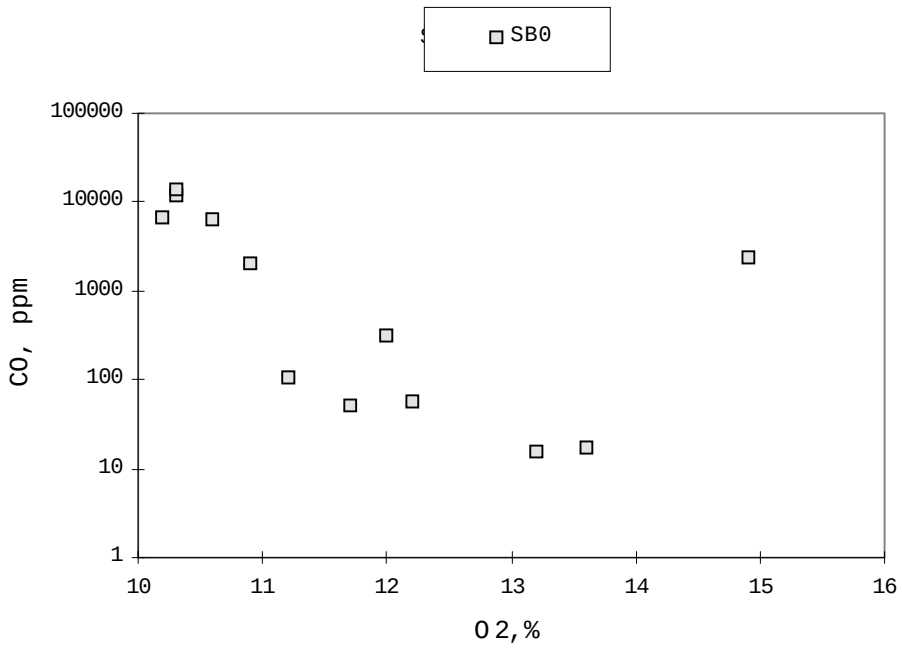

Figure 2.13 CO/O_2 Ratio measured by IPEP.

Temperature in the Furnace Chamber

The non-continuous fuel supply also caused of temperature variation in the furnace (from 800 to 1250°C) within short time intervals (Figure 2.14). We do not have this data from the entire measuring period and we can just conclude that the combustion conditions was very variable regarding temperature when we discuss the behaviour of Cs-137.

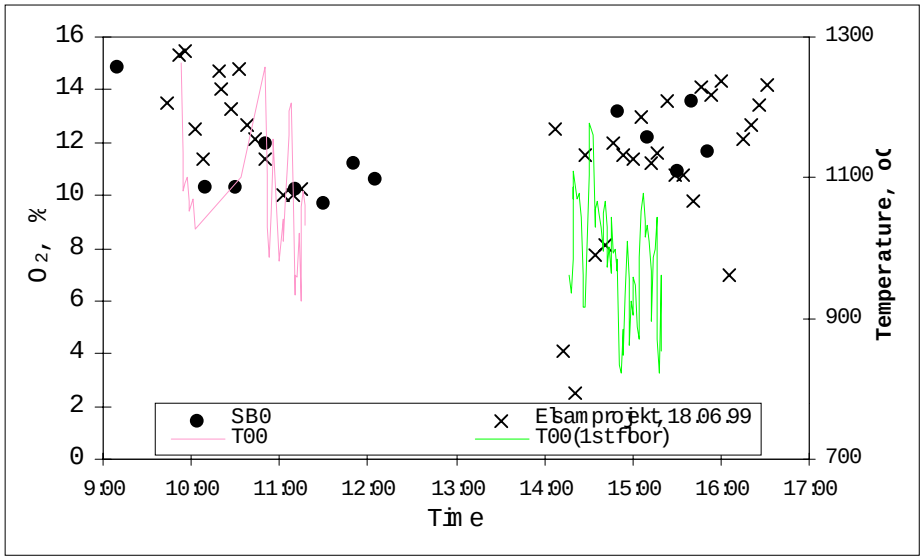

Figure 2.14 Furnace Bed Temperature (T00) and O_2 Concentration in Flue Gas. 18.06.99

The live steam output also reflected the variations in combustion conditions as illustrated in Figure 2.15 to Figure 2.17. Apparently the boiler was run at fuel load during 16/6, whereas it was running at reduced power during 17/6 and 18/6.

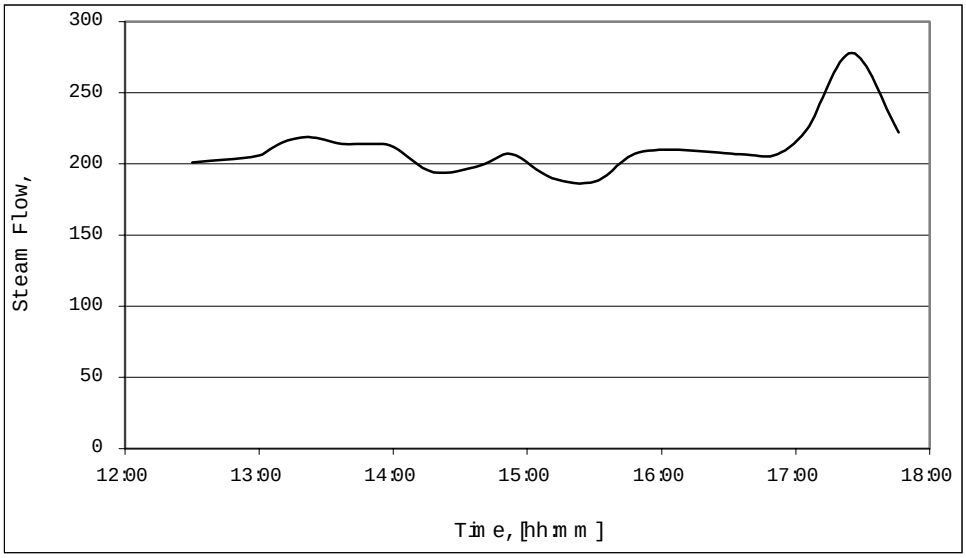

Figure 2.15 Boiler Live Steam Flow (16.06.99)

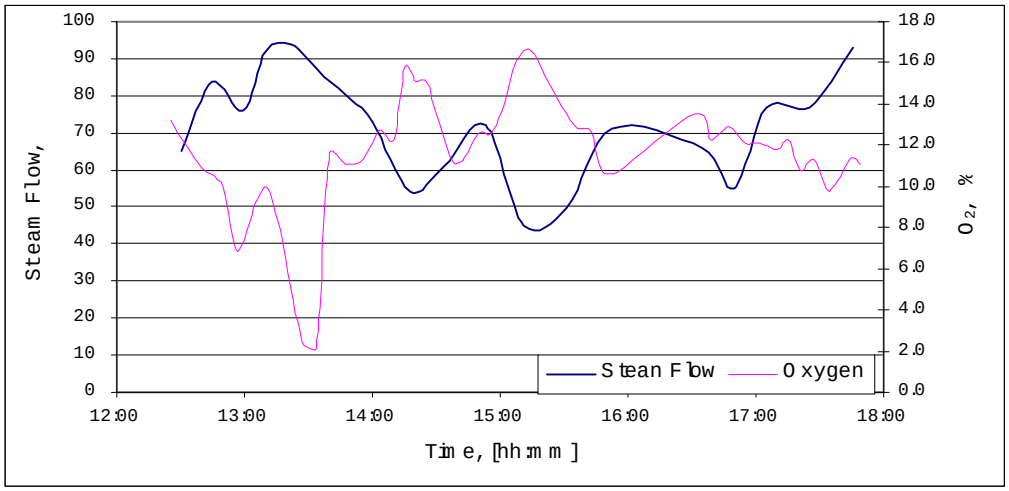

Figure 2.16 Boiler Live Steam Flow and Flue Gas Oxygen Content (17.06.99)

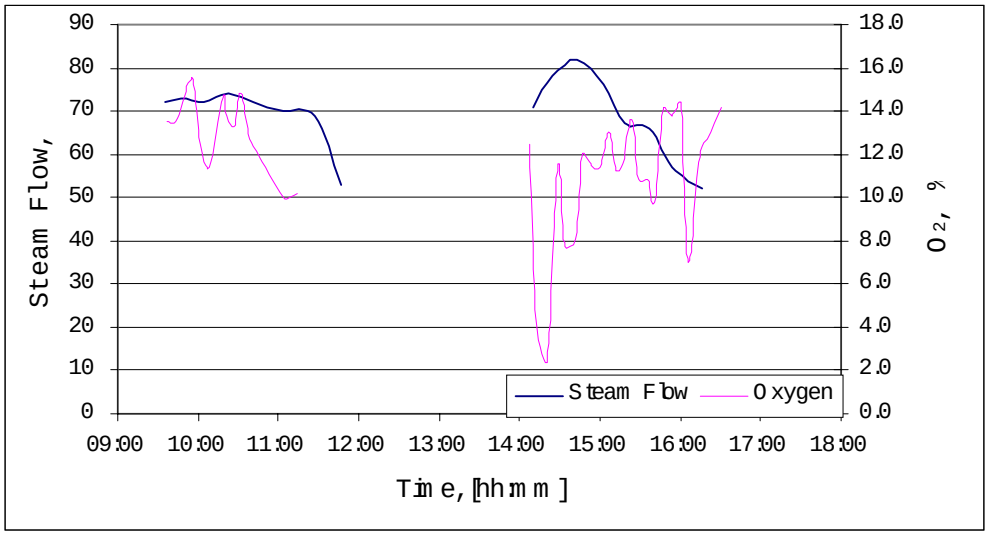

Figure 2.17 Boiler Live Steam Flow and Flue Gas Oxygen Content (18.06.99)

Flue Gas Flow in Test Facility Duct

The dynamic characteristics of flue gas flow between furnace and stack are mainly defined by the stack height, therefore the flue gas flow rate did not vary much, only within some 4%. However, as it follows from the results of traversing, the air velocity profile along the duct height is non-uniform. The flow velocity in the lower part of the duct channel, where the dust gravity is likely to be highest, is 40% higher than that in the upper part.

As for flue gas flow parameters inside the capture facility, they varied within a larger range (see Figure 2.18, Figure 2.19 and Figure 2.20). This was caused by periodic changes in the settings controlling the flow rate and alteration of intervals between the baghouse cleaning cycles.

Both these two circumstances lead to problems when trying to extract a iso-kinetic flue gas stream from the underground duct into the bag house facility. It can be concluded that over all the obtained data from the test facility is not representative for the exhaust flue gas. Single parameters, such as specific activity of sub-micron aerosol, will still be valid.

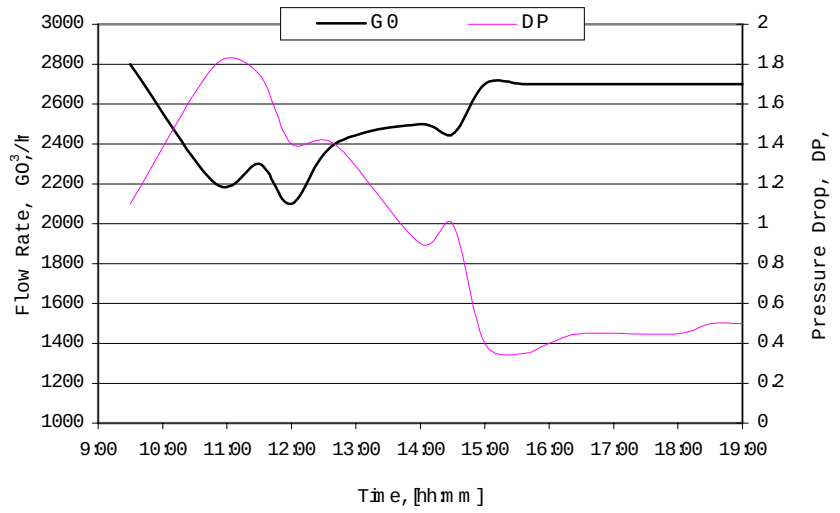

Figure 2.18 Flue gas flow rate and pressure drop in test facility 16.06.99.

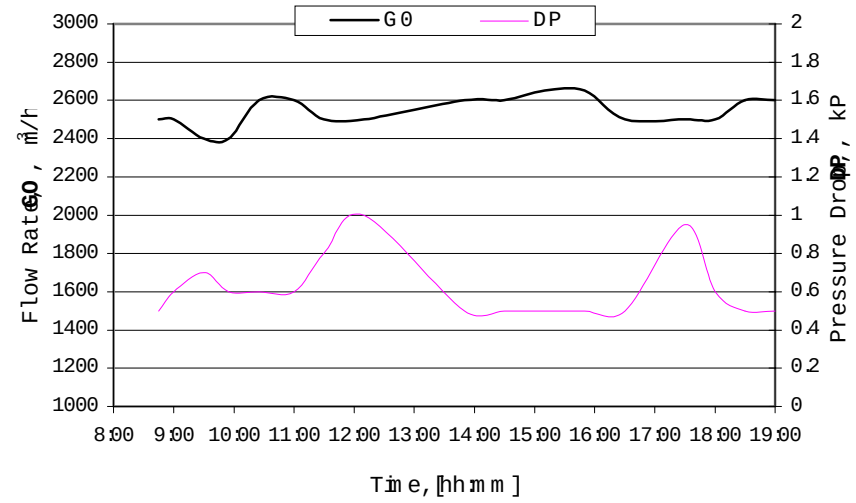

Figure 2.19 Flue gas flow rate and pressure drop in test facility 17.06.99.

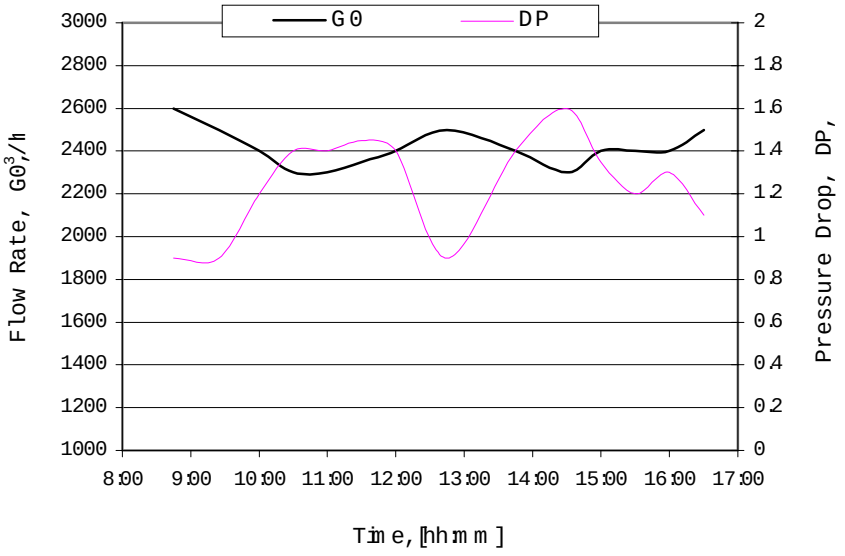

Figure 2.20 Flue Gas flow rate and pressure drop in the test facility 18.06.99.

Conclusion on Stable Time Regimes

From the above review of the test regimes and combustion conditions, one can make the following resume:

- Several time intervals can be singled out, within which the results of aerosol measurements and the samples taken from the duct can be referred to a conditionally stable regime of combustion. They are as follows:
- 12:00 to 13:30, 15:30 to 17:00, and 18:00 to 19:00
- 9:30 to 12:30, 14:00 to 16:30, and 17:00 to 19:00
- 9:30 to 11:30, and 15:00 to 18:00
- Uneven distribution of the flue gas velocity in the main duct does not allow us to consider the extraction of gas flow to the capture facility as sampling attributed to isokinetic conditions.
- The evident variations of oxidising conditions and inequality of fuel should cause sufficient differences of data on aerosols. First of all, it concerns the data on radioactivity since chemistry and volatility of caesium and its species are mainly defined by conditions in a furnace.

Instability of oxidising conditions was also a main reason of periodic sooting (every 5-10 minutes) and thus, was a source of the lesser-contaminated fine dust containing carbon. The latter distorts the picture of aerosol formation.

3 Baghouse Measurements

In order to test the capture efficiency of the baghouse facility a number of different measurements were carried out. Size specific number concentrations were measured together with total mass concentration and size distribution according to mass.

These measurements were made at different locations. The schematic position of the sampling ports fitted into the pipes is shown in figure 1.5. Based on these measurements it is possible to evaluate the performance of the cyclone and the baghouse filter as a function of particle size.

The first day of the test was spent preparing and testing equipment. Next day, Tuesday the 15/6, there were no measurements done at the baghouse due to problems with the fan. A full test programme was carried out over the last three days of the week.

3.1 Test Facility Run Procedure

The baghouse test facility was only operated during daytime and it had to be restarted every morning.

The by-pass circuit with filters was preheated prior to the actual test in order to exceed the dew point and avoid the condensation of flue gas moisture on filter bags. This is achieved by running the circulation fan with the SG2 sliding gate open and the SG1 / SG3 sliding gates closed (see Fig. 1.5). The idling circulation along the by-pass circuit is maintained until the temperature of air in the system exceeds 40^{o}C (app. 1 hour run).

Then the idling circulation flow is stopped by closing the SG2 sliding gate, and the SG1 / SG3 sliding gates are opened simultaneously. A fraction of the boiler flue gas stream (approx. 2,900 m^3 per hour) is iso-kinetically taken from the boiler outlet duct and enters the test facility.

In Table 3.1 an example of temperature parameters at three main points along the by-pass circuit during a start-up is given. For the log numbers of temperature measurement positions see Fig. 3.1.

Table 3.1 Temperature variations along the duct of the test facility during the start-up procedure.

Procedure	Time	T11, °C	T12, °C	T13, °C
Idling circulation	6:10 (start)	20	20	20
	8:00	42	40	36
Actual run	8:22 (start)	55	40	36
	8:25	68	53	50
	8:28	195	110	68
	8:30	198	127	75
	8:45	200	135	95

In the cyclone the coarse fly ash particles are selected from fine aerosols and accumulated in a hopper (container Z1, see Fig. 1.5) equipped with special sliding gate opening/damming the dust flow down to the container. The coarse dust from the container is manually emptied by the end of each day into the plastic bag for further analysis. Every day, during each test run, several samples were taken from a port positioned between the sliding gate and the container by a special sampling device for time-dependent characterisation of the ash.

After the cyclone, the flue gas enters the baghouse and the flue gas stream is evenly divided among the two modules. In the baghouse the fine dust is captured on the surface and pores of filter material, and the dust cake is then shaken off into two containers Z2 (see Fig. 1.5) by means of bypass cleaning cycles. The removed fine dust is collected in a container (one container for each module), and each container is emptied manually by the end of each day into a plastic bag for further analysis. Likewise the coarse dust sampling from a cyclone, during each day of the test, several samples were also taken by a special sampling device from a sampling port positioned between the sliding gate and the container.

After the baghouse, the clean flue gas returns back into the boiler outlet duct through a baghouse fan. The fan is equipped with a short circuit with a gate-type slide valve (SG4, see Fig. 1.5) in order to adjust the flow regime of the filter system to that of the boiler outlet duct thus providing a stable flue gas flow rate through the whole by-pass circuit.

When the test is completed the SG1 / SG3 sliding gates (see Fig. 1.5) are closed and the SG2 sliding gate is opened. The baghouse fan blowing with air for half an hour cleans out the by-pass circuit.

For characterisation of the test parameters and collection of data several ports for positioning the probes and measuring tools are arranged as shown in the schematic diagrams (Fig. 1.5 and Fig. 3.1).

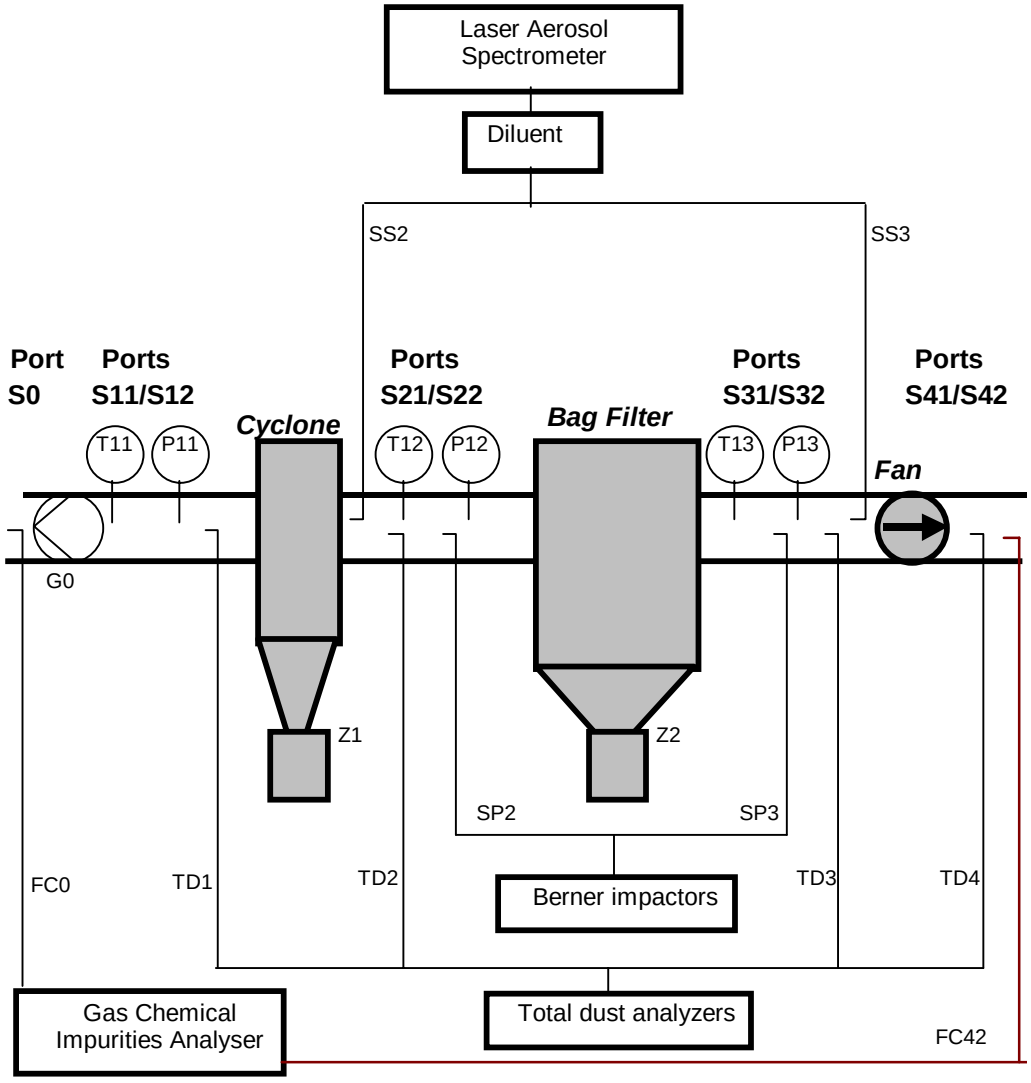

Figure 3.1 Functional scheme of sampling and measurements at the baghouse test facility.

Plan for the Baghouse Test

For detailed characterisation of the target mass flows the following measurements and samplings were provided by IPEP and RISØ, as listed in Tables 3.2 and 3.3 below.

Table 3.2 List of the objects / parameters sampled / measured by IPEP

Log No	Target object	Sampling procedure in situ	Parameters to be analysed	Measurement procedure ↻ - in situ; 💻 - in lab
TD1 TD2 TD4 AD1 AD2 AD4	Aerosols	From the S12/S21/S41 ports by iso-kinetic probes	Total Dust content before and after the cyclone, Total dust content after the baghouse, Activity of Dust samples	💻 Dust mass flow, Elemental analysis, Granulometry, Radiological measurements of different fractions
SS2 SS3	Aerosols	From the S22/S31 ports by iso-kinetic probe	Spectrum of particulate Size in micron and sub-micron diapason	↻ On-line laser spectrum analysis of aerosols fractions
FCB0 FC0 FC42	Flue gas	Performed by IPEP from the SB0/S0/S42 ports	Flue gas Chemistry (O_2, CO_2, CO, NO_X, SO_X) and moisture	↻ On-line direct analysis of different gases and chemical impurities
ED0 ED1 ED2 ED3	Radioactive exposure		Exposure Dose rate from different compartments of the facility	↻ Direct measurements of exposure dose rate by dosimeter

Table 3.3 List of the objects / parameters sampled / measured by RISØ

Log No	Target object	Sampling procedure in situ	Parameters to be fixed	Measurement procedure ↻ - in situ; 💻 - in lab
TD1 TD2 TD3 AD1 AD2 AD3	Aerosols	From the S11/S22/S32 sampling points by iso-kinetic probe	Total Dust content before and after the cyclone, Total dust content after the baghouse, Activity of Dust samples	↻ Dust mass flow 💻 Radiological measurements of fractions
SP1 SP2 SP3 AP1 AP2 AP3	Aerosols	From the S11/S22/S31 sampling points by Berner impactor	Size distribution of Particulate in sub-micron diapason, Activity of each Particulate fraction	↻ Mass fraction of particulate of different size 💻 Elemental analysis of different frac-tions, Radiological measurements of fractions, NAA analysis

The general physical parameters of flue gas (flow rate, pressure, pressure drop, and temperature) that characterise the conditions of test performance in different positions of test facility are presented in Annex A.

3.2 Laser Measurements

The aerosol laser spectrometry was carried out continuously of flue gas iso-kinetically sampled from two ports (S22 and S31). These measurements made it possible to evaluate the variations with time in the content of fine aerosols in flue gas. It was found that the aerosol concentration varied significantly even within relatively short time intervals. This ties in with the visual impression of the intensity of smoke escaping from the stack. The smoke generally changed with 5-10 minutes intervals between being very dark and thick and being transparent. Therefore, representative measurements/samplings were performed only in a few test intervals when dust load variations were comparatively small. These results are presented in Tables 3.4 and 3.5. More detailed results of the laser spectrometer measurements are given in Appendix B.

Based on the measurements before and after the filter, filter efficiencies have been calculated as a function of particle size. These figures are presented in the bottom of the Tables 3.4 and 3.5. No distinct variation with particle size could be observed. It should be noted that the concentrations above 0.4 µm are based on relatively few counted particles and there is thus a significant uncertainty associated with these figures.

Table 3.4 Particle number size distribution measured by consecutive aerosol laser spectrometry. Results are presented from two ports - before and after the baghouse filter. Data is from 17/6.

Time	0,2-0,25 µm	0,25-0,3 µm	0,3-0,4 µm	0,4-0,5 µm	0,5-0,7 µm	0,7-1,0 µm	1,0-2,0 µm	Comments
17.06.99, Port log. # S22, N_2 dilution ratio = 135; Volume of probe = 50 cm^3								
9:49	96660	34965	11475	7020	945	675	0	Gray smoke
9:51	108405	38340	12555	7965	405	405	270	
9:52	88560	31995	13905	8370	1215	675	270	
9:53	110160	33075	13230	11475	1080	540	0	
Avrg.	**100946**	**34594**	**12791**	**8708**	**911**	**574**	**135**	
17.06.99, Port log. # S31, N_2 dilution ratio = 4.5; Volume of probe = 50 cm^3								
10:12	6935	2421	743	369	41	59	36	Gray smoke
10:15	6597	1994	594	203	9	0	9	
10:16	6512	2034	657	324	14	27	9	
10:17	6804	2462	639	338	36	23	14	
Avrg.	**6712**	**2228**	**658**	**309**	**25**	**27**	**17**	
Filter eff.	**93,4%**	**93,6%**	**94,9%**	**96,5%**	**97,3%**	**95.3%**	**87.4%**	

Table 3.5 Particle number size distribution measured by consecutive aerosol laser spectrometry. Results are presented from two ports - before and after the baghouse filter. Data from is from 18/6.

Time	0,2-0,25 µm	0,25-0,3 µm	0,3-0,4 µm	0,4-0,5 µm	0,5-0,7 µm	0,7-1,0 µm	1,0-2,0 µm	Comments
18.06.99, Port log. # S31, N_2 dilution ratio = 4.5; Volume of probe = 50 cm^3								
12:53	927	68	23	5	5	5	0	Smoke is
12:54	635	36	9	9	0	0	0	almost
12:56	450	14	5	0	0	0	0	transparent
12:57	1040	131	18	14	5	0	0	
Avrg.	**763**	**62**	**14**	**7**	**3**	**1**	**0**	
18.06.99, Port log. # S22, N_2 dilution ratio = 9.0; Volume of probe = 50 cm^3								
13:02	144000	8235	1773	1404	369	414	99	Smoke is
13:04	179703	8136	1782	1836	594	441	117	almost
13:05	183483	8307	2079	1953	387	279	36	transparent
13:06	241857	9252	2223	2250	423	432	135	
Avrg.	**187261**	**8483**	**1964**	**1861**	**443**	**392**	**97**	
Filter efficiency	**99,6%**	**99,3%**	**99,3%**	**99,6%**	**99,3%**	**99,7%**	**100%**	

3.3 Total Dust Measurements by Risø

Measuring Equipment

Risoe has assembled a portable system for total dust measurements according to the German standard VDI 2066 part 7. Figure 3.2 below shows the complete system for the sampling excluding the measuring head, which is shown in Figure 3.3. From the inlet the system features a cooling spiral, a water separator, a drying column, a pump with a bypass valve for flow control, a flow meter, a gas meter and a thermometer mounted with the gas meter for correction to normal cubic metres sampled. The measuring head for 'in-pipe' sampling uses 5-cm Ø quartz fibre filter paper for filtration. The nozzle is exchangeable with inlet diameters from 6 mm to 20 mm. This enables a coarse regulation of the inlet flow. The fine-tuning, ensuring iso-kinetic sampling is done by regulation of the bypass valve at the suction pump.

This system had prior to the test in Belarus been tested at Danish power plants, with good results both concerning durability and quality of results. That is, two systems are available for simultaneous sampling at two locations, e.g. before and after a filter.

Figure 3.2 Complete mount for total dust measurements. On the left the cooling circuit with a water separator underneath. In the centre a drying column.

Figure 3.3 Measuring head/filter holder for total dust measurements. The filter holder uses 5 cm Ø quartz fibre filters. The sampling aperture can be adjusted by exchanging the front end of the filter house

Results of the Dust Measurements

In total 29 total dust measurements were made. The details of the measurements are listed in Table 3.7 together with the results of the mass and ^{137}Cs activity analysis. Measuring locations:

- S1 Before the cyclone
- S2 After the cyclone before the baghouse
- S3 After the baghouse

Hereafter, the suffixes 'L' or 'R' indicate that samples were taken from the left or right port. 'LR' means that traversing was performed in both ports.

All TD mass concentration results are stated for dry air at 20 ^{o}C, but they are not corrected for oxygen content.

The first measurement on Monday 14/6 was an initial test. There were no measurements on Tuesday the 15/6.

Due to the very unstable flue gas conditions traversing was stopped on 18/6 and thus only one sampling port is listed as a position for sampling carried out on this day. This simplification enabled us to increase the number of measurements done this day. In general, larger variation in TD was observed

making it very difficult to compare consecutive measurements and undermining any positive benefit of traversing.

In general there were big variations in both mass and activity concentrations. This was also observed in the data on particulate concentration obtained with laser spectrometry. The mass concentration varied on a small time scale - an order of magnitude in 10 minutes. The variations in the activity concentration were smaller, but it is unfortunate that the highest activities were achieved early during the test period where fewer measurements were made.

Table 3.6 Review of the Total Dust measurements made by Risø. All mass and activity concentrations are given for a temperature of 20 ^{o}C and dry air.

			Duration	Mass	Volume	Mass /volume	Activity		Activity /mass	Activity /volume
ID	Position	Start time	[minutes]	[mg]	[m^3]	[mg/m^3]	[Bq]	``+/-	[Bq/g]	[Bq/m^3]
TD01	S2-L	14.06-17:30	5	33.53	0.085	396	0.20	0.013	6	2.39
TD02	S2-L	16.06-10:17	4	46.34	0.097	480	0.29	0.013	6	2.99
TD03	S1-LR	16.06-12:12	8	48.84	0.061	795	0.53	0.024	11	8.71
TD04	S2-LR	16.06-12:13	8	56.33	0.104	538	0.72	0.029	13	6.83
TD05	S3-LR	16.06-14:36	240	2.60	1.966	1.3	0.066	0.009	25	0.033
TD07	S2-L	16.06-15:09	8	7.16	0.131	54.5	0.26	0.017	36	1.95
TD08	S2-R	16.06-16:49	16	7.88	0.278	28.3	0.38	0.021	48	1.36
TD09	S1-LR	17.06-09:59	4	21.97	0.067	327	0.18	0.010	8	2.67
TD10	S3-LR	17.06-08:37	240	1.67	3.410	0.49	0.029	0.008	17	0.01
TD11	S2-LR	17.06-10:03	8	3.62	0.185	19.6	0.12	0.014	32	0.63
TD12	S2-LR	17.06-12:01	4	13.68	0.065	211	0.10	0.014	7	1.55
TD13	S2-LR	17.06-15:14	8	4.48	0.151	29.7	0.24	0.019	55	1.62
TD14	S3-LR	17.06-14:13	180	2.53	2.922	0.87	0.061	0.009	24	0.021
TD15	S1-LR	17.06-16:29	8	17.02	0.133	128	0.20	0.014	12	1.53
TD16	S2-LR	17.06-17:30	4	29.37	0.096	308	0.25	0.014	8	2.58
TD17	S1-L	18.06-09:05	4	2.79	0.067	42	0.099	0.0098	35	1.47
TD18	S2-L	18.06-09:05	4	2.70	0.064	42	0.120	0.012	44	1.89
TD19	S2-L	18.06-11:35	8	9.69	0.132	74	0.20	0.016	20	1.48
TD20	S1-L	18.06-09:40	4	7.06	0.067	106	0.083	0.014	12	1.24
TD21	S1-L	18.06-10:05	5	19.60	0.064	304	0.12	0.016	6	1.93
TD22	S1-L	18.06-10:23	20	57.62	0.364	158	0.44	0.04	8	1.19
TD23	S1-L	18.06-11:35	8	8.14	0.130	63	0.157	0.0194	19	1.21
TD24	S2-L	18.06-15:22	12	17.67	0.174	102	0.26	0.0189	15	1.49
TD26	S3-L	18.06-14:36	120	0.32	1.802	0.18	0.017	0.0051	51	0.01
TD27	S2	18.06-14:46	12	16.81	0.1835	91.6	0.269	0.0166	16	1.47
TD28	S2-L	18.06-15:45	12	6.47	0.1958	33.0	0.321	0.0181	50	1.64
TD29	S2-L	18.06-16:14	12	7.32	0.1954	37.5	0.42	0.0224	57	2.15

When TD measurements made at the same time before and after the cyclone (TD17 *vs*. TD18, and TD19 *vs*. TD23) are compared an increase in mass load is observed. This is of course peculiar. However, the increase is not significant. But it repeats itself for the activity measurements that show a 15 to 29 % increase after the cyclone. This is an increase of three standard deviations on the activity measurements. Another set of measurements shows a reduction of 32% (TD03 *vs*. TD04). This is in better agreement with the amount of ashes collected at the cyclone and below the baghouse filters. Here the reduction is similar for the ^{137}Cs activity measurements as well.

By comparing the samples made at positions S1 and S2 with the samples from S3 some estimates can be made of the filter efficiency. These calculations are presented in Table 3.7. Please note that Ratio2 and Ratio3 are based on measurements both before and after the cyclone, whereas Ratio1 and Ratio4 give the 'pure' filter efficiency. It can be seen that Ratio1 gives a comparatively low filter efficiency. The explanation could simply be that the two samples taken before the filter are not representative for the input as they only cover 10 % of the sampling time after the filter. In addition, both the TD07 and TD08 measurements were performed within the time interval of very unstable combustion

conditions in the furnace. In general, the filter efficiency calculation gave a stable result both when based on mass and activity measurements.

Table 3.7 Calculations of filter efficiency for four sets of filter samples. The second and third columns show the ID of the after filter sample and the pre-filter samples, respectively. The fourth column shows the total sample collection time before and after the filter in minutes.

ID	After filter sample	Before filter Samples	Fraction covered	Filter efficiency, %	
				Mass	Activity
Ratio1	TD05	TD07, TD08; both from S2	24/240	96.4	97.9
Ratio2	TD10	TD09 (from S1), TD11, TD12; both S2	16/240	99.7	99.5
Ratio3	TD14	TD13 (S2), TD15(S1), TD16(S2)	20/180	99.4	99.6
Ratio4	TD26	TD24, TD27, TD28, TD29; all S2	48/120	99.7	99.4

As it was realised already during the tests that the dust concentrations were very variable, longer sample times before the filter were applied on the last day of the tests. Ratio4 probably gives the best estimate of the filter efficiency as the sampling before the filter covers 40 % of the after filter sampling time. The dust levels before and after the filter are illustrated in Figure 3.5. Between the TD measurements before the filter a number of impactor measurements were made. These are included in a new figure in the section dealing with the impactor measurements.

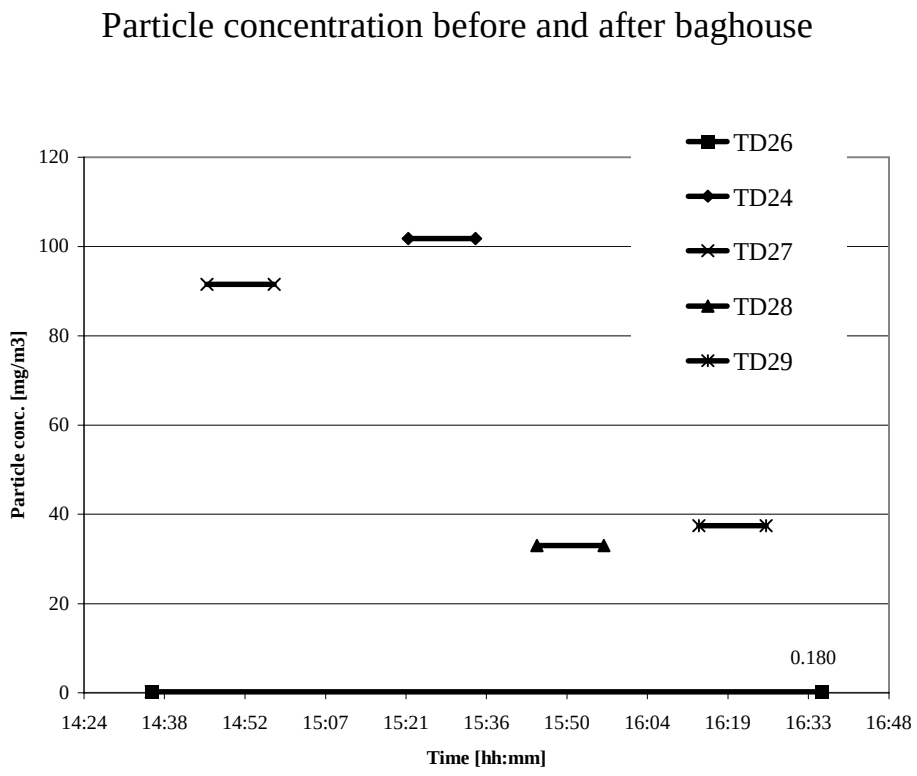

Figure 3.4 Four TD measurements before the baghouse are shown together with one TD measurement after the baghouse (TD26).

3.4 Dust Measurements by IPEP

The total dust content was determined by the exterior filtration method. A certain volume of flue gas was iso-kinetically taken from the identified ports (S12, S21 and S41) and pumped through the cascade impactors where the aerosols were entrapped. The filters were weighed, and the results are presented in Table 3.9.

Table 3.9. Total dust content in flue gas

ID	Date	Time	Sampling duration Minutes	Volume Nm^3	Mass Collected g	Dust Content g/m^3	Smoke
TD1	17.06.99	9:15	2	0,036	0,1010	2,8	Thick black smoke
TD2	17.06.99	9:15	5	0,038	0,0431	1,13	Thick black smoke
TD4	17.06.99	12:28	332	43,68	0,2289	0,005	
TD1	17.06.99	14:50	8	0,17	0,0257	0,15	Almost transparent
TD2	17.06.99	15:04	13	0,17	0,007	0,04	Almost transparent
TD1	17.06.99	16:10	10	0,21	0,0274	0,13	Almost transparent
TD4	18.06.99	10:00	405	65,6	0,0871	0,0013	
TD1	18.06.99	10:25	4	0,09	0,0363	0,41	Dark gray smoke
TD2	18.06.99	10:47	5	0,042	0,0140	0,33	Dark gray smoke
TD1	18.06.99	14:41	19	0,35	0,0171	0,05	Light gray smoke
TD2	18.06.99	16:05	25	0,39	0,0081	0,021	Light gray smoke

These results are subject to the same problems as described above. It was impossible to run the boiler steadily enough to be in agreement with quality of data anticipated and the high precision instrumentation used. The boiler personnel tried to stoke the fire-box steadily, but the main reason is that the boiler has a fixed grate. The heap of chips in furnace did not move along the grate, but was growing until it subsided down from time to time. Nevertheless, the average picture can be obtained from the above results. In Table 3.10, the efficiency of different elements of the test capture system is presented as calculated on the basis of the above data.

Table 3.10. Average efficiency of capture system. These efficiencies are comparable to those achieved by ESP filters (Electro Static Precipitators), but at least one order of magnitude lower than those achieved by common bag house filter installations.

Date	Average dust content			Capture efficiency, %		
	Before cyclone $mg\ m^{-3}$	Before baghouse $mg\ m^{-3}$	After baghouse $mg\ m^{-3}$	Cyclone %	Bag house %	Total system %
17.06.99	1.03	0.585	0.005	43	99.1	99.5
18.06.99	0.23	0.18	0.0013	22	99.3	99.4
Average	0.708	0.38	0.00315	46	99.2	99.6

3.5 Impactor Measurements

Equipment

For the impactor measurements two identical Berner low-pressure impactors (BLPI) from Hauke GmbH were used. These have 10 stages and cut-off diameters from 30 nm up to 16 μm. They were calibrated by Hillamo and Kaupinen, 1991. As the pipe diameters at the filter test plant are relatively narrow, 200 mm, compared to the impactor dimension, 110 mm diameter, a gas stream was iso-kinetically extracted. The dimension of the measuring head was determined after measurement of the flow rate on the first day of the test. To avoid condensation of vapour in the impactors they were pre-

heated and placed in insulation material before they were mounted in the set-up. Figure 3.5 shows a diagram illustrating the mounting of the impactor. The 4" fitting was screwed into the thread in the sampling port. The insulated impactor could be moved back and forth through the fitting enabling traversing.

A set-up with a pre-filtration system was prepared for sampling before the cyclone in case of an overload with big particles. However, the first measurements showed that the fine mode aerosol below one micrometer dominated the particle size distribution. Therefore it was not necessary to have the pre-filtration cyclone installed in the sampling line before the impactor.

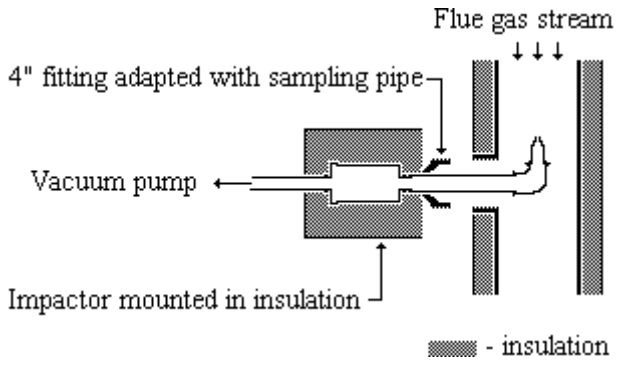

Figure 3.5 Principle diagram of the impactor mounting on the side of the main bag house duct.

The impactor results have been corrected to dry air at 0 ^{o}C . Also the impactor flow rate was corrected, according to the paper by Valmari et al. (1998). The mass flow rate declines with the square root of the relative temperature increase when doing in-stack measurements.

A total of 22 impactor measurements were made. 21 of these gave useful results. All impactor samples have been weighed and all the mass size distributions can be seen in Appendix A. A total of 5 impactor ^{137}Cs size distributions have been measured.

Table 3.11 Review of impactor measurements. 'ID' is the sample batch identification. 'Pos.' is the measurement position code. 'Imp' is the identity of the impactor used. 'Qual' is a subjective judgement of the quality of the sample. Three types of collector surface were used: 'Alu-g' is an aluminium foil coated with vacuum grease, 'Alu-ng' is the same without grease and the third was a teflon foil. All concentrations are given for dry air at 0 ^oC.

ID	Pos.	Imp.	Collector surface	Foil numbers	Start time	Duration [minutes]	Volume [m^3]	Total collected [mg]	[mg/m^3]
IMP-1	S1	25-43	Alu-g	402-411	16.06-15:05	8	0.206		
IMP-2	S2L	25-22	Alu-g	442-451	16.06-18:05	8	1.549	41.41	26.7
IMP-3	S3	25-43	Alu-ng	412-421	16:06-14:32	240	6.168	11.08	1.80
IMP-4	S3	25-43	Alu-ng	352-361	17.06-08:45	240	6.168	6.03	0.98
IMP-5	S1	25-22	Alu-g	422-431	17.06-09:00	2	0.051	22.56	3.66
IMP-6	S2	25-22	Alu-g	392-401	17.06-10:06	4	0.102	13.46	132.5
IMP-7	S2	25-22	Teflon	242-251	17.06-12:16	1.33	0.034	2.12	62.5
IMP-8	S3	25-22	Alu-g	452-461	17.06-14:45	180	4.572	3.92	0.86
IMP-9	S2	25-43	Alu-g	462-471	17.06-15:33	1.33	0.034	1.17	34.3
IMP-10	S1	25-43	Teflon	252-261	17.06-16:30	1.33	0.034	1.66	48.5
IMP-11	S2	25-22	Alu-ng	362-371	17.06-18:20	1	0.025	0.47	18.7
IMP-12	S1L	25-22	Alu-g	472-481	18.06-09:29	1	0.025	4.19	165.0
IMP-13	S2L	25-43	Alu-g	432-441	18.06-09:29	1	0.026	3.64	141.4
IMP-14	S1L	25-22	Teflon	272-281	18.06-11:05	1	0.025	6.62	260.8
IMP-15	S2	25-43	Teflon	262-271	18.06-11:05	1	0.026	6.11	237.7
IMP-16	S2	25-43	Teflon	282-291	18.06-14:00	0.75	0.019	9.37	485.9
IMP-17	S2	25-22	Alu-ng	342-351	18.06-14:00	0.75	0.019	11.43	600.0
IMP-18	S3T	25-22	Teflon	292-301	18.06-14:36	120	3.048	1.95	0.64
IMP-19	S2L	25-43	Alu-ng	372-381	18.06-15:05	1	0.026	7.60	295.5
IMP-20	S2L	25-43	Teflon	302-311	18.06-16:02	0.5	0.013	0.76	0.25
IMP-21	S2L	25-43	Alu-ng	382-391	18.06-17:36	1	0.026	0.80	30.9
IMP-22	S2L	25-22	Alu-g	482-491	18.06-17:36	1	0.025	0.73	28.7

Figure 3.6 shows the effect of the cyclone by comparing IMP-12 and IMP-13. The impactor only samples relatively small particles, with its top size being approximately 16 micron. Particles of this size or smaller are inefficiently collected in the cyclone, as indicated by the relatively small change in the mass loading illustrated in the figure. However, the total dust did not show any significant reduction in the level before and after the cyclone.

Another example of the particle size distribution after the filter is given in Figure 3.7. These data were collected on the same day and should be nominal duplications of the after cyclone data illustrated in Figure 3.6. As is evident, the distributions differ substantially in both shape and magnitude. These differences are likely to be associated with shifts from sooting to non-sooting conditions in the furnace. The bulk of the sample illustrated in Figure 3.8 may be soot rather than fly ash.

In Figure 3.8 a size distribution measured after the filter is shown. It is a relatively flat distribution, but with an indicated maximum at about 0.2 microns. The concentration is about two orders of magnitude below the pre-filter data indicating capture efficiencies of approximately 99% at all sizes in the bag house filter. Such capture efficiencies are high in absolute terms, but are low compared to what is expected from filters of this quality. Elemental analyses of these samples, that have yet to be completed, will allow us to more precisely determine the fractions of soot in the sample.

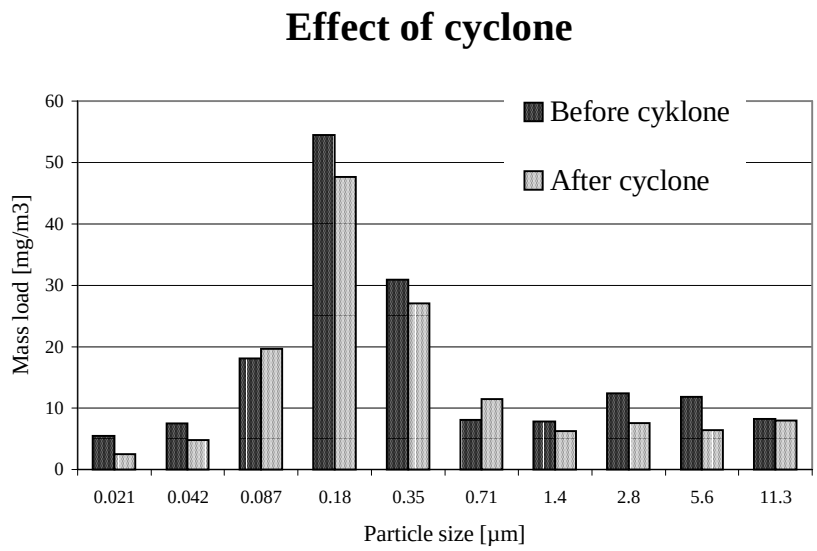

Figure 3.6 Particle size distribution measured 18/6 before and after the cyclone. Results are from impactor measurements IMP-12 and IMP-13.

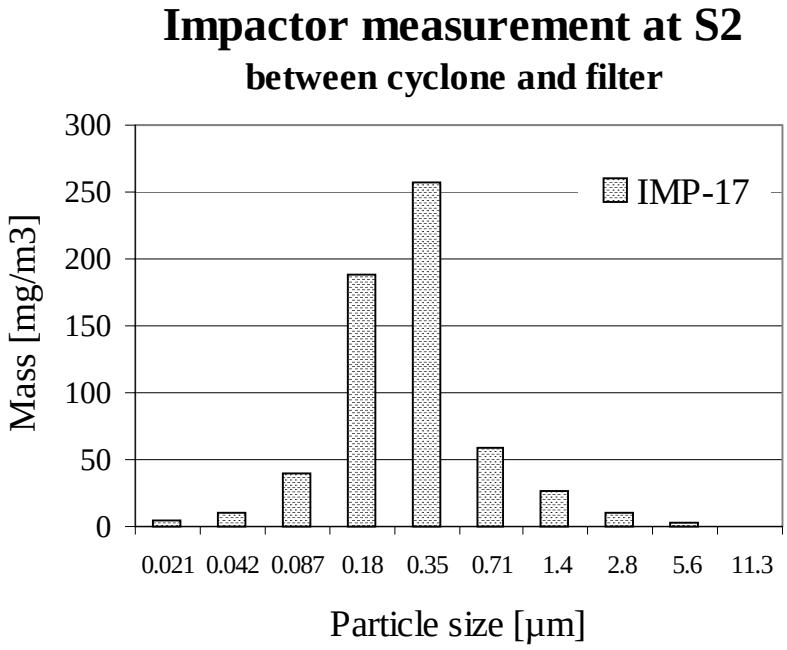

Figure 3.7 Impactor measurement IMP-17 taken at S2 18/6 1999.

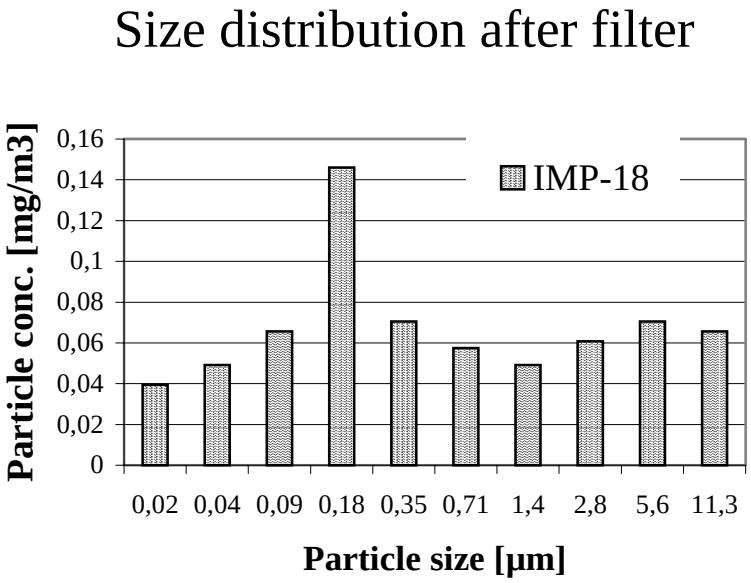

Figure 3.8 Particle size distribution after the filter.

Cs-137 Measurements for Impactor Samples

A number of impactor samples were selected for activity measurements. A 65 % Germanium detector was used for the measurements. In order to have sufficient material for the analysis only series were more than 3 mg was deposition in total on the 10 collectors was analysed. preferably 10 mg. The activity size distributions are all shown in Appendix C. A discussion of the activity measurements is given in Chapter 4.

Table 3.8 Review of Cs-137 measurements on impactor samples.

Measure-ment	Measure-ment	**Sub micron**			**Supra micron**		
		Mass	Activity	Specific activity	Mass	Activity	Specific act.
ID	Position	[mg]	[Bq]	[Bq/g]	[mg]	[Bq]	[Bq/g]
IMP 3	S3	4.1	0.123	30	7.0	0.045	6
IMP 4	S3	3.9	0.0656	17	2.2	0.034	16
IMP 5	S1	20.8	0.179	9	1.7	0.034	20
IMP 6	S2	6.7	0.2791	42	6.8	0.150	22
IMP 12	S1	3.2	0.085	27	1.0	0.023	23
IMP 13	S2	2.9	0.058	20	0.7	0.023	31
IMP 17	S2	10.7	0.012	1		BDL*	

*BDL - Below Detection Limit

In Figure 3.9 an activity size distribution is shown together with a mass size distribution. The activity has a distinct maximum for the fine mode aerosol whereas the mass distribution is bimodal by nature. This pattern can arise from nucleation and aerosol formation of the radionuclides themselves, condensation of radionuclides on small particles, or generation of fine radionuclide particles during combustion. Elemental analyses of the samples should allow these various mechanisms to be distinguished.

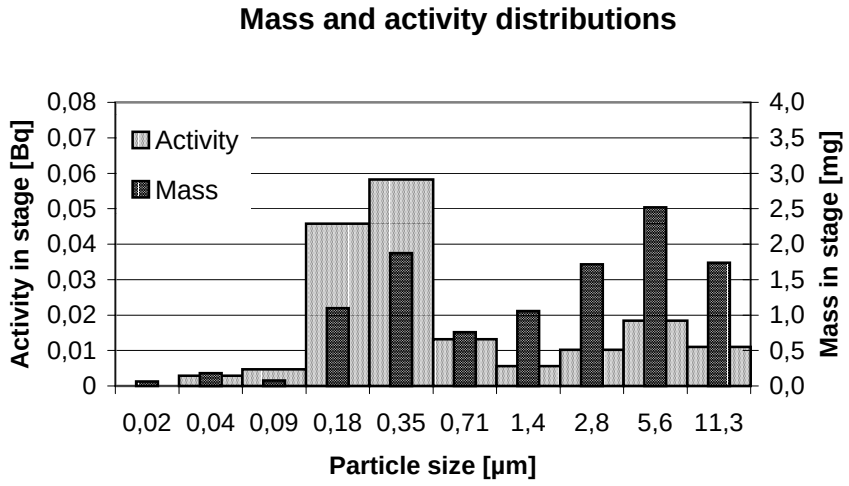

Figure 3.9 Mass and activity (IMP4)

3.6 Discussion of Dust Measurements

Comparison between the various data is difficult due to the large time variations in the aerosol load. In general IPEP achieved higher values, but the relationship they found between before and after the filter was in good agreement with Risø measurements. Risø impactor measurements and total dust measurements was also in good agreement.

In order to make a more systematic comparison and evaluation of the results a number of data sets have been selected for the stable periods during each of the three days of the actual test.

Data Selection

The measurements of dust content were carried out with different methods in the four main sampling points of the test facility (boiler outlet, before cyclone, before baghouse, after baghouse) by all three groups of researchers (IPEP, RISØ, and Elsamprojekt). The review of data is given in the charts below (Figure 3.10, Figure 3.11 and Figure 3.12. In these charts, the data on oxygen variations are also shown. The black bars show the dust content at the boiler outlet and before the cyclone. The red and green (blue) ones indicate the data on dust content before and after the filter correspondingly. Prefix "IMP" denotes the data obtained by impactor measurements.

The time intervals of unstable regimes are marked in abscissa (time argument) by the black segments. As can be seen, a part of the results does not fit into the time intervals of stable regimes, and these results are not analysed further.

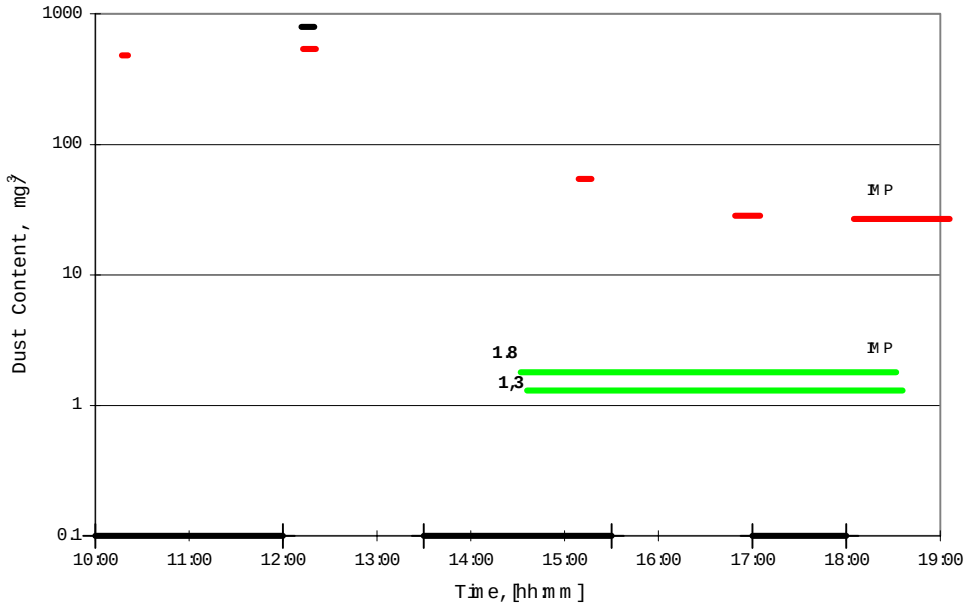

Figure 3.10 Results of total dust measurements by RISØ, 16.06.99.

Not many measurements were performed on the 16th of June, the first day of actual test. It follows from Figure 3.10 that only one set of data can be chosen, taking into account also the fact that the error for the impactor measurements may be high due to the rather long duration of measurements after the filter, half of which are associated with unstable regimes. The chosen series of 16/06/99 is shown in Table 3.9.

Table 3.9 Data selected from 16/06/99.

Series ID	Date	Time interval	Sampling point	Sample ID
TD-C/1-16**	16.06 99	12:12 – 12:20	Before cyclone, S11	TD03
	16.06.99	12:13 – 12:21	After cyclone, S22	TD04

** - RISØ

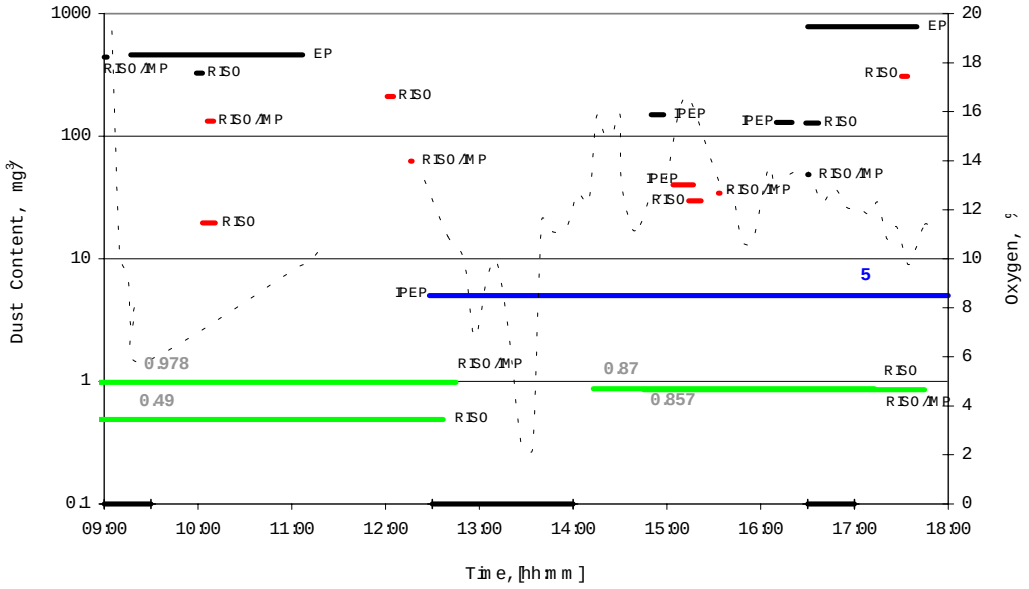

Figure 3.11 Results of dust measurements by IPEP, Elsamprojekt, RISØ 17.06.99. Dot line shows oxygen concentration.

The Figure 3.11 draws the attention to a large difference between the data on dust concentration before cyclone obtained by Elsamprojekt at the point SB1 (the boiler duct) and those obtained by other groups at the point S11 (the test facility inlet duct). The lower content detected at the point S11 indicates an extent of non-isokinetic extraction of flue gas from the boiler duct to the capture system, as it was also assumed from analysis in section 2.3.

There is a large difference between the results obtained by IPEP and RISØ after the baghouse filter. There may be two likely explanations for this. First of all, in the IPEP measurements, a significant fraction of the measurement time was during unstable conditions. Secondly, since IPEP's sampling point (S41) was located far downstream from RISØ's point (S31/S32), the influence of duct non-compactness could be sufficiently high to detect some extraneous fine dust from the surface air around the facility. In any case, IPEP's results after the filter should not be considered.

The data on dust concentration for sample TD11 before the filter are set too low compared, e.g., to the data of IMP-6 obtained at the same time from the neighbouring port. Here we almost certainly have a fatal experimental error (i.e. accidental loss of mass). Therefore, the series listed in *Table 3.10* was chosen for the further evaluation:

Table 3.10 Data selected from 1706/99.

Series ID	Date	Time interval	Sampling point	Sample ID
IMP-F/4-17**	17.06 99	10:06 – 10:10	Before filter, S22	IMP-6
	17.06.99	8:45 – 12:45	After filter, S31	IMP-4
TD-F/5-17**	17.06 99	12:01 – 12:05	Before filter, S22	TD12
	17.06.99	8:37 – 12:37	After filter, S32	TD10
IMP-F/6-17**	17.06 99	12:16 – 12:18	Before filter, S22	IMP-7
	17.06.99	8:45 – 12:45	After filter, S31	IMP-4
TD-C/2-17*	17.06 99	14:50 – 14:58	Before cyclone, S12	
	17.06.99	15:04 – 15:17	After cyclone, S21	
TD-F/7-17**	17.06 99	15:14 – 15:22	Before filter, S22	TD13
	17.06.99	14:13 – 17:13	After filter, S32	TD14
IMP-F/8-17**	17.06 99	15:33 – 15:35	Before filter, S22	IMP-9
	17.06.99	14:45 – 17:45	After filter, S31	IMP-8
TD-F/9-17**	17.06 99	17:30 – 17:34	Before filter, S22	TD16
	17.06.99	14:13 – 17:13	After filter, S32	TD14

* - IPEP

** - RISØ

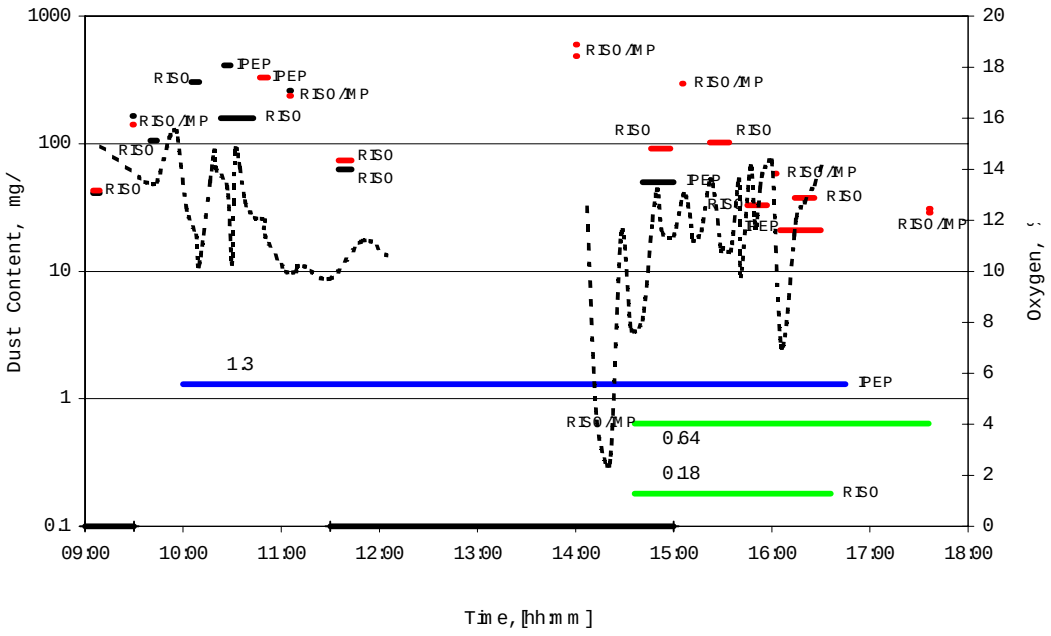

Figure 3.12 Results of dust measurements by IPEP and RISØ, 18.06.99. Dot line shows oxygen concentration

On 18.06.99 (Figure 3.12), there were longer periods of stable operation of the furnace compared to the previous dates. The results are in better agreement. Nevertheless, the comment related to IPEP's measurements in the point S41 should be the same as that given above. The second discrepancy, which is difficult to explain, is the negative difference between the dust content detected by Risø before and after the cyclone between 11:35 and 11:43.

Based on analysis, the data listed in Table 3.12 were selected to further evaluate the filter efficiency.

Table 3.11 Data selected from 18/06/99

Series ID	Date	Time interval	Sampling point	Sample ID
IMP-C/1-18**	18.06 99	9:29 – 9:30	Before cyclone, S11	IMP-12
	18.06 99	9:29 – 9:30	After cyclone, S22	IMP-13
TD-C/2-18*	18.06 99	10:25 – 10:29	Before cyclone, S12	
	18.06 99	10:47 – 10:52	After cyclone, S21	
IMP-C/3-18**	18.06 99	11:05 – 11:06	Before cyclone, S11	IMP-14
	18.06 99	11:05 – 11:06	After cyclone, S22	IMP-15
IMP-F/2-18**	18.06 99	15:05 – 15:06	Before filter, S22	IMP-19
	18.06 99	14:36 – 17:36	After filter, S31	IMP-18
TD-F/3-18**	18.06 99	15:22 – 15:34	Before filter, S22	TD24
	18.06 99	14:36 – 16:36	After filter, S32	TD26
TD-F/4-18**	18.06 99	15:45 – 15:57	Before filter, S22	TD28
	18.06 99	14:36 – 16:36	After filter, S32	TD26
TD-F/5-18**	18.06 99	16:14 – 16:26	Before filter, S22	TD29
	18.06 99	14:36 – 16:36	After filter, S32	TD26
IMP-F/6-18**	18.06 99	16:02 – 16:03	Before filter, S22	IMP-20
	18.06 99	14:36 – 17:36	After filter, S31	IMP-18
IMP-F/7-18**	18.06 99	17:36 – 17:37	Before filter, S22	IMP-21
	18.06 99	14:36 – 17:36	After filter, S31	IMP-18
IMP-F/8-18**	18.06 99	17:36 – 17:37	Before filter, S22	IMP-22
	18.06 99	14:36 – 17:36	After filter, S31	IMP-18

* - IPEP

** - RISØ

An interesting pattern is observed when analysing the dust concentration after the baghouse (Figure 3.13). The filter efficiency was improving during the test as the filter material was covered with dust.

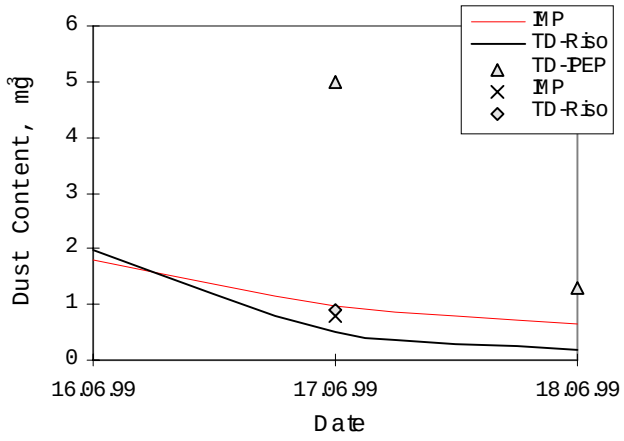

Figure 3.13 Concentration of dust in air after the baghouse plotted as function of time. Total dust (TD) and impactor (IMP) measurements made by different teams.

Cyclone Capture Efficiency from Dust Concentration Data

The cyclone capture efficiency, as calculated on a basis of selected series, is presented in Figure 3.14. The deviation is large due to non-coincident intervals of time of measurements in some series (e.g.,

TD-C/2-17). Overall the cyclone efficiency was low. This is also confirmed by the amount of ash collected in the cyclone and baghouse catches. The former contained much less mass of ash compared to the baghouse container. The reason for this is that the flue gas mainly consisted of relatively small particles with diameters below the cyclone capture efficiency curve.

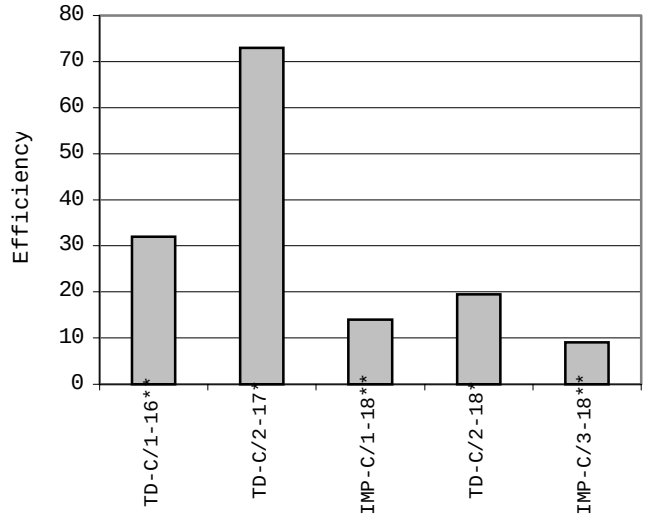

Figure 3.14 Efficiency of Cyclone (in %) based on five data sets from stable periods of operation.

Baghouse Capture Efficiency from Dust Concentration Data

In Figure 3.15, the calculated filter capture efficiencies are shown, as calculated on the basis of the series chosen. As expected, the results of impactor measurements correspond to a lower efficiency than total filter measurements. The impactor does not reflect the total picture of dust content in the flow before baghouse. After the baghouse, both methods gave practically identical results.

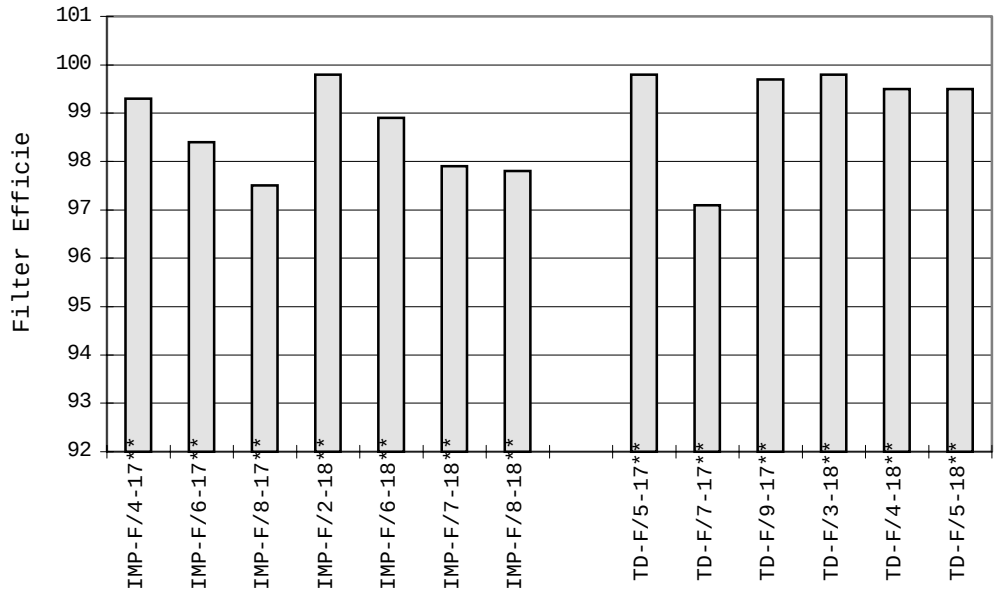

Figure 3.15 Efficiency of Baghouse Filter based on thirteen selected data sets from periods of stable operation.

Based on the selected data, the average values listed in Table 3.12 for the baghouse filter efficiency were obtained.

Table 3.12 Summary of filter efficiency measurements

Method	Average efficiency, %	Min/Max, %
Total dust measurements	99.2	97.1 / 99.8
Impactor measurements	98.5	97.5 / 99.8
Laser spectrometry	91.7	83.6 / 99.6

Filter Efficiency as a Function of Particle Size

In Figure 3.16 and Figure 3.17 the baghouse filter efficiency for different aerosol fractions is presented. Like the aerosol laser spectrometry data (see section 3.2), these results do not disclose the dependence of filter efficiency on aerosol fractions, at least within the investigated range of particle size.

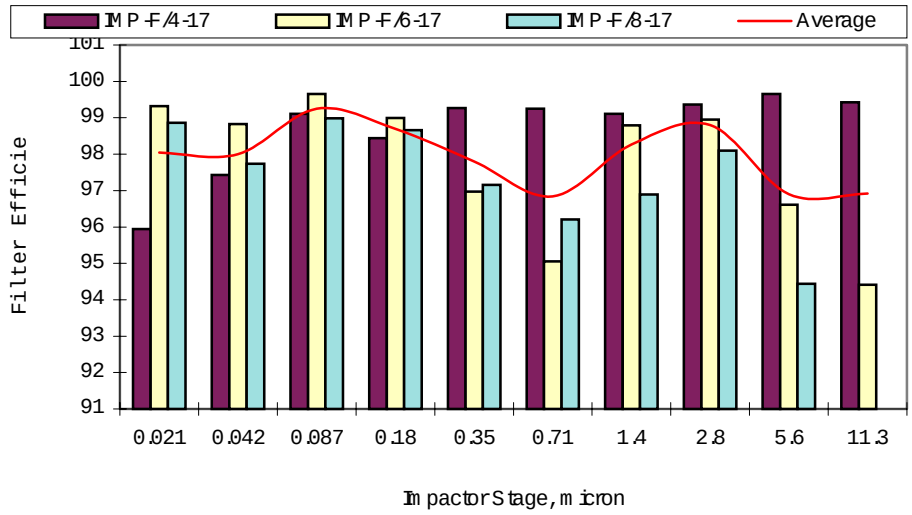

Figure 3.16 Filter efficiency according to different impactor stages, 17.06.99.

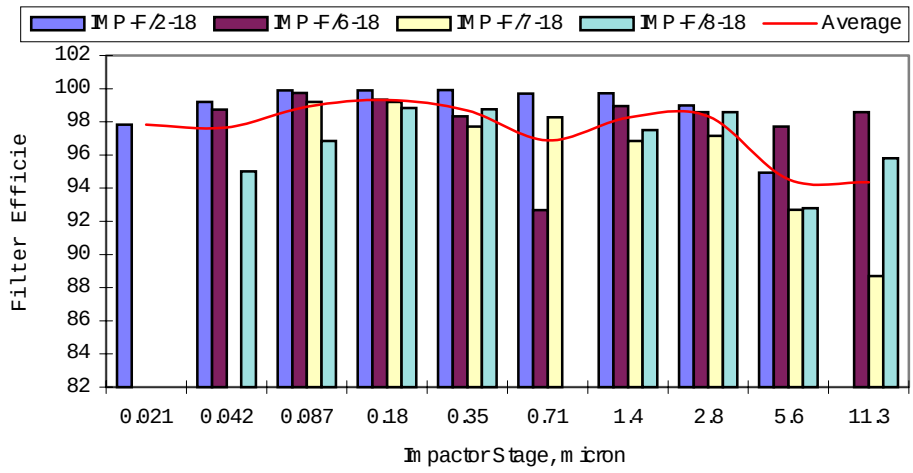

Figure 3.17 Filter Efficiency According to Different Impactor Stages (18.06.99)

4 Activity Measurements

4.1 Fuel, Ash and Slag Analysis

During the test, several samples of fly ash and bottom ash were taken from the designated ports and placed in plastic flasks. In addition, the ashes collected in the containers under the cyclone and filters (Z1, Z2) were manually poured into plastic bags by the end of each day.

The samples of slag and bottom ash were taken from the furnace chamber after the entire test burn had been carried out and combustion in furnace had been extinguished. All samples were transported to IPEP for further analysis and distribution among other participants. The time of sampling and volume of samples are summarised in Table 4.1.

The samples of wood fuel were collected manually from the feed conveyer right before entering the feed hopper of the combustor chamber. A description of these samples is given in Table 4.2.

Table 4.1 Description of ash samples

Time of sampling	**Port Z1**		**Port Z2(1)**		**Port Z2(2)**		**Port Z0, slag and bottom ash**
	Volume, cm^3	Mass, g	Volume, cm^3	Mass, g	Volume, cm^3	Mass, g	
15.06.99							
19:00-20:00	12						
16.06.99							
15:10-16:10	7		13		10		
9:30-19:00		≈200		≈200		≈200	
17.06.99							
9:45-11:00			13			0,39	
11:15-12:15		0,34		0,28	-	-	
12:30-13:30	-	-	1,5	0,16		0,13	
14:00-15:00	-	-	4		-	-	
15:20-16:20	4		8			0,026	
16:30-17:30	-	-	-	-	-	-	
17:45-18:45	5		7,5		-	-	
8:30-19:00		≈500		≈1000		≈1000	
18.06.99							
8:50-9:50		0,086		0,18		0,02	
10:10-11:10	1	0,44	1	0,13		0,015	
11:20-12:20		0,14	-	-	-	-	
12:35-13:35		0,46	3	0,22	-	-	
14:00-15:00		0,06	20		-	-	
15:10-16:10	-	-	1	0,12	-	-	
16:20-17:20	5		15		22		
8:15-17:20		100		500		500	
20.06.99							
10:00							80 litres
18.06.99							
10:00-16:45			Moisture condensate from flue gas from the **S41 port**, total volume = 0.4 litre				

Table 4.2 Description of fuel samples

Time of sampling	*Log. # of sample: W1*		
	Type of fuel	Approximate weight, kg	Moisture content [%]
16.06.99			
15:30	Sawdust and shavings	1	35.7
17.06.99			
9:35	Sawdust, shavings and chips	2	37.3
10:35	Sawdust, shavings and chips	2	40.6
11:35	Sawdust, shavings and chips	3	37.8
12:35	Sawdust, shavings and chips	2	35.5
13:35	Sawdust, shavings and chips	2	55.6
14:35	Chips	3	48.7
15:35	Chips	3	47.1
16:35	Chips	2	40.2
17:35	Chips	3	31.2
18:35	Chips	3	34.7
18.06.99			
8:40	Shavings and chips	2.5	55.6
9:40	Shavings and chips	3	32.2
10:40	Shavings and chips	3	45.8
15:40	Shavings and chips	2	42.0
16:40	Shavings and chips	3	42.6

The probe preparation and following radiological measurements for biomass samples were provided in accordance with the guidance "Determination of Content and Forms of Artificial Radionuclides in Environmental Objects", Up-to-Date Methods of Separation and Determination of Radioactive Elements, Moscow, 1989. Total ^{137}Cs content in wood fuel samples after drying at 105°C and coarse grinding (until approx. 1 mm x 1 mm) was determined in a three-dimensional geometry by the gamma-gay spectrometry. The samples had a volume of approx. 103.7 cm^3.

The ^{137}Cs specific activity of ashes was measured by the gamma-spectrometer in three-dimensional geometry. The samples subjected to radiological analysis had a volume of approx. 13.7 cm^3.

The small content of ^{137}Cs in the total dust samples was measured using a low-background spectrometer with Ge(Li) detector system and a guard annulus NaI(Tl) detector to provide gamma-ray spectrometry of the small samples with low activity level. The method is based on the anti-coincidence mode that gives the sensitivity of 0.1 Bq/probe in case of two-dimensional geometry, the counting time being 7,200 seconds or less. The detector was calibrated with different container dimensions and sample densities. The detecting time varied from 2-3 hours to 30-50 hours depending on the mass of the sample. All equipment has been verified (certificate No. BY/112.02.2.0.0464, of 18.05.98). The results are shown in Appendix D.

As can be seen by comparing the results in Appendix D with Table 4.3, the results of the ash and slag contamination analyses performed at IPEP are in good agreement with corresponding results from analyses performed at Risø. The results is discussed further in the next section and summarised in Table 4.4.

The Risø results were obtained from measurement of 200 cm^3 samples in Risø standard geometry on a high purity Ge detector. The Canberra Genie software system was applied for the data treatment. The analyses were density corrected, and in sample preparation, precautions were made to eliminate the influence of static electricity. Loss on ignition (indicating the principally combustible part of the ash samples) was determined by heating to 550°C for 2 hours. As can be seen, the cyclone ash, which is rich on large particles, has a comparatively lower loss on ignition than does the fly ash, consisting of small particles with large surface-to-mass relationship, to which gas will have condensed. Practically no loss on ignition was detected for the slag samples.

Table 4.3 Specific activity of ash and slag samples measured at Risø.

ID	Sample	Date	Loss on ignition	Bq ^{137}Cs activity [Bq g^{-1}]
A	Cyclone ash	16/6. 99	39.8 %	3.0 ± 0.1
B	Fly ash 1	16/6. 99	72.6 %	11.9 ± 0.3
C	Fly ash 2	16/6. 99	77.7 %	10.7 ± 0.3
D	Cyclone ash	17/6. 99	38.0 %	4.4 ± 0.1
E	Fly ash 1	17/6. 99	79.0 %	10.3 ± 0.3
F	Fly ash 2	17/6. 99	82.4 %	9.4 ± 0.2
G	Slag < 2mm	All week	~0	1.6 ± 0.05
H	Slag > 2mm	All week	~0	1.8 ± 0.05

4.2 Discussion of Cs-137 in Aerosols and Ashes

Radioactivity of Samples from Facility Compartments

The results of daily measurements of ^{137}Cs content in ashes sampled from different ports are shown in Fig. 4.1 - 4.3. The analysis of the samples taken from the catches of two baghouse modules (Fig. 4.3) gave differing data on specific activity. The fly ash captured in the right module Z2(2) has lower activity than that in the left module Z2(1). One can derive two reasons. The baghouse design may have some elements, which could result in inertial separation of ash particles. In this case, the right module might collect larger number of bigger particles of dust (soot) that has low activity. The likely reason is that the right baghouse module has lower efficiency in the sub-micron diapason (probably resulting from certain defects in a filter bag).

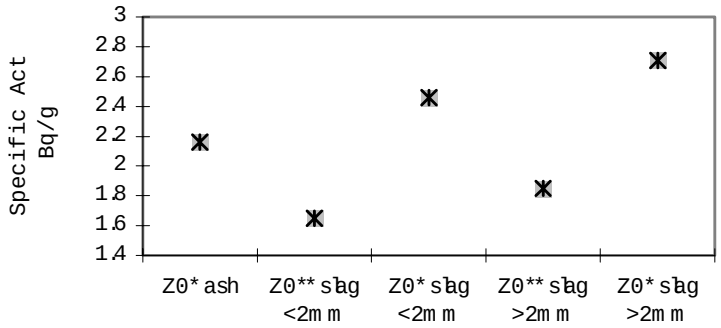

Figure 4.1 Specific Activity of Bottom Ash and Slag (- IPEP; ** - RISØ)*

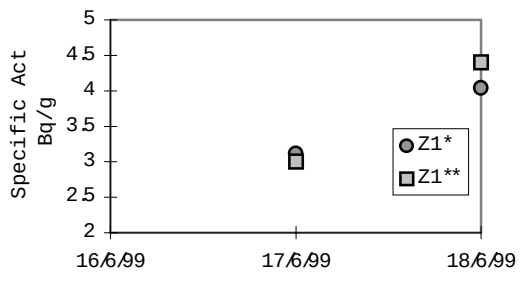

Figure 4.2 Specific Activity of Cyclone Ash

(* - IPEP; ** - RISØ)

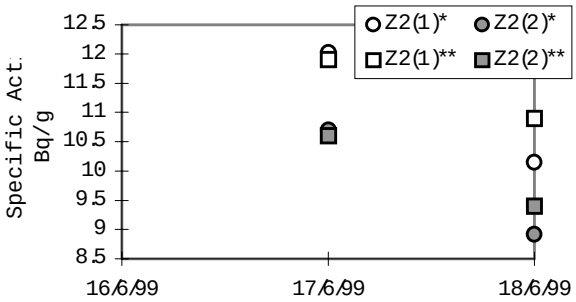

Figure 4.3 Specific Activity of Baghouse Ash

(* - IPEP; ** - RISØ)

Some samples of fly ash were taken from special ports several times during a day. The results of their analysis are given in Fig. 4.4 and 4.5. These data are in a good agreement with the averaged activity of the samples ($Z1_{cont}$ $Z2_{cont}$) taken at the end of each day from the catches (see Fig. 4.2 and 4.3).

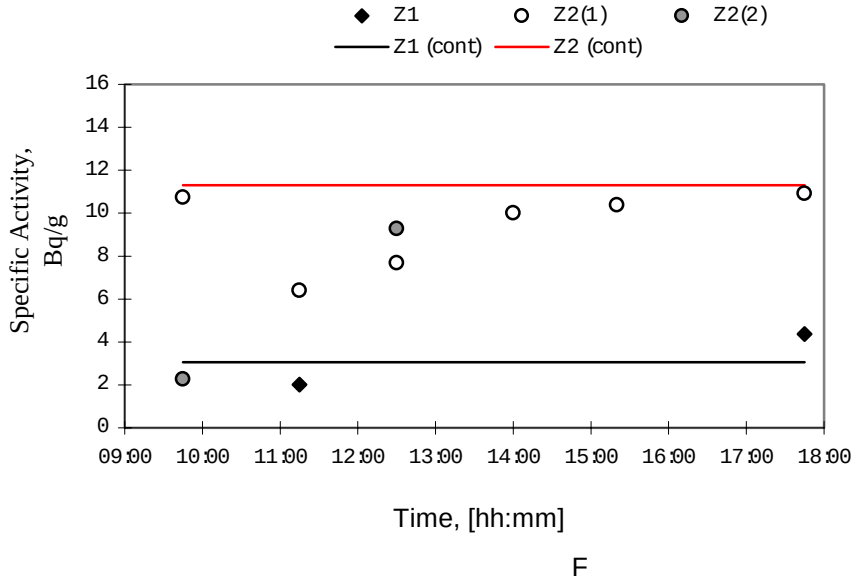

F

Figure 4.4 Specific Activity of Time-dependent Ash Samples (17.06.99)

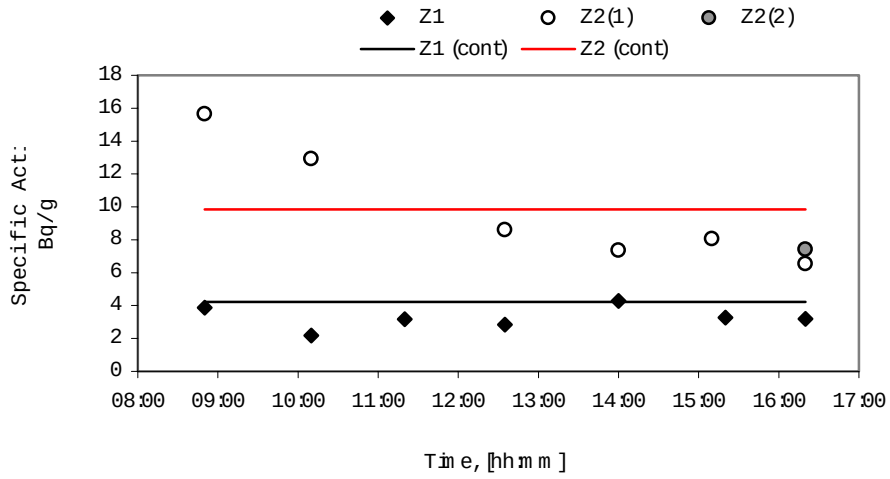

Figure 4.5 Specific Activity of Time-dependent Ash Samples (18.06.99)

From the above data, the following averaged values of the ^{137}Cs content in ashes sampled from furnace, cyclone and baghouse can be derived:

Table 4.4 Summary of specific activities for slag and fly ashes.

Material	Date	Specific activity [Bq/g]	Max/Min [Bq/g]
Bottom ash and slag (Z0)	18.06.99	2.1	2.7 / 1.6
Coarse ash from cyclone (Z1)	17.06.99	3.1	4.4 / 2.0
	18.06.99	3.5	4.4 / 2.2
Fine fly ash from baghouse (Z2)	17.06.99	9.4	12.0 / 3.0
	18.06.99	9.6	6.5 / 15.6

Radioactivity of Samples Collected by Total Filter and Impactor

As was noted in Chapter 2, the unstable oxidizing conditions in furnace led to periodical heavy sooting. This resulted in a wide fluctuation in the content of low-active organic dust (carbon particles) in the flue gas flow. The higher number of such particles, the higher total dust content, and the lower the specific activity of dust.

In Figure 4.6 and Figure 4.7, the dependence of the specific activity of the samples entrapped by total filters and impactor foils in three sampling points (S1, S2, and S3) is plotted as a function of the inverse value of dust concentration measured using the same filters and foils. These graphs confirm the above assumption.

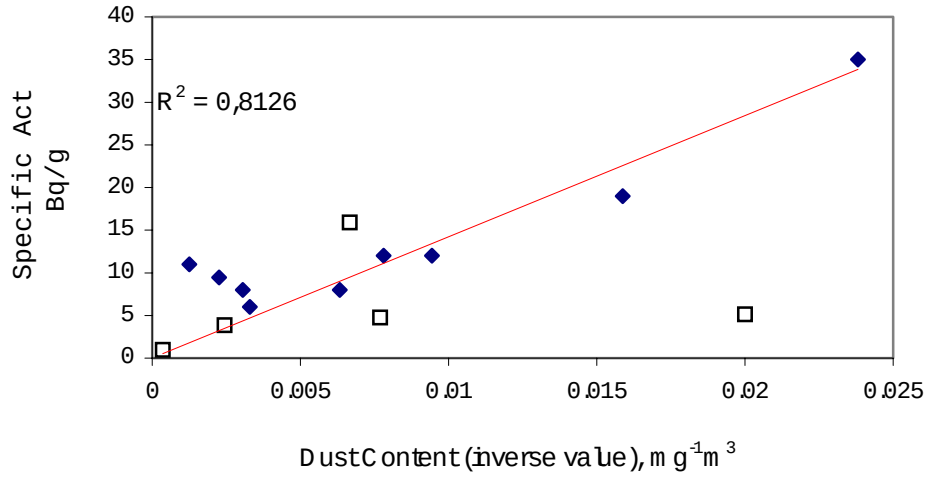

Figure 4.6 Specific Activity of Aerosols vs. *Inverse Dust Content measured at port S1 (before the baghouse cyclone)*

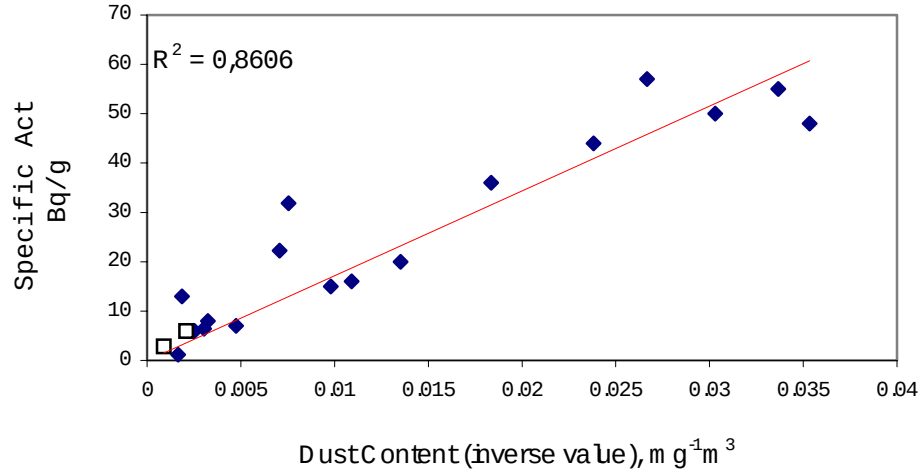

Figure 4.7 Specific Activity of Aerosols vs. *Inverse Dust Content measured at port S2 (before the baghouse filter)*

In this correlation, the proportionality coefficient is related to the value of the ^{137}Cs content in a unit volume of flue gas, which is mostly defined by (i) the rate of vapour formation of ^{137}Cs and its species, (ii) the absorption/condensation/nucleation characteristics of ^{137}Cs, and (iii) the number of the ^{137}Cs-containing aerosol particles. In the case of presence of non-contaminated aerosols, this value (volumetric activity) has a slight dependence on the total dust concentration (see Fig. 4.8 and 4.9).

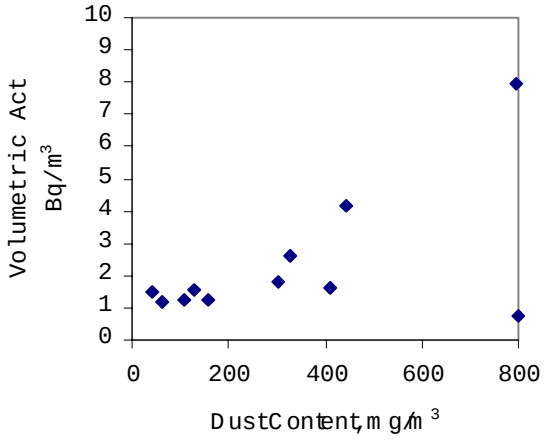

Figure 4.8 Volumetric Activity at S1

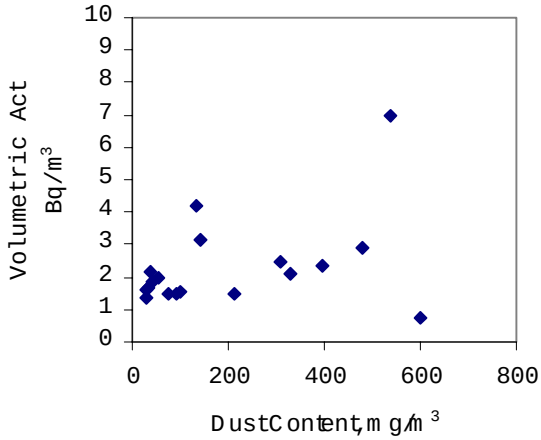

Figure 4.9 Volumetric Activity before filter at S2

A somewhat different picture would be expected for the specific values of aerosol activity after the baghouse filter. Here, the mass specific activity should not depend on the dust content, since in the after-filter flow, the submicron aerosols dominate, carrying the major part of the activity. In fact, it was the case in this test (see Fig. 4.10). As for the volumetric activity, it depends proportionally on the amount of dust per unit volume, since this dust mostly consists of the contaminated particulate (Fig. 4.11).

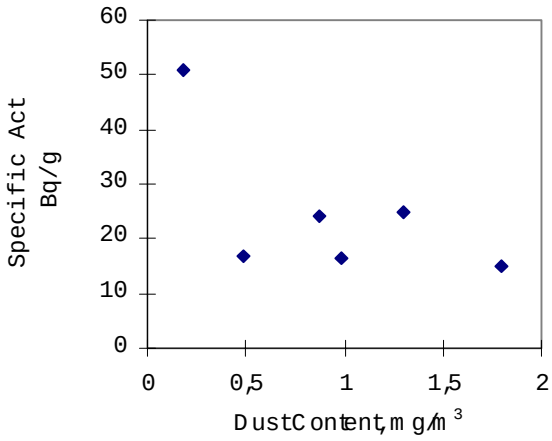

Figure 4.10 Specific Activity (after filter, S3)

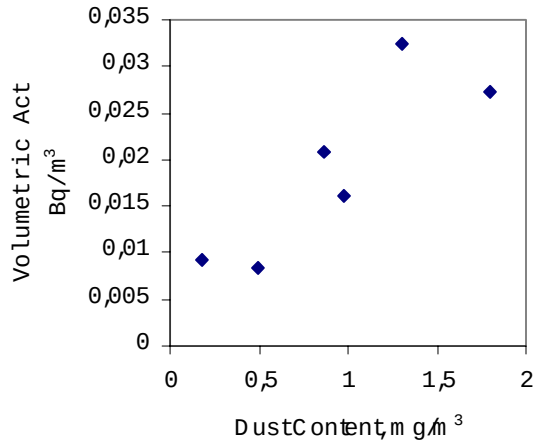

Figure 4.11 Volumetric Activity (after filter, S3)

Activity of Different Fractions According to Impactor Data

Due to the relatively low radioactivity level in the fuel and small amount of material collected on the impactor foils the ^{137}Cs content was mostly below the detection limit of the applied gamma spectrometer. At Risø, six samples were analysed for which the data on radioactivity of aerosols entrapped on the impactor foils of 10 stages were obtained.

It is difficult to make any comprehensive evaluation or modelling on this background. Some results received from the same sampling point and under similar conditions differ significantly (see *Figure 4.12* and *Figure 4.13*).

Specific Activity of Samples:	Surface Activity of Samples:
IMP-3, Port S3	IMP-3, Port S3
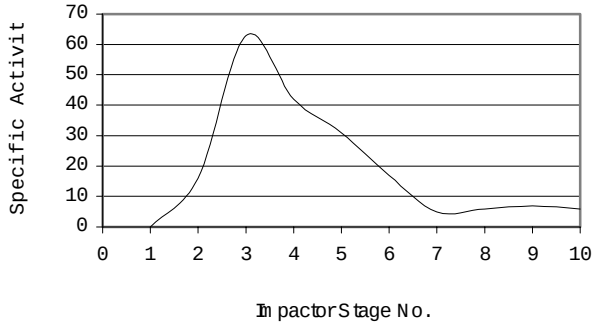	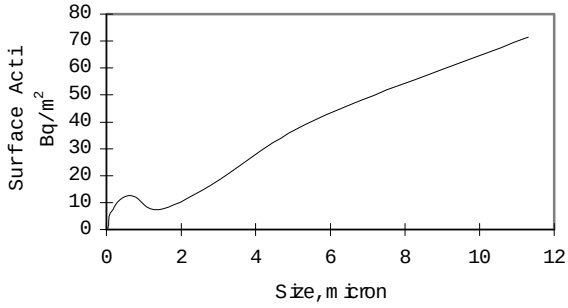
IMP-4, Port S3	IMP-4, Port S3
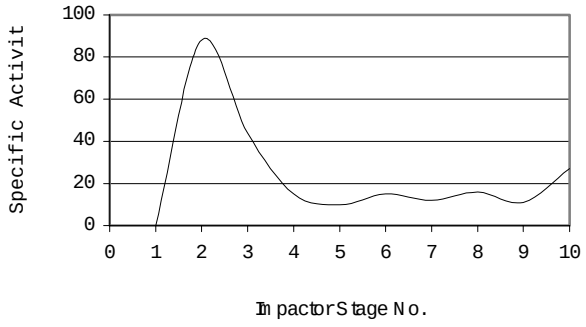	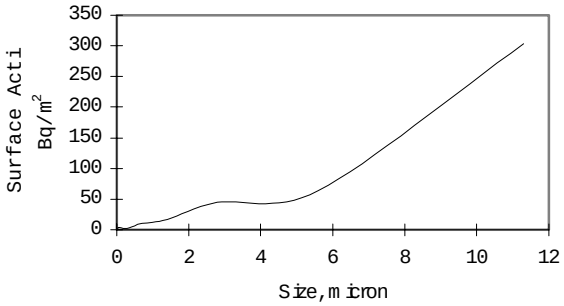
IMP-5, Port S1	IMP-5, Port S1
	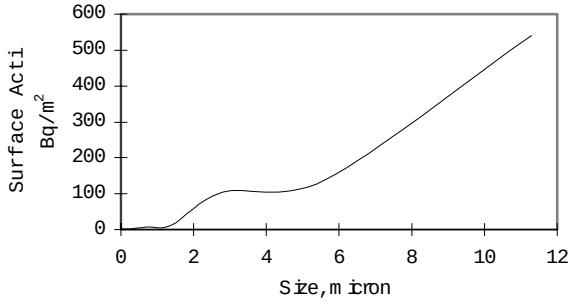
IMP-12, Port S1	IMP-12, Port S1
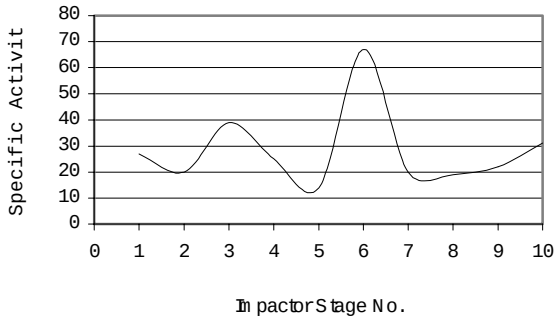	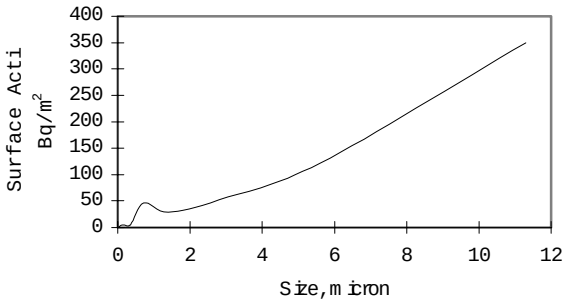

Continued on the next page

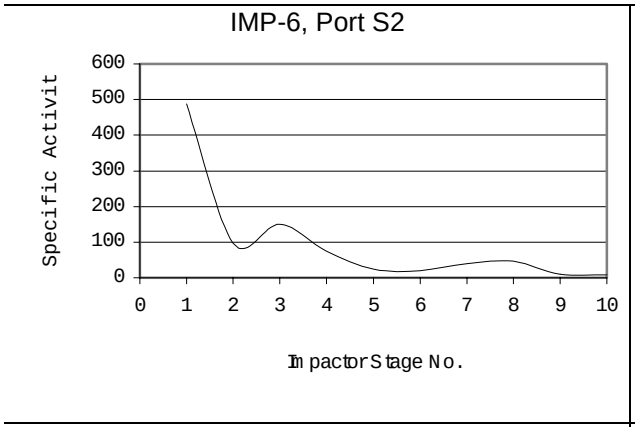

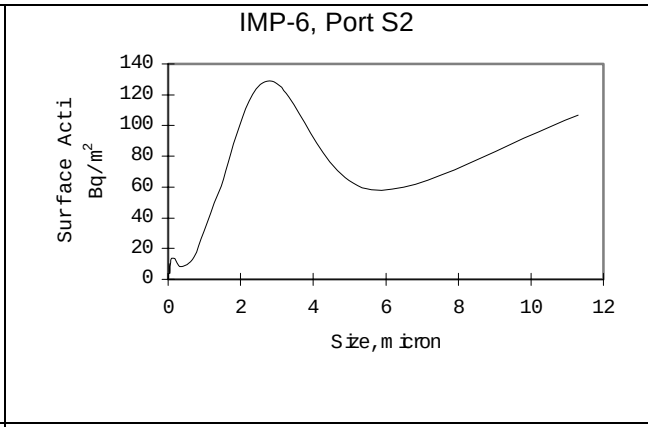

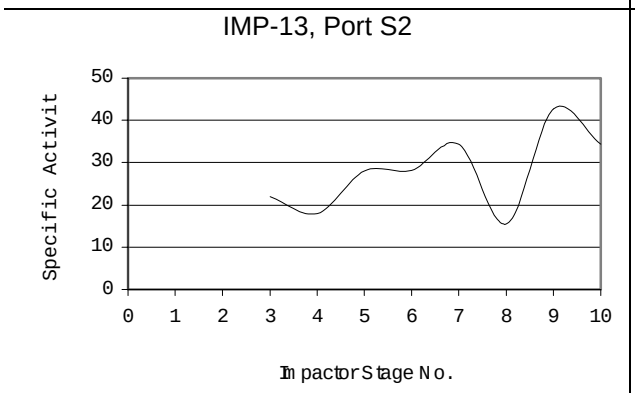

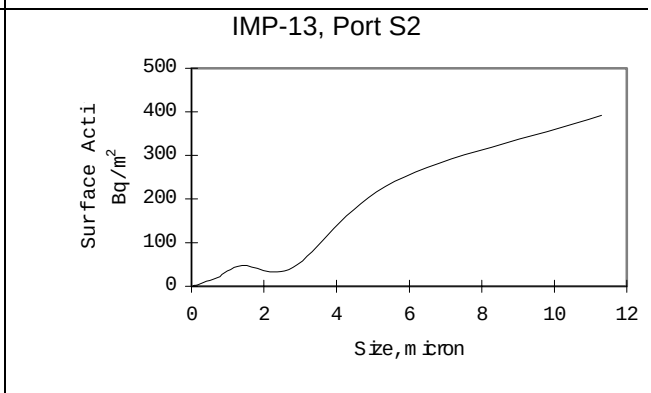

Figure 4.12 Specific Activity of Samples

Figure 4.13. Surface Activity of Samples

Efficiency of Cyclone and Baghouse with Regard to Radioactivity

It follows from the generalisation of measurements of the ^{137}Cs content in ash samples (Chapter 4.2) that the volumetric activity of aerosols in the sampling points S1, S2 and S3 has the mean values shown in Table 4.5.

Table 4.5 Mean volumetric activities in the baghouse facility.

Sampling point	Volumetric activity, Bq/m^3	Standard deviation, Bq/m^3
Before cyclone (S1)	2.33	0.96
Before baghouse (S2)	2.30	0.77
After baghouse (S3)	0.019	0.01

From these data, the capture efficiency of the cyclone and filter can be estimated with regard to radioactivity. This is shown in Table 4.6.

Table 4.6 Capture efficiencies for Cs-137 based on all results.

System	Capture efficiency, %	Max / Min, %
Cyclone	1.3	53.5 / -124
Baghouse	99.2	99.7 / 98.1

The above values are calculated on the basis of generalisation of the results of all measurements. At the same time, by analogy with the dust capture efficiency, it is possible to make an assessment of efficiency within each measurement series chosen (see Chapter 3.1). The results of such an estimation are presented below in Fig. 4.14 and 4.15 and Table 4.7.

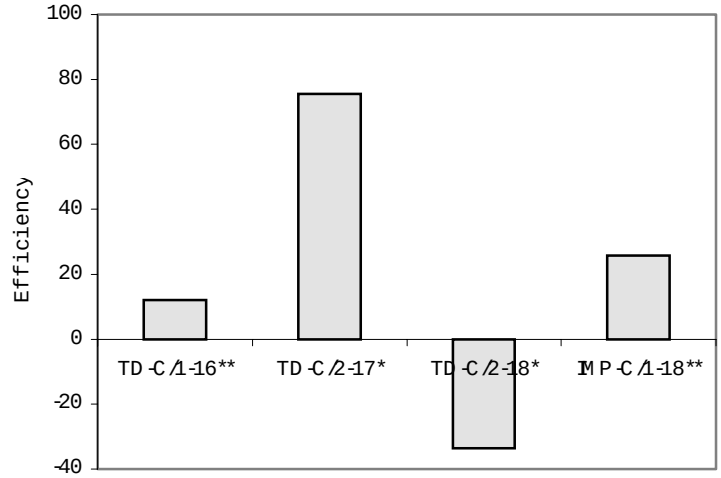

Figure 4.14 Radioactivity Capture Efficiency of Cyclone

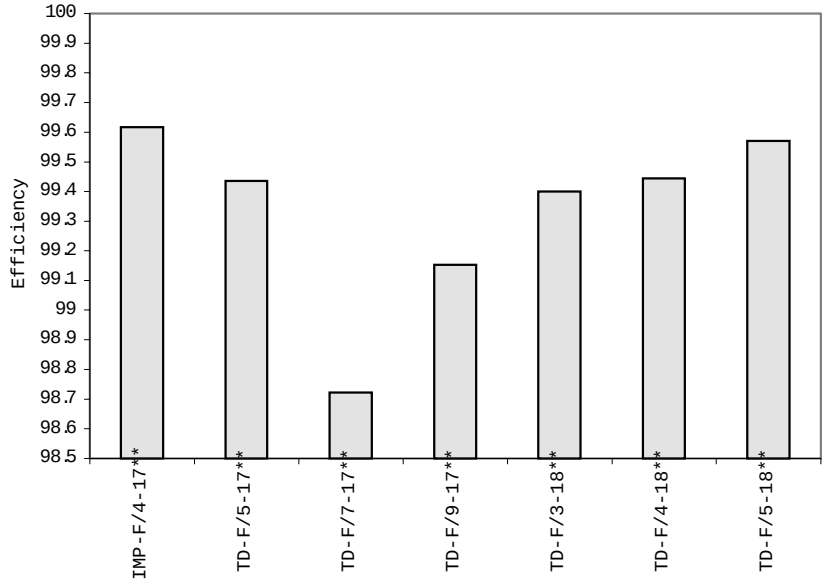

Figure 4.15 Radioactivity Capture Efficiency of Baghouse Filter.

Table 4.7 Capture efficiencies for Cs-137 based on selected results.

System	Capture efficiency, %	Max / Min, %
Cyclone	4.8	25.8 / -33.5
Baghouse	99.3	99.6 / 98.7

The results in Table 4.7 do not differ from the previous ones in Table 4.6, but the deviations are smaller.

As can be seen from comparison of the results, in almost all cases the baghouse efficiency of capture of dust is lower than that of radioactivity. As for the capture efficiency of the cyclone, the opposite is the case, i.e. the efficiency of dust treatment is higher. These results are in line with the fact that ^{137}Cs is carried mainly by fine aerosol fractions.

5 Conclusions

A series of in situ tests has been conducted in Belarus to examine the fate of radiocaesium in the process of energy production in a boiler system fired with contaminated biomass from the Belarussian forests contaminated by the Chernobyl accident. Of particular interest in this context is the emission to the atmosphere of radiocaesium from the stack of the bio-energy plant.

Aerosol laser spectrometry measurements before and after the filter system at the test plant show that the impact on particles in the range between ca. 0.2 µm and 2.0µm is rather homogeneous and highly significant. Impactor measurements confirm this and show that the cyclone before the filter as expected generally has a great effect on the super micron particles. The size distribution of particles between the cyclone and the filter exhibits a nice Gaussian-like shape with a GMD of about 250 nm. The coarse particles have here been removed from the flue gas stream.

The smaller particles are efficiently filtered in the baghouse filter mounted at the plant. Total dust measurements show that the radiocaesium contaminant capture efficiency of the cyclone is slightly less than a factor of 2. However, after the exhaust air has passed through the baghouse filter only ca. 0.3 to 0.6 % of the caesium remains. This result was observed by two independent measuring teams.

Overall, laser measurements, total dust measurements and impactor measurements gave a filter efficiency of about 99.5 % for the entire baghouse construction.

In the preliminary assessment of the potential consequences of radiocaesium stack releases from a power plant fired with contaminated biomass, as reported in the final report of Phase 1a of the project, it was assumed that 10 % of the radiocaesium in the fuel would be released from the stack. This estimate was considered to be 'probably conservative'. The results of the tests described in the present report demonstrate that this assumption must in fact be considered highly conservative. If the in situ findings in Belarus were applied in the preliminary stack release consequence analysis from the Phase 1a report, it would thus reduce the number of expected fatal cancers by a factor of ca. 20. The estimate would then be that there would be less than one case of fatal cancer from 100 years operation of power plants fired with an annual total of 1,000,000 tonnes of biomass. It should however be stressed that a proper and fully covering consequence analysis in relation to the construction of any specific biomass-fired power plant would demand the incorporation of site- and case-specific data.

The test in Belarus also provided a unique opportunity to study the factor by which the radiocaesium in the fuel is concentrated in the various types of ash produced in the plant. As expected, the organic content in the slag was negligible, increasing in the cyclone ash, and greatest in the fly ash (72-82 %). The specific radiocaesium activity was found to increase in the order slag - cyclone ash - fly ash. Relative to the fuel content the radiocaesium concentration factor was about 15 in the slag, 30 in the cyclone ash and 90 in the fly ash. Although these figures tie in with the general observations of Hedvall et al. (1996), who examined the ash concentration of radiocaesium in 13 Swedish biomass fired power plants, the absolute values of the concentration factors are critically dependent on process-specific parameters, and may be associated with significant variations. For instance, Hedvall et al. in a few cases recorded higher concentration factors for bottom ash than for fly ash.

Fuel rich (reducing) conditions in the furnace significantly alter the chemical transformations and volatility of caesium. Such conditions occurred frequently during these investigations. Reducing conditions enhance the volatility of caesium in every major component in the furnace, including particles, deposits, grate ash, and slag.

Definitive field data on the fate of caesium during combustion require better control and characterisation of combustion conditions than was achieved during this test.

6 Acknowledgement

The work reported here received funding from Wheelabrator Environmental Systems, Inc., USA, USA Department of Energy's Initiatives for Proliferation Prevention (IPP) programme and Energistyrelsen, Danish Ministry of Environment and Energy.

We are grateful to the support provided by each of these institutions.

7 References

Steven G. Buckley, Melissa M. Lunden, Allen L. Robinson, David C. Allen, Albert Sandoval, Alexandre grebenkov, and Larry Baxter: ”Fate of Sr and Cs in Biomass Combustion”.

DIN 1942. Abnahmeversuche an Dampferzeugern (VDI-Dampferzeugerregeln). Deutsche Norm, Februar 1994.

Alexandre J. Grebenkov: ”Baghouse Filter for Pilot-Scale Facilities. Field Test Results. IPEP’s contribution to the Joint Test at Rechitza Drev Sawmill”, October 1999.

Hedvall, R., Erlandsson, B. and Matsson, S., Cs-137 in fuels and ash products from biofuel power plants in Sweden, J. Environ. Radioactivity 31, no. 1, pp. 103-117, 1996.

Hillamo, R.E. and E.I. Kauppinen, On the Performance of the Berner Low Pressure Impactor, Aerosol Science and Technology, Vol. 14, pp. 33-47, 1991.

Helle Junker, Jens-Martin Jensen, Henrik Boye Jørgensen, Jørn Roed, Kasper Andersson, Pieter D. Kofman, Ebbe Bøllehuus, Larry Baxter, Alexandre Grebenkov: “Chernobyl Bioenergy Project. Power Production from Radioactively Contaminated Biomass and Forest Litter in Belarus. Final Report, Phase 1”, September 1998.

Valmari, Tuomas; Esko I. Kauppinen, Juha Kurkela, Jorma K. Jokiniemi, George Sfiris and Hannu Revitzer; Fly ash formation and depotion during fluidized bed combustion of willow, J. of Aerosol Science, Vol. 29, no. 4, pp. 445 - 459, 1998.

Appendix A

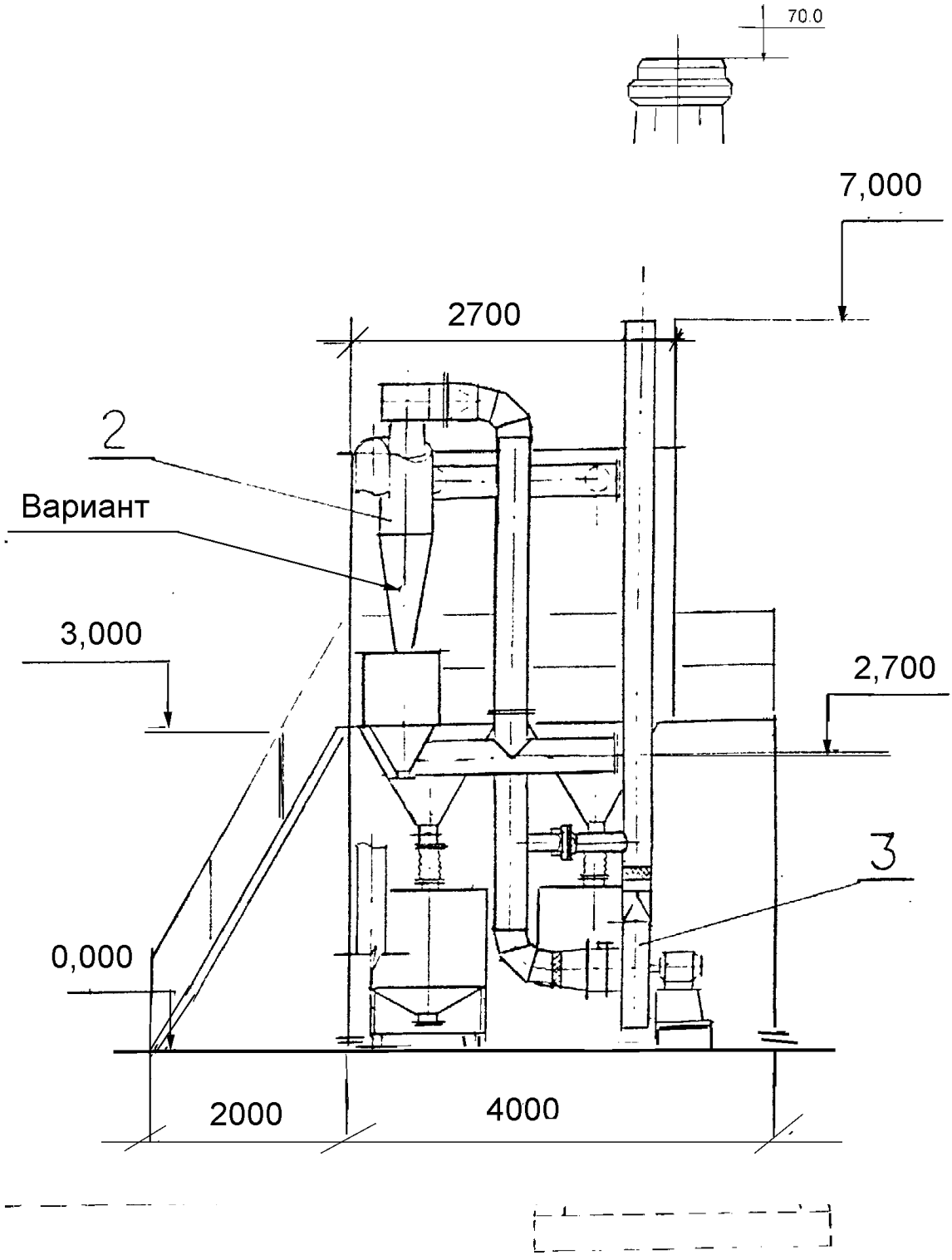

Figure A.1 Baghouse assembling at the Rechitza Drew Sawmill boiler. Front-site view.

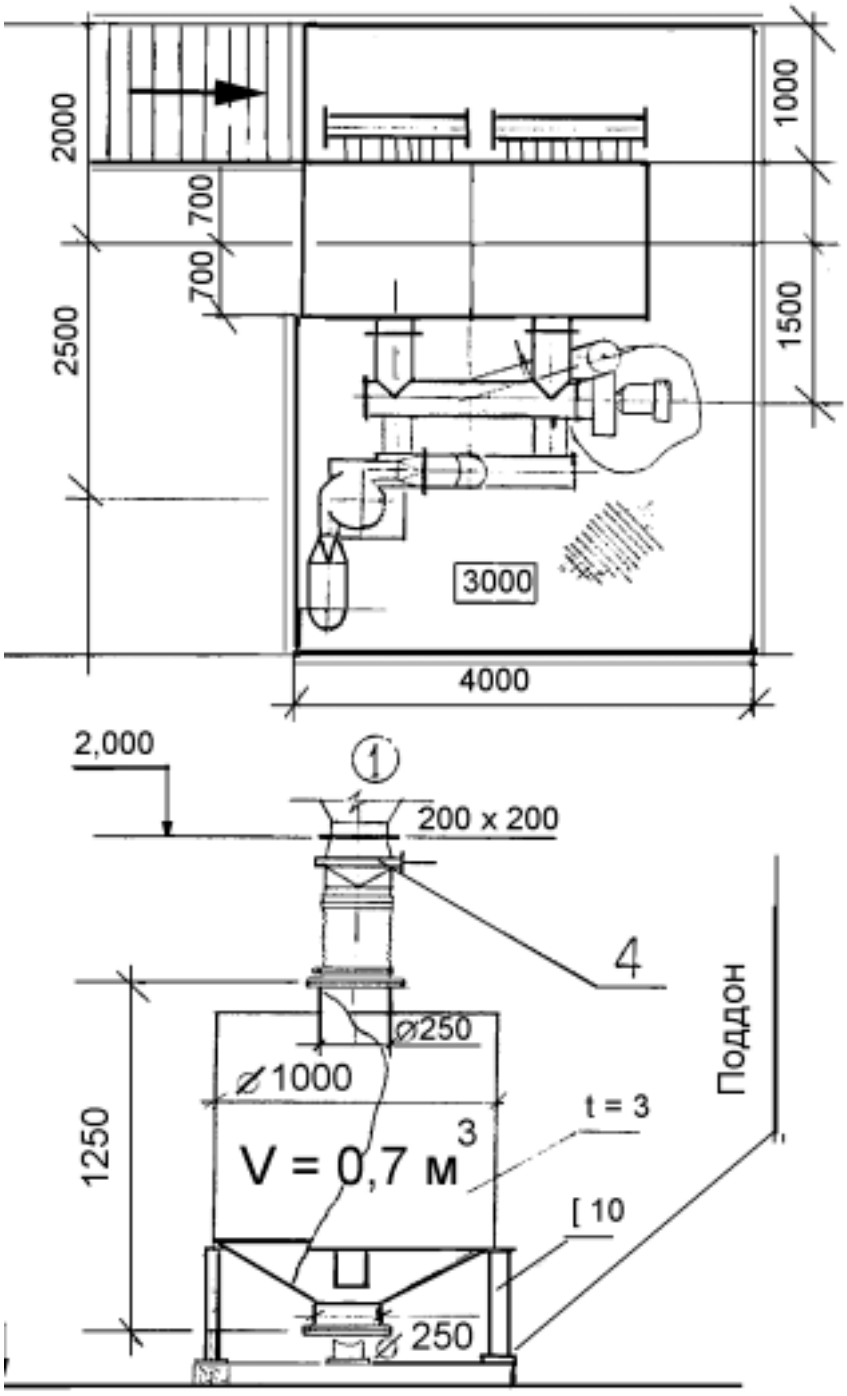

Figure A.2

Baghouse filter at RechiDrev Sawmill site. Air-site view (above)
Flue gas fan (below)

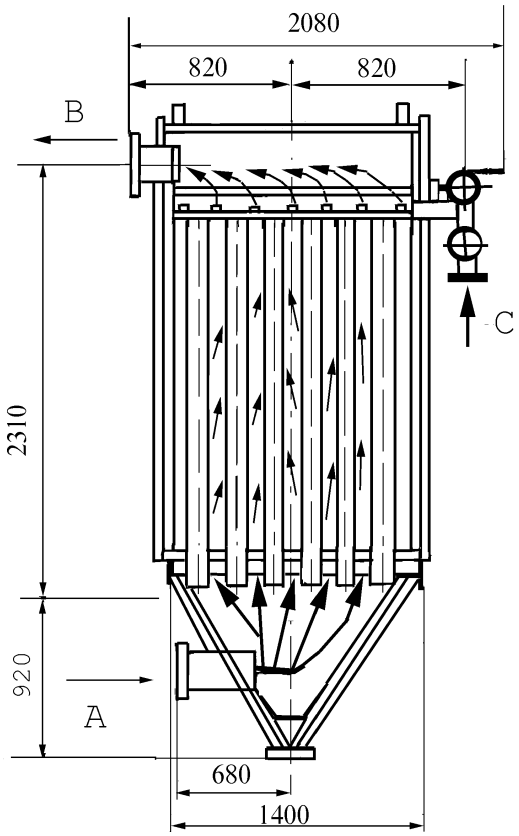

Figure A.3 Scheme of single baghouse casing.
A - incoming air.
B - filtered air out.
C - compressed air for bag cleaning.

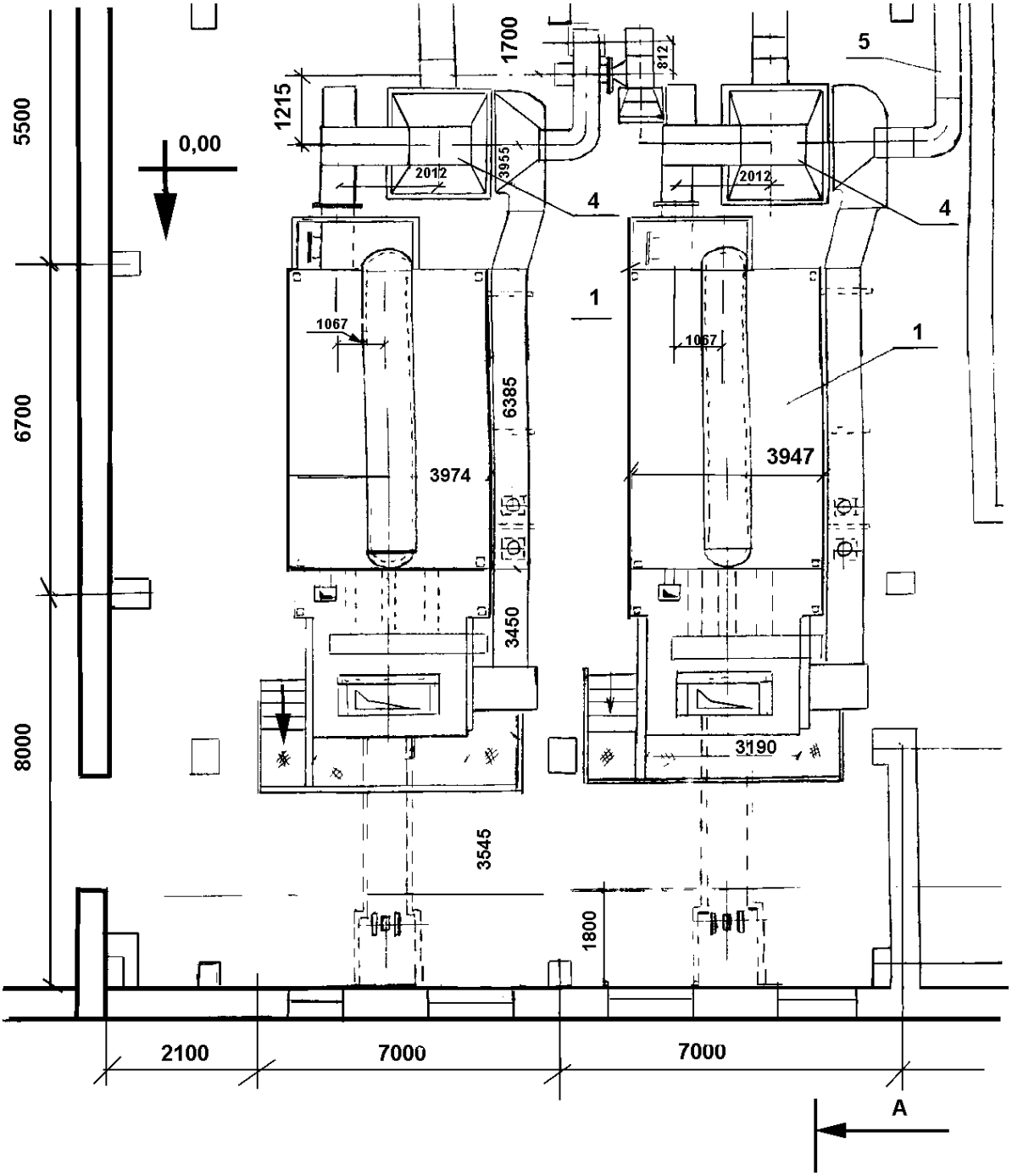

Figure A.4 Boiler house at Rechitza Drew Sawmill. Air view on wood fired boilers

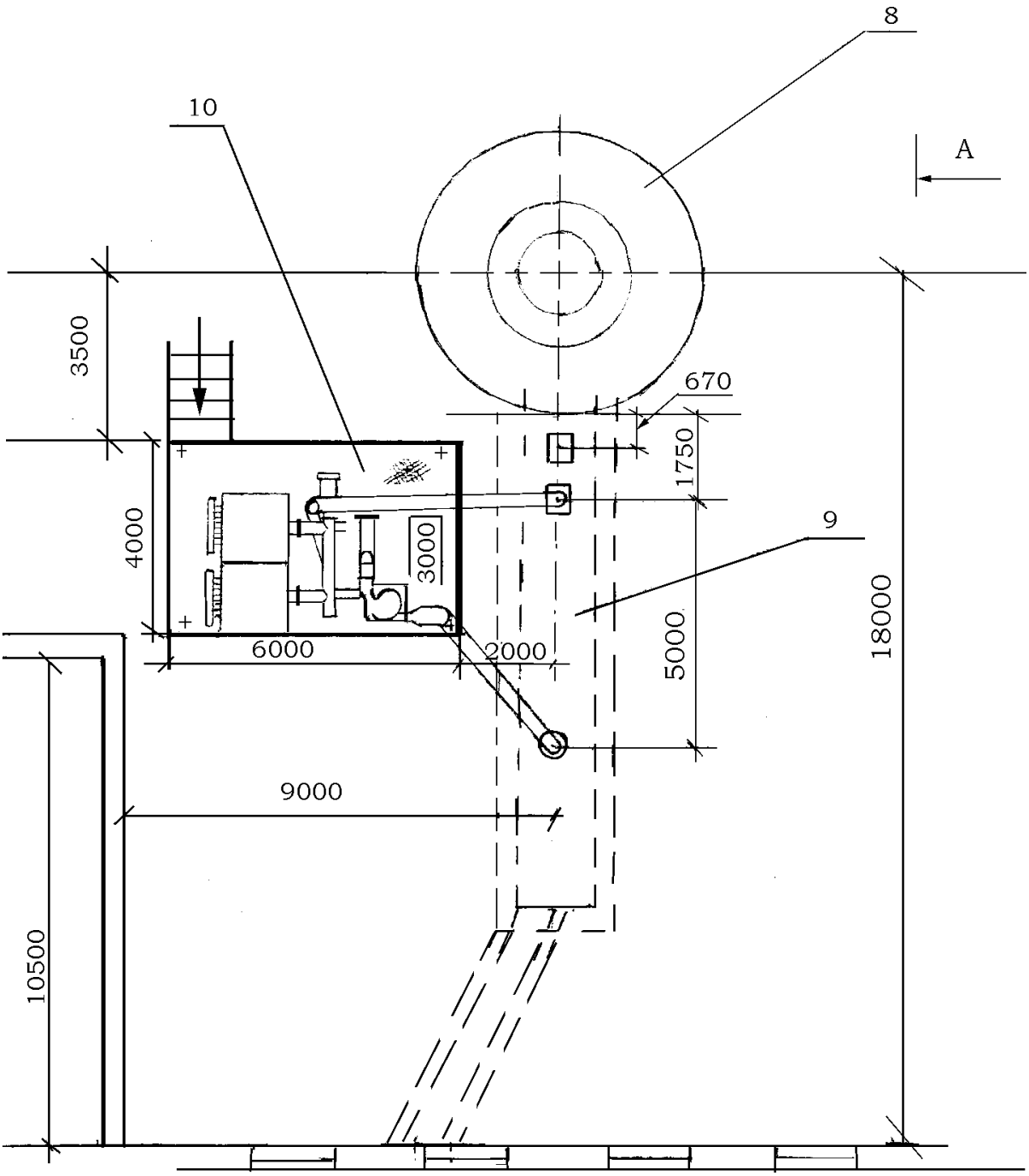

Figure A.5 Baghouse filter at Rechitza Drew Sawmill site. Air-site view.
8 - Chimney; 9 - Flue gas trunk chest; 10 - Baghouse filter

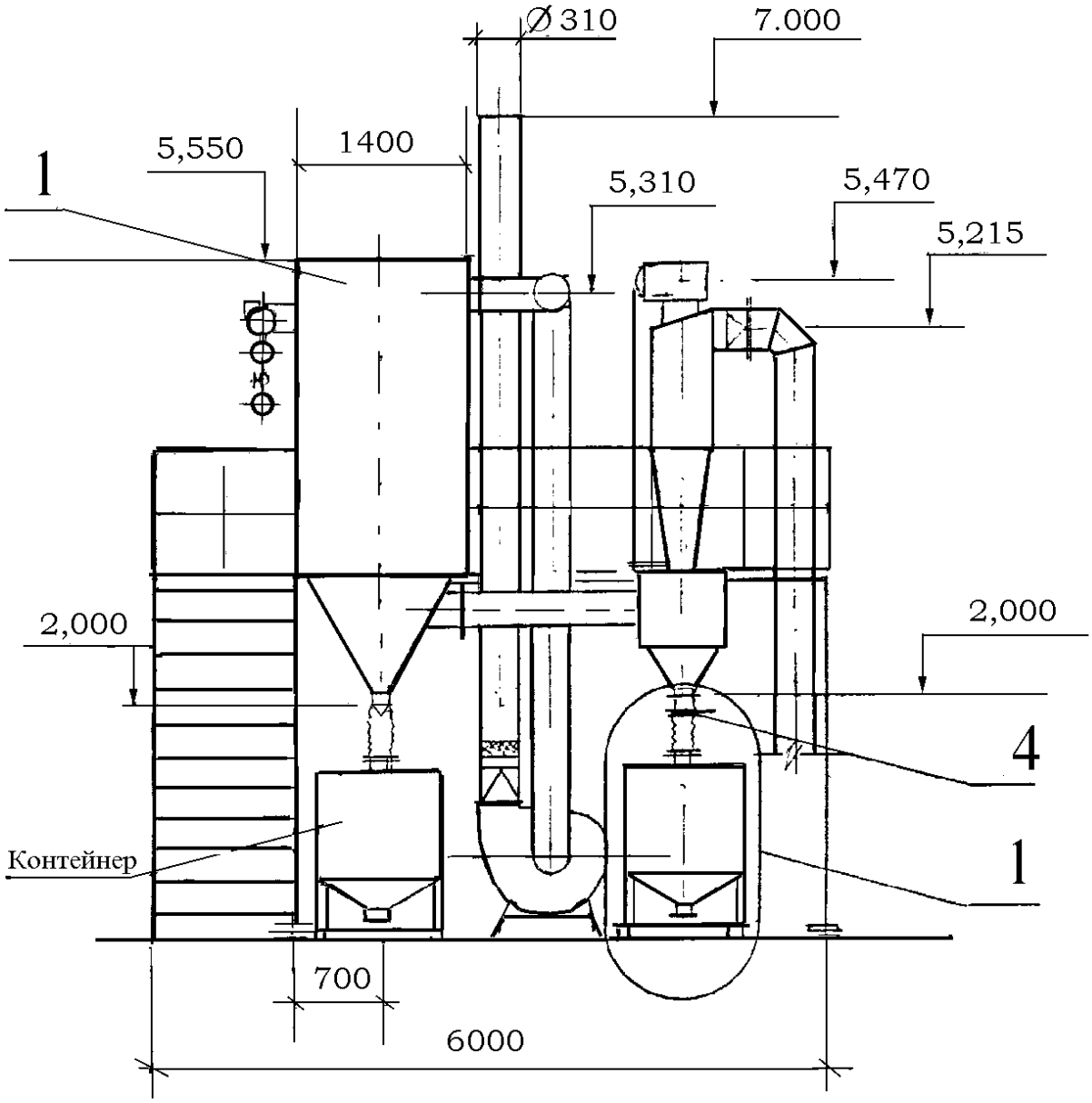

Figure A.6 Baghouse filter at RechiDrev Sawmill site. Back-site view.

1 top - Baghouse filter casing
1 bottom - fly ash container below cyclone

Appendix B

Raw Data of Impactor Measurements

ID	Pos.	Impactor ID	Collector surface	Foil numbers	Start time	Duration [min.]	Volume [m^3]
IMP-1	S1	25-43	Alu-grease	402-411	16.06.99-15:05	8	0.206
IMP-2	S2L	25-22	Alu-grease	451-442	16.06.99-18:05	61	1.549
IMP-3	S3	25-43	Alu-ng	412-421	16:06.99-14:32	240	6.168
IMP-4	S3	25-43	Alu-ng	352-361	17.06.99-08:45	240	6.168
IMP-5	S1	25-22	Alu-grease	422-431	17.06.99-09:00	2	0.051
IMP-6	S2	25-22	Alu-grease	392-401	17.06.99-10:06	4	0.102
IMP-7	S2	25-22	Teflon	242-251	17.06.99-12:16	1.333	0.034
IMP-8	S3	25-22	Alu-grease	452-461	17.06.99-14:45	180	4.572
IMP-9	S2	25-43	Alu-grease	462-471	17.06.99-15:33	1.333	0.034
IMP-10	S1	25-43	Teflon	252-261	17.06.99-16:30	1.333	0.034
IMP-11	S2	25-22	Alu-ng	362-371	17.06.99-18:20	1	0.025
IMP-12	S1L	25-22	Alu-grease	472-481	18.06.99-09:29	1	0.0254
IMP-13	S2L	25-43	Alu-grease	432-441	18.06.99-09:29	1	0.0257
IMP-14	S1L	25-22	Teflon	272-281	18.06.99-11:05	1	0.0254
IMP-15	S2	25-43	Teflon	262-271	18.06.99-11:05	1	0.0257
IMP-16	S2	25-43	Teflon	282-291	18.06.99-14:00	0.75	0.019
IMP-17	S2	25-22	Alu-ng	342-351	18.06.99-14:00	0.75	0.019
IMP-18	S3TL	25-22	Teflon	292-301	18.06.99-14:36	120	3.048
IMP-19	S2L	25-43	Alu-ng	372-381	18.06.99-15:05	1	0.026
IMP-20	S2L	25-43	Teflon	302-311	18.06.99-16:02	0.5	0.013
IMP-21	S2L	25-43	Alu-ng	382-391	18.06.99-17:36	1	0.026
IMP-22	S2L	25-22	Alu-grease	482-491	18.06.99-17:36	1	0.025

IMP-2		Filter ID	1. pre mass	2. pre mass	1. post mass	2. post mass	Sample mass		Conc.	
	[µm]	[ ]	[g]	[g]	[g]	[g]	[g]	[mg]	[mg/m^3]	[%]
	0,021	442	0,08829		0,08881	0,08889	0,00056	0,56	0,361	1%
Flow	0,042	443	0,08847		0,09051	0,09029	0,00193	1,93	1,246	5%
1,5494	0,087	444	0,08811		0,09081	0,09081	0,00270	2,7	1,743	7%
m^3	0,18	445	0,08782		0,09014	0,09013	0,00232	2,315	1,494	6%
	0,35	446	0,08825		0,09194	0,09193	0,00368	3,685	2,378	9%
	0,71	447	0,08825		0,09832		0,01007	10,07	6,499	24%
	1,4	448	0,08810		0,10286		0,01476	14,76	9,526	36%
	2,8	449	0,08764		0,09218		0,00454	4,54	2,930	11%
	5,6	450	0,08833		0,08897	0,08896	0,00063	0,635	0,410	2%
	11,3	451	0,08887		0,08911	0,08905	0,00021	0,21	0,136	1%
								41,4	26,723	100%

Impactor measurement at S2

between cyclone and filter

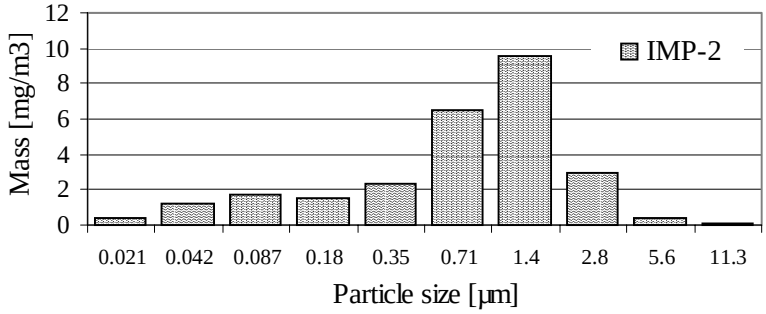

IMP-3		Filter ID	1. pre mass	2. pre mass	1. post mass	2. post mass	Sample mass		Conc.	
	[µm]	[ ]	[g]	[g]	[g]	[g]	[g]	[mg]	[mg/m^3]	[%]
	0,021	412	0,08829		0,08838	0,08833	0,00007	0,065	0,011	1%
Flow	0,042	413	0,08898		0,08919	0,08913	0,00018	0,18	0,029	2%
6,168	0,087	414	0,08839		0,08850	0,08843	0,00007	0,075	0,012	1%
m^3	0,18	415	0,08881		0,08992	0,08989	0,00110	1,095	0,178	10%
	0,35	416	0,08837		0,09028	0,09021	0,00187	1,875	0,304	17%
	0,71	417	0,08814		0,08891	0,08889	0,00076	0,76	0,123	7%
	1,4	418	0,08897		0,09004	0,09001	0,00106	1,055	0,171	10%
	2,8	419	0,08937		0,09110	0,09107	0,00171	1,715	0,278	15%
	5,6	420	0,08754		0,09008	0,09004	0,00252	2,52	0,409	23%
	11,3	421	0,08827		0,09001	0,09001	0,00174	1,74	0,282	16%
								11,1	1,796	100%

Impactor measurement at S3

after the bag house filter

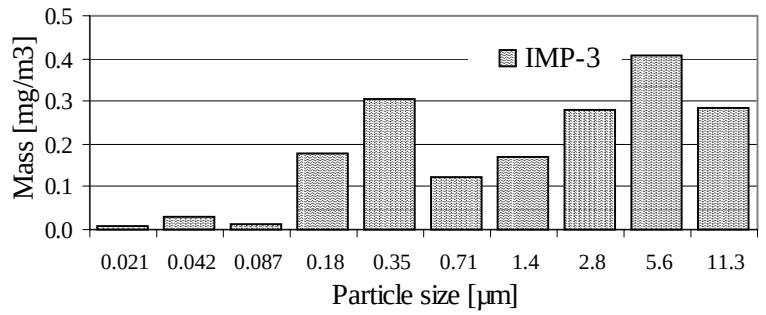

IMP-4	[µm]	Filter ID [ ]	1. pre mass [g]	2. pre mass [g]	1. post mass [g]	2. post mass [g]	Sample mass [g]	[mg]	Conc. [mg/m^3]	[%]
	0,021	352	0,08773		0,08778	0,08776	0,00004	0,04	0,006	1%
Flow	0,042	353	0,08808		0,08821	0,08819	0,00012	0,12	0,019	2%
6,168	0,087	354	0,08770		0,08789	0,08785	0,00017	0,17	0,028	3%
m^3	0,18	355	0,08812		0,08954	0,08945	0,00137	1,375	0,223	23%
	0,35	356	0,08748		0,08878	0,08872	0,00127	1,27	0,206	21%
	0,71	357	0,08751		0,08843	0,08839	0,00090	0,9	0,146	15%
	1,4	358	0,08843		0,08894	0,08891	0,00050	0,495	0,080	8%
	2,8	359	0,08783		0,08841	0,08840	0,00058	0,575	0,093	10%
	5,6	360	0,08849		0,08920	0,08914	0,00068	0,68	0,110	11%
	11,3	361	0,08859		0,08903	0,08897	0,00041	0,41	0,066	7%
							Sum	6,035	0,978	100%

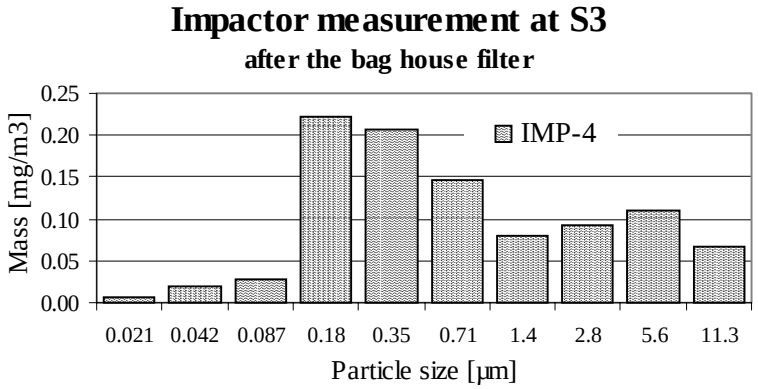

IMP-5	[µm]	Filter ID [ ]	1. pre mass [g]	2. pre mass [g]	1. post mass [g]	2. post mass [g]	Sample mass [g]	[mg]	Conc. [mg/m^3]	[%]
	0,021	422	0,08808		0,08822	0,08818	0,00012	0,12	0,019	1%
Flow	0,042	423	0,08847		0,08902	0,08900	0,00054	0,54	0,088	2%
0,0508	0,087	424	0,08803		0,08974	0,08971	0,00170	1,695	0,275	8%
m^3	0,18	425	0,08816		0,09841		0,01025	10,25	1,662	45%
	0,35	426	0,08801		0,09416		0,00615	6,15	0,997	27%
	0,71	427	0,08796		0,09003		0,00207	2,07	0,336	9%
	1,4	428	0,08821		0,08909		0,00088	0,88	0,143	4%
	2,8	429	0,08834		0,08873	0,08873	0,00039	0,39	0,063	2%
	5,6	430	0,08721		0,08745	0,08743	0,00023	0,23	0,037	1%
	11,3	431	0,08739		0,08763	0,08761	0,00023	0,23	0,037	1%
								22,555	3,657	100%

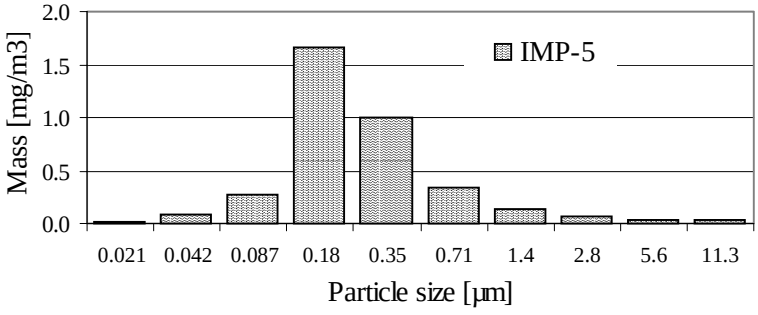

IMP-6	[µm]	Filter ID [ ]	1. pre mass [g]	2. pre mass [g]	1. post mass [g]	2. post mass [g]	Sample mass [g]	[mg]	Conc. [mg/m^3]	[%]
	0,021	392	0,08742		0,08744	0,08743	0,00002	0,015	0,148	0%
Flow	0,042	393	0,08752		0,08764	0,08755	0,00008	0,075	0,738	1%
0,1016	0,087	394	0,08757		0,08790	0,08788	0,00032	0,32	3,150	2%
m^3	0,18	395	0,08875		0,09020	0,09020	0,00145	1,45	14,272	11%
	0,35	396	0,08753		0,09038	0,09039	0,00286	2,855	28,100	21%
	0,71	397	0,08894		0,09093	0,09092	0,00199	1,985	19,537	15%
	1,4	398	0,08820		0,08911	0,08911	0,00091	0,91	8,957	7%
	2,8	399	0,08818		0,08968	0,08965	0,00149	1,485	14,616	11%
	5,6	400	0,08858		0,09179	0,09177	0,00320	3,2	31,496	24%
	11,3	401	0,08859		0,08975	0,08976	0,00117	1,165	11,467	9%
			0,09286		0,09314	0,09305		13,460	132,480	100%

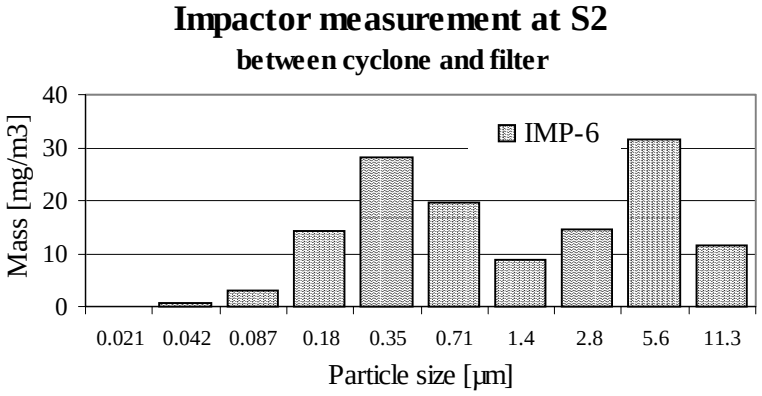

IMP-7	[µm]	Filter ID [ ]	1. pre mass [g]	2. pre mass [g]	1. post mass [g]	2. post mass [g]	Sample mass [g]	[mg]	Conc. [mg/m^3]	[%]
	0,02	242	0,33041	0,33040	0,33043	0,33044	0,00003	0,03	0,886	1%
Flow	0,04	243	0,32921	0,32921	0,32931	0,32922	0,00006	0,055	1,624	3%
0,03386	0,08	244	0,33240	0,33239	0,33269	0,33265	0,00028	0,275	8,122	13%
m^3	0,18	245	0,32886	0,32886	0,32956	0,32966	0,00075	0,75	22,151	35%
	0,35	246	0,33302	0,33303	0,33328	0,33323	0,00023	0,23	6,793	11%
	0,71	247	0,33189	0,33189	0,33203	0,33195	0,00010	0,1	2,953	5%
	1,4	248	0,33120	0,33125	0,33144	0,33146	0,00023	0,225	6,645	11%
	2,8	249	0,32866	0,32865	0,32895	0,32896	0,00030	0,3	8,860	14%
	5,6	250	0,32997	0,32997	0,33008	0,33008	0,00011	0,11	3,249	5%
	11,3	251	0,33263	0,33263	0,33265	0,33269	0,00004	0,04	1,181	2%
								2,115	62,466	100%

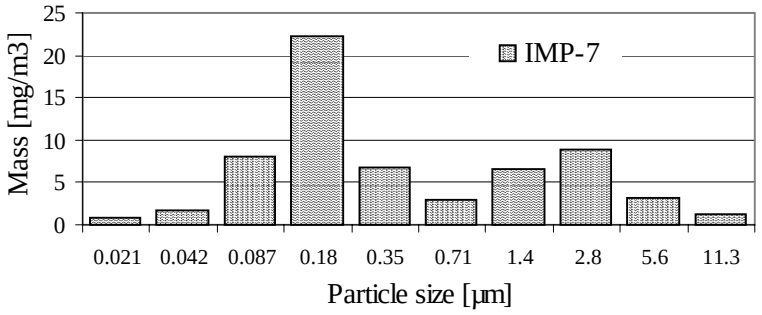

IMP-8	[µm]	Filter ID [ ]	1. pre mass [g]	2. pre mass [g]	1. post mass [g]	2. post mass [g]	Sample mass [g]	[mg]	Conc. [mg/m^3]	[%]
	0,021	452	0,08812		0,08816	0,08822	0,00007	0,07	0,015	2%
Flow	0,042	453	0,08827		0,08844	0,08840	0,00015	0,15	0,033	4%
4,572	0,087	454	0,08746		0,08757	0,08761	0,00013	0,13	0,028	3%
m^3	0,18	455	0,08822		0,08890	0,08890	0,00068	0,68	0,149	17%
	0,35	456	0,08825		0,08879	0,08870	0,00049	0,495	0,108	13%
	0,71	457	0,08710		0,08746	0,08740	0,00033	0,33	0,072	8%
	1,4	458	0,08713		0,08766	0,08760	0,00050	0,5	0,109	13%
	2,8	459	0,08815		0,08870	0,08864	0,00052	0,52	0,114	13%
	5,6	460	0,08809		0,08871	0,08873	0,00063	0,63	0,138	16%
	11,3	461	0,08745		0,08787	0,08786	0,00041	0,415	0,091	11%
								3,920	0,857	100%

Impactor measurement at S3

after the bag house filter

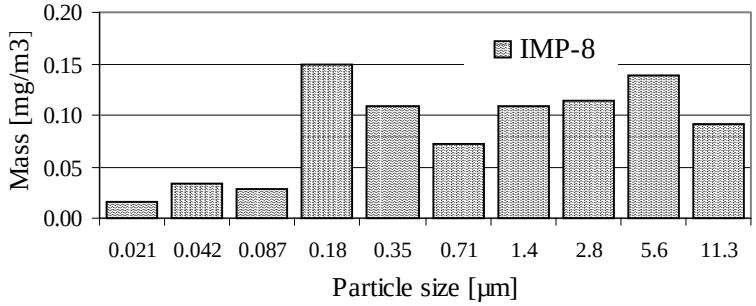

IMP-9	[µm]	Filter ID [ ]	1. pre mass [g]	2. pre mass [g]	1. post mass [g]	2. post mass [g]	Sample mass [g]	[mg]	Conc. [mg/m^3]	[%]
	0,02	462	0,08815		0,08818	0,08821	0,00004	0,045	1,314	4%
Flow	0,04	463	0,08980		0,08984	0,08986	0,00005	0,05	1,460	4%
0,03426	0,08	464	0,08962		0,08974	0,08969	0,00009	0,095	2,773	8%
m^3	0,18	465	0,08873		0,08913	0,08909	0,00038	0,38	11,092	32%
	0,35	466	0,08946		0,08959	0,08959	0,00013	0,13	3,795	11%
	0,71	467	0,08919		0,08924	0,08927	0,00006	0,065	1,897	6%
	1,4	468	0,08849		0,08861	0,08861	0,00012	0,12	3,503	10%
	2,8	469	0,08828		0,08851	0,08846	0,00021	0,205	5,984	17%
	5,6	470	0,08807		0,08815	0,08816	0,00009	0,085	2,481	7%
	11,3	471	0,08816		0,08818	0,08814	0,00000	-	0,000	0%
								1,175	34,298	100%

Impactor measurement at S2

between cyclone and filter

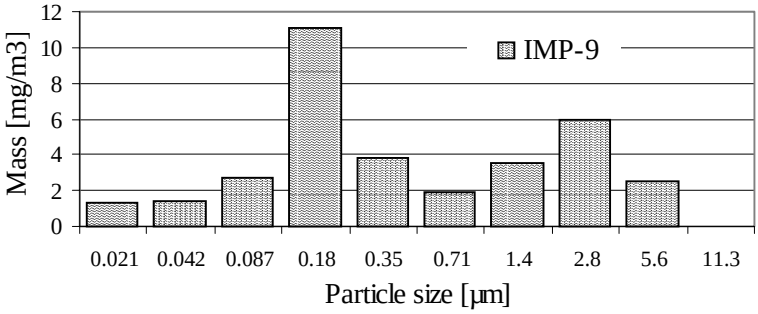

IMP-10		Filter ID	1. pre mass	2. pre mass	1. post mass	2. post mass	Sample mass		Conc.	
	[µm]	[ ]	[g]	[g]	[g]	[g]	[g]	[mg]	[mg/m^3]	[%]
	0,02	252	0,32893	0,32890	0,32899	0,32898	0,00007	0,07	2,0	4%
Flow	0,04	253	0,32993	0,32993	0,33005	0,33001	0,00010	0,1	2,9	6%
0,0342	0,08	254	0,33127	0,33123	0,33155	0,33154	0,00029	0,295	8,6	18%
m^3	0,18	255	0,33344	0,33332	0,33398	0,33393	0,00057	0,575	16,8	35%
	0,35	256	0,33362	0,33362	0,33377	0,33379	0,00016	0,16	4,7	10%
	0,71	257	0,33220	0,33218	0,33226	0,33225	0,00006	0,065	1,9	4%
	1,4	258	0,33026	0,33027	0,33029	0,33030	0,00003	0,03	0,9	2%
	2,8	259		0,33008	0,33009	0,33008	0,00000	0,005	0,1	0%
	5,6	260	0,33137	0,33197	0,33203	0,33198	0,00033	0,335	9,8	20%
	11,3	261	0,33141	0,33135	0,33144	0,33137	0,00002	0,025	0,7	2%
								1,660	48,5	100%

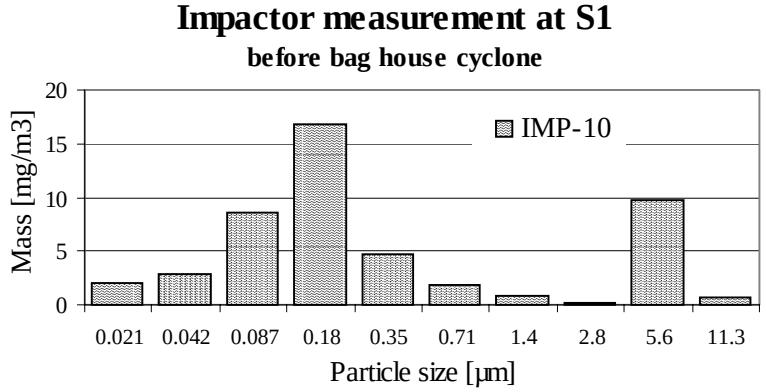

IMP-11		Filter ID	1. pre mass	2. pre mass	1. post mass	2. post mass	Sample mass		Conc.	
	[µm]	[ ]	[g]	[g]	[g]	[g]	[g]	[mg]	[mg/m^3]	[%]
	0,02	362	0,08774		0,08788	0,08783	0,00012	0,115	4,528	24%
Flow	0,04	363	0,08773		0,08767	0,08766	-0,00007	-0,065	-2,559	-14%
0,0254	0,08	364	0,08789		0,08796	0,08795	0,00007	0,065	2,559	14%
m^3	0,18	365	0,08815		0,08824	0,08825	0,00009	0,095	3,740	20%
	0,35	366	0,08826		0,08830	0,08831	0,00004	0,045	1,772	9%
	0,71	367	0,08792		0,08800	0,08799	0,00007	0,075	2,953	16%
	1,4	368	0,08800			0,08806	0,00006	0,06	2,362	13%
	2,8	369	0,08855		0,08863	0,08860	0,00006	0,065	2,559	14%
	5,6	370	0,08797		0,08802	0,08798	0,00003	0,03	1,181	6%
	11,3	371	0,08794		0,08792	0,08794	-0,00001	-0,01	-0,394	-2%
								0,475	18,701	100%

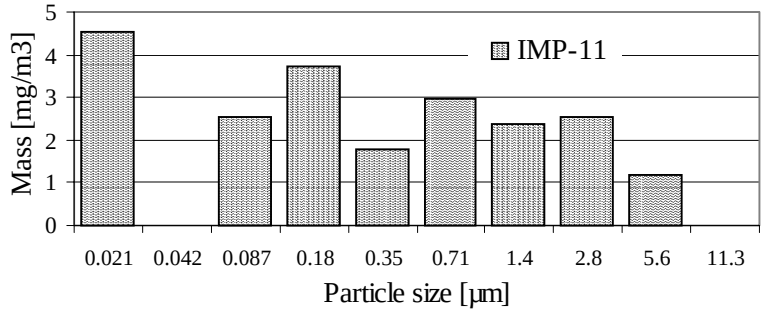

IMP-12	[µm]	Filter ID [ ]	1. pre mass [g]	2. pre mass [g]	1. post mass [g]	2. post mass [g]	Sample mass [g]	[mg]	Conc. [mg/m^3]	[%]
	0.021	472	0.08719		0.08738	0.08728	0.00014	0.14	5.512	3%
Flow	0.042	473	0.08755		0.08770	0.08778	0.00019	0.19	7.480	5%
0.0254	0.087	474	0.08733		0.08768	0.08790	0.00046	0.46	18.110	11%
m^3	0.18	475	0.08787		0.08925	0.08926	0.00139	1.385	54.528	33%
	0.35	476	0.08792		0.08863	0.08878	0.00079	0.785	30.906	19%
	0.71	477	0.08785		0.08806	0.08805	0.00020	0.205	8.071	5%
	1.4	478	0.08905		0.08928	0.08922	0.00020	0.2	7.874	5%
	2.8	479	0.08918		0.08943	0.08956	0.00031	0.315	12.402	8%
	5.6	480	0.08884		0.08914	0.08914	0.00030	0.3	11.811	7%
	11.3	481	0.08865		0.08881	0.08891	0.00021	0.21	8.268	5%
								4.190	164.961	100%

Impactor measurement at S1

before bag house cyclone

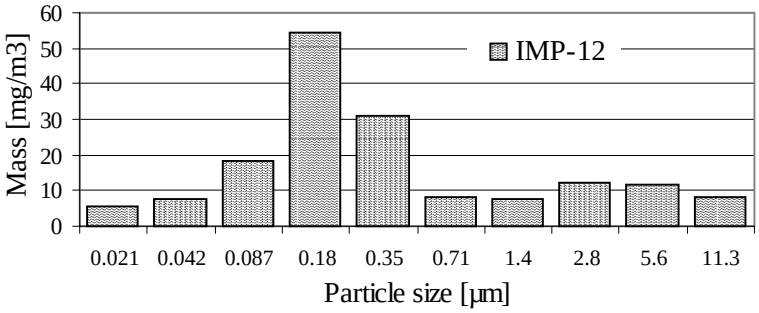

IMP-13	[µm]	Filter ID [ ]	1. pre mass [g]	2. pre mass [g]	1. post mass [g]	2. post mass [g]	Sample mass [g]	[mg]	Conc. [mg/m^3]	[%]
	0,02	432	0,08759		0,08767	0,08764	0,00006	0,065	2,529	2%
Flow	0,04	433	0,08833		0,08840	0,08851	0,00013	0,125	4,864	3%
0,0257	0,08	434	0,08802		0,08851	0,08854	0,00050	0,505	19,650	14%
m^3	0,18	435	0,08710		0,08831	0,08834	0,00123	1,225	47,665	34%
	0,35	436	0,08892		0,08963	0,08960	0,00070	0,695	27,043	19%
	0,71	437	0,08886		0,08914	0,08917	0,00030	0,295	11,479	8%
	1,4	438	0,08903		0,08919	0,08919	0,00016	0,16	6,226	4%
	2,8	439	0,08841		0,08866	0,08855	0,00020	0,195	7,588	5%
	5,6	440	0,08908		0,08927	0,08922	0,00016	0,165	6,420	5%
	11,3	441	0,08906		0,08927	0,08926	0,00021	0,205	7,977	6%
								3,635	141,440	100%

Impactor measurement at S2

between cyclone and filter

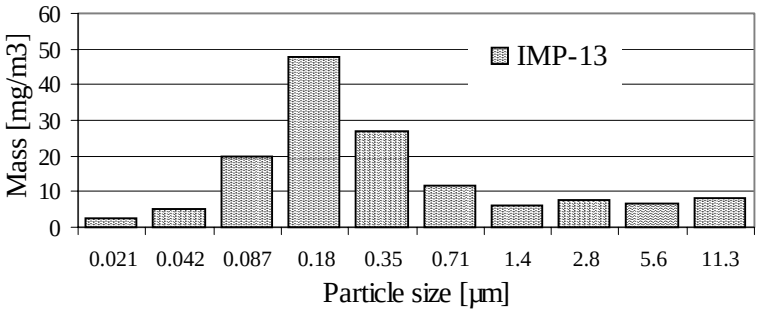

IMP-14		Filter ID	1. pre mass	2. pre mass	1. post mass	2. post mass	Sample mass		Conc.	
	[µm]	[ ]	[g]	[g]	[g]	[g]	[g]	[mg]	[mg/m^3]	[%]
	0,02	272	0,32859	0,32861	0,32870	0,32871	0,00011	0,105	4,134	2%
Flow	0,04	273	0,32982	0,32982	0,33014	0,33015	0,00033	0,325	12,795	5%
0,0254	0,08	274	0,32922	0,32923	0,32980	0,32981	0,00058	0,58	22,835	9%
m^3	0,18	275	0,32997	0,32995	0,33269	0,33254	0,00265	2,655	104,528	40%
	0,35	276	0,32995	0,32992	0,33140	0,33132	0,00143	1,425	56,102	22%
	0,71	277	0,33191	0,33195	0,33261	0,33264	0,00070	0,695	27,362	10%
	1,4	278	0,32943	0,32943	0,32971	0,32982	0,00033	0,335	13,189	5%
	2,8	279	0,33197	0,33198	0,33224	0,33209	0,00019	0,19	7,480	3%
	5,6	280	0,32876	0,32876	0,32890	0,32885	0,00012	0,115	4,528	2%
	11,3	281	0,33056	0,33059	0,33081	0,33074	0,00020	0,2	7,874	3%
								6,625	260,827	100%

Impactor measurement at S1

before bag house cyclone

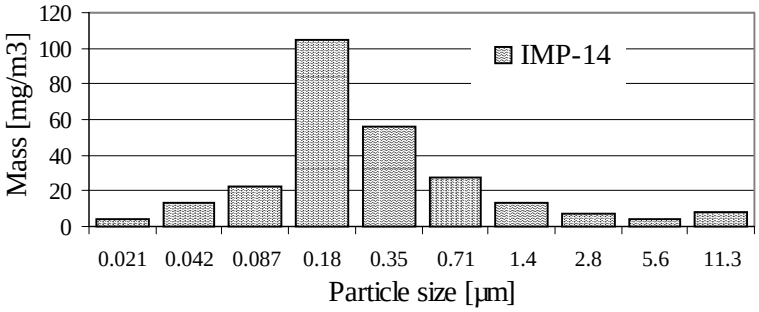

IMP-15		Filter ID	1. pre mass	2. pre mass	1. post mass	2. post mass	Sample mass		Conc.	
	[µm]	[ ]	[g]	[g]	[g]	[g]	[g]	[mg]	[mg/m^3]	[%]
	0,02	262	0,33080	0,33078	0,33087	0,33093	0,00011	0,11	4,280	2%
Flow	0,04	263	0,33046	0,33043	0,33061	0,33076	0,00024	0,24	9,339	4%
0,0257	0,08	264		0,32901	0,32945	0,32951	0,00047	0,47	18,288	8%
m^3	0,18	265		0,32953	0,33213	0,33209	0,00258	2,58	100,389	42%
	0,35	266		0,32976	0,33102	0,33100	0,00125	1,25	48,638	20%
	0,71	267	0,33245	0,33250	0,33310	0,33306	0,00061	0,605	23,541	10%
	1,4	268	0,33156	0,33159	0,33187	0,33193	0,00032	0,325	12,646	5%
	2,8	269	0,32969	0,32970	0,32990	0,32996	0,00024	0,235	9,144	4%
	5,6	270	0,33180	0,33178	0,33184	0,33200	0,00013	0,13	5,058	2%
	11,3	271	0,32980	0,32983	0,33001	0,32995	0,00017	0,165	6,420	3%
								6,110	237,743	100%

Impactor measurement at S2

between cyclone and filter

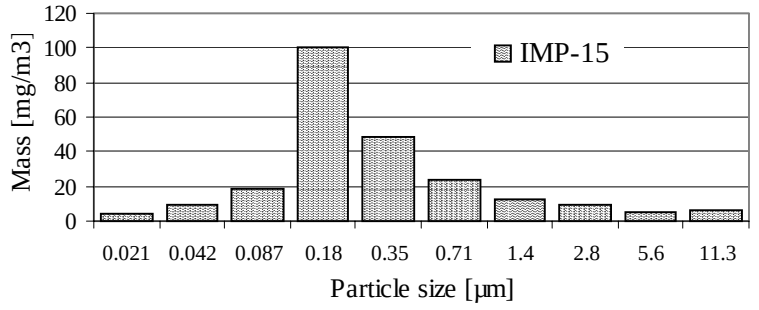

IMP-16		Filter ID	1. pre mass	2. pre mass	1. post mass	2. post mass	Sample mass		Conc.	
	[µm]	[ ]	[g]	[g]	[g]	[g]	[g]	[mg]	[mg/m^3]	[%]
	0,02	282	0,32965	0,32964	0,32971	0,32969	5,5E-05	0,055	2,853	1%
Flow	0,04	283	0,32831	0,32829	0,32858	0,32855	0,000265	0,265	13,748	3%
0,0193	0,08	284	0,32661	0,32664	0,32742	0,3274	0,000785	0,785	40,726	8%
m^3	0,18	285	0,33539	0,33541	0,33821		0,00281	2,81	145,785	30%
	0,35	286	0,32836	0,32835	0,33195		0,003595	3,595	186,511	38%
	0,71	287	0,32946	0,32948	0,33036		0,00089	0,89	46,174	10%
	1,4	288	0,33036	0,33032	0,33087	0,33081	0,0005	0,5	25,940	5%
	2,8	289	0,32524	0,32525	0,32548	0,32552	0,000255	0,255	13,230	3%
	5,6	290	0,32864	0,32863	0,32879	0,32873	0,000125	0,125	6,485	1%
	11,3	291	0,32858	0,3286	0,32869	0,32866	8,5E-05	0,085	4,410	1%
								9,365	485,863	100%

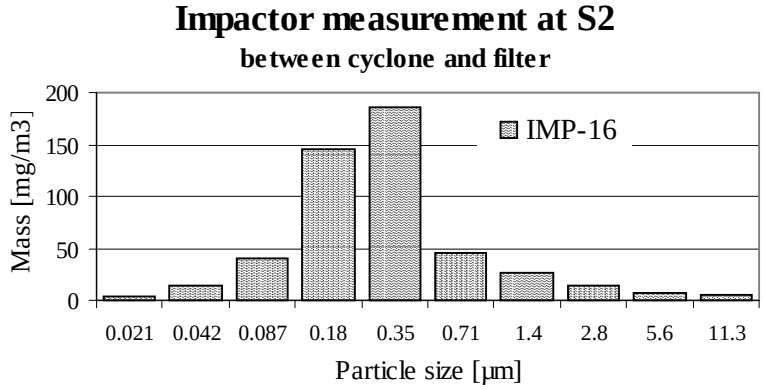

IMP-17		Filter ID	1. pre mass	2. pre mass	1. post mass	2. post mass	Sample mass		Conc.	
	[µm]	[ ]	[g]	[g]	[g]	[g]	[g]	[mg]	[mg/m^3]	[%]
	0,02	342	0,08833	0,08833	0,08838	0,08847	0,00009	0,095	5,0	1%
Flow	0,04	343	0,08805	0,08805	0,08826	0,08826	0,00021	0,21	11,0	2%
0,01905	0,08	344	0,08775	0,08774	0,08850	0,08852	0,00077	0,765	40,2	7%
m^3	0,18	345	0,08782	0,08780	0,09131	0,09146	0,00357	3,575	187,7	31%
	0,35	346	0,08821	0,08819	0,09327	0,09294	0,00490	4,905	257,5	43%
	0,71	347	0,08827	0,08828	0,08938	0,08941	0,00112	1,12	58,8	10%
	1,4	348	0,08901	0,08905	0,08953	0,08955	0,00051	0,51	26,8	4%
	2,8	349	0,08895	0,08895	0,08917	0,08912	0,00020	0,195	10,2	2%
	5,6	350	0,08809	0,08811	0,08820	0,08813	0,00006	0,065	3,4	1%
	11,3	351	0,08850	0,08844	0,08849	0,08843	-0,00001	-0,01	-0,5	0%
							Sum	11,4	600	100%

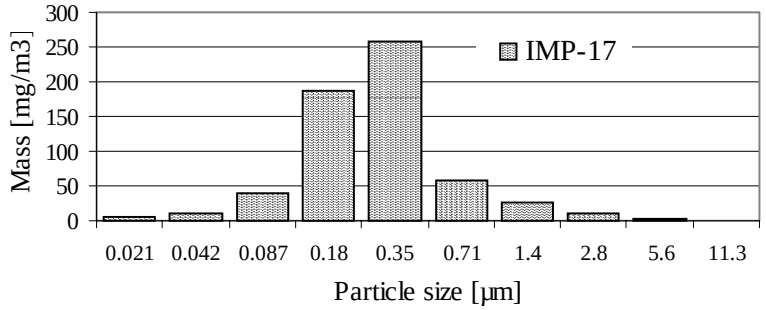

IMP-18		Filter ID	1. pre mass	2. pre mass	1. post mass	2. post mass	Sample mass		Conc.	
	[µm]	[ ]	[g]	[g]	[g]	[g]	[g]	[mg]	[mg/m^3]	[%]
	1	292	0,32788	0,32790	0,32802	0,32800	0,00012	0,12	0,039	6%
Flow	2	293	0,33063	0,33061	0,33076	0,33078	0,00015	0,15	0,049	8%
3,048	3	294	0,32888	0,32884	0,32906	0,32885	0,00009	0,095	0,031	5%
m^3	4	295	0,32981	0,32983	0,33036	0,33017	0,00045	0,445	0,146	23%
	5	296	0,33265	0,33263	0,33288	0,33283	0,00022	0,215	0,071	11%
	6	297	0,32925	0,32926	0,32942	0,32944	0,00018	0,175	0,057	9%
	7	298	0,32946	0,32948	0,32954	0,32970	0,00015	0,15	0,049	8%
	8	299	0,32880	0,32881	0,32895	0,32903	0,00018	0,185	0,061	9%
	9	300	0,33376	0,33373	0,33400	0,33392	0,00022	0,215	0,071	11%
	10	301	0,32748	0,32747	0,32765	0,32770	0,00020	0,2	0,066	10%
							Sum	1,950	0,640	100%

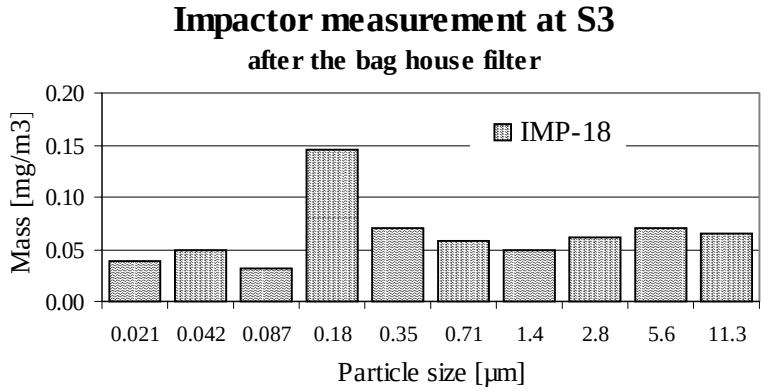

IMP-19		Filter ID	1. pre mass	2. pre mass	1. post mass	2. post mass	Sample mass		Conc.	
	[µm]	[ ]	[g]	[g]	[g]	[g]	[g]	[mg]	[mg/m^3]	[%]
	1	372	0,08799		0,08805	0,08802	0,00005	0,0450	1,8	1%
Flow	2	373	0,08820		0,08836	0,08836	0,00016	0,1600	6,2	2%
0,0257	3	374	0,08837		0,08915	0,08912	0,00076	0,7650	29,8	10%
m^3	4	375	0,08844		0,09153	0,09214	0,00340	3,3950	132,1	45%
	5	376	0,08860		0,09072	0,09068	0,00210	2,1000	81,7	28%
	6	377	0,08806		0,08858	0,08854	0,00050	0,5000	19,5	7%
	7	378	0,08882		0,08924	0,08929	0,00045	0,4450	17,3	6%
	8	379	0,08880		0,08896	0,08895	0,00016	0,1550	6,0	2%
	9	380	0,08839		0,08842	0,08843	0,00004	0,0350	1,4	0%
	10	381	0,08889		0,08890	0,08887	0,00000	-0,0050	-0,2	0%
							Sum	7,5950	295,5	100%

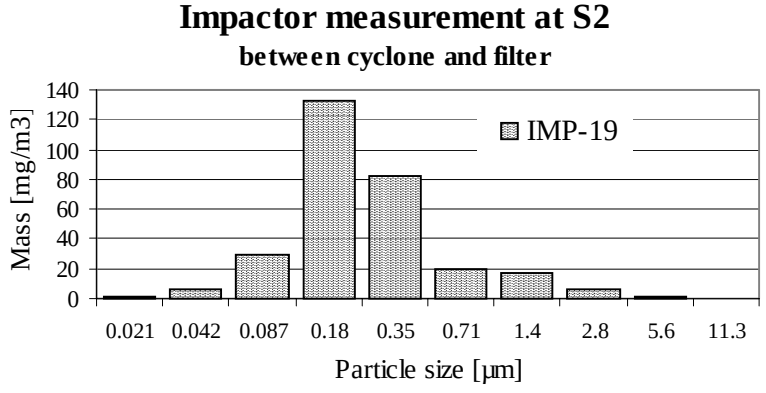

IMP-20		Filter ID	1. pre mass	2. pre mass	1. post mass	2. post mass	Sample mass		Conc.	
	[µm]	[ ]	[g]	[g]	[g]	[g]	[g]	[mg]	[mg/m^3]	[%]
	1	302	0,33375	0,33372	0,33369	0,33377	-0,00001	-0,005	-0,002	-1%
Flow	2	303	0,32519	0,32514	0,32521	0,32522	0,00005	0,05	0,016	7%
0,01285	3	304	0,32756	0,32758	0,32773	0,32771	0,00015	0,15	0,049	20%
m^3	4	305	0,32759	0,32757	0,32779	0,32793	0,00028	0,28	0,092	37%
	5	306	0,32801	0,32801	0,32809	0,32804	0,00005	0,055	0,018	7%
	6	307	0,32821	0,32819	0,32823	0,32819	0,00001	0,01	0,003	1%
	7	308	0,32716	0,32713	0,32722	0,32719	0,00006	0,06	0,020	8%
	8	309	0,32904	0,32903	0,32910	0,32908	0,00006	0,055	0,018	7%
	9	310	0,32704	0,32712	0,32712	0,32712	0,00004	0,04	0,013	5%
	10	311	0,32638	0,32633	0,32647	0,32636	0,00006	0,06	0,020	8%
							Sum	0,755	0,248	100%

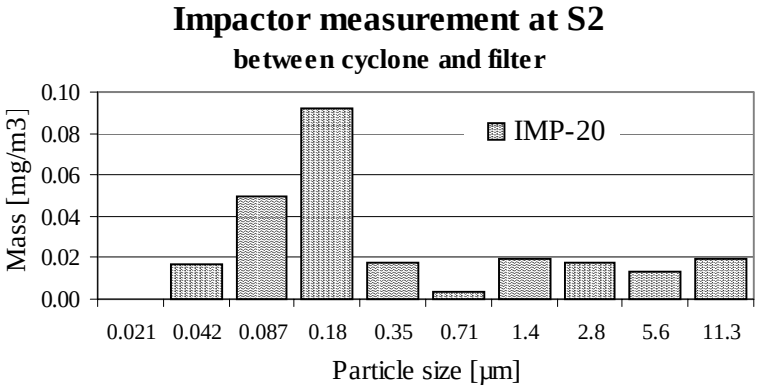

IMP-21		Filter ID	1. pre mass	2. pre mass	1. post mass	2. post mass	Sample mass		Conc.	
	[µm]	[ ]	[g]	[g]	[g]	[g]	[g]	[mg]	[mg/m^3]	[%]
	0,02	382	0,08833		0,08831	0,08826	-0,00005	-0,045	-1,751	-6%
Flow	0,04	383	0,08802		0,08801	0,08796	-0,00003	-0,035	-1,362	-4%
0,0257	0,08	384	0,08802		0,08812	0,08812	0,00010	0,1	3,891	13%
m^3	0,18	385	0,08804		0,08854	0,08849	0,00048	0,475	18,482	60%
	0,35	386	0,08768		0,08775	0,08777	0,00008	0,08	3,113	10%
	0,71	387	0,08782		0,08793	0,08788	0,00009	0,085	3,307	11%
	1,4	388	0,08769		0,08773	0,08773	0,00004	0,04	1,556	5%
	2,8	389	0,08803		0,08809	0,08808	0,00005	0,055	2,140	7%
	5,6	390	0,08772		0,08775	0,08774	0,00002	0,025	0,973	3%
	11,3	391	0,08742		0,08744	0,08743	0,00002	0,015	0,584	2%
							Sum	0,795	30,934	100%

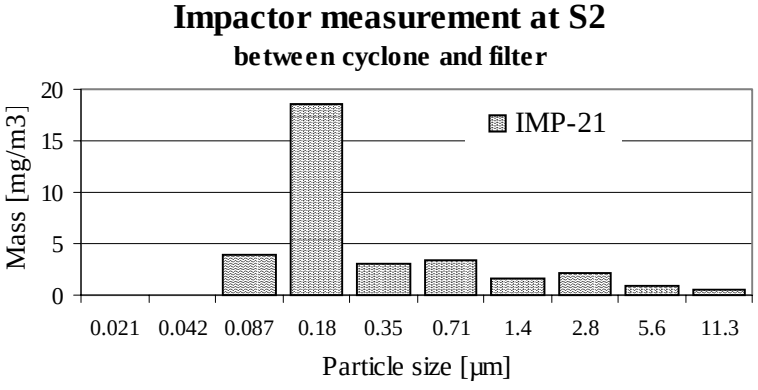

IMP-22	[µm]	Filter ID [ ]	1. pre mass [g]	2. pre mass [g]	1. post mass [g]	2. post mass [g]	Sample mass [g]	[mg]	Conc. [mg/m^3]	[%]
	0,02	482	0,08928		0,08927	0,08928	-0,00001	-0,005	-0,197	-1%
Flow	0,04	483	0,09807		0,09808	0,09811	0,00002	0,025	0,984	3%
0,0254	0,08	484	0,08836		0,08841	0,08836	0,00002	0,025	0,984	3%
m^3	0,18	485	0,08879		0,08909	0,08913	0,00032	0,32	12,598	44%
	0,35	486	0,08890		0,08905	0,08904	0,00014	0,145	5,709	20%
	0,71	487	0,08871		0,08869	0,08872	0,00000	-0,005	-0,197	-1%
	1,4	488	0,08867		0,08872	0,08872	0,00005	0,05	1,969	7%
	2,8	489	0,08833		0,08840	0,08848	0,00011	0,11	4,331	15%
	5,6	490	0,08943		0,08941	0,08950	0,00003	0,025	0,984	3%
	11,3	491	0,08844		0,08842	0,08854	0,00004	0,04	1,575	5%
							Sum	0,730	28,740	100%

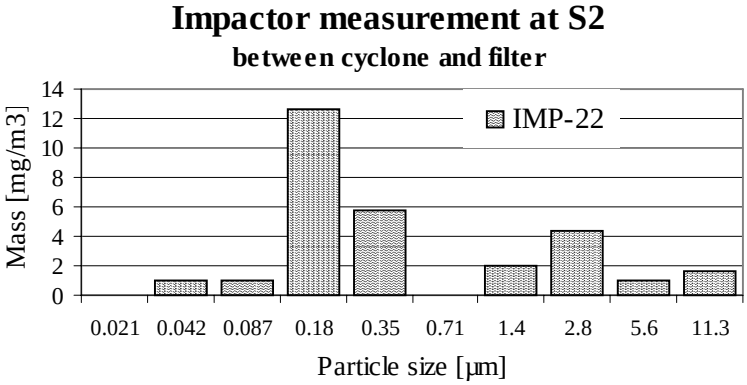

Appendix C

Review of activity measurement on impactor foils. The data have been summed for particles less than 1 µm (stage 1 to 6) and particles larger than 1 µm (stage 7 - 10) for activity and mass. Specific activities have then been calculated for the two size groups.

Measurement		Particles smaller than 1 µm			Particles larger than 1 µm		
ID	Position	Mass [mg]	Activity [Bq]	Specific act. [Bq/g]	Mass [mg]	Activity [Bq]	Specific act. [Bq/g]
IMP 3	S3	4,1	0,123	30	7,0	0,045	6
IMP 4	S3	3,9	0,0656	17	2,2	0,034	16
IMP 5	S1	20,8	0,179	9	1,7	0,034	20
IMP 6	S2	6,7	0,2791	42	6,8	0,150	22
IMP 12	S1	3,2	0,085	27	1,0	0,023	23
IMP 13	S2	2,9	0,058	20	0,7	0,023	31
IMP 17	S2	10,7	0,012	1		BDL	

Detailed results:

IMP 3 Stage	Par. Size [µm]	Cs-137 [Bq]	s.d. [Bq]	Load [mg]	Mass load [mg/m3]	Specifi act. [Bq/g]
1	0.021	-0.0023	0.0038	0.0650	0.01	-35
2	0.042	0.0029	0.0038	0.1800	0.03	16
3	0.087	0.0047	0.0048	0.0750	0.01	63
4	0.18	0.0458	0.0052	1.0950	0.18	42
5	0.35	0.0582	0.0061	1.8750	0.30	31
6	0.71	0.0132	0.0041	0.7600	0.12	17
7	1.4	0.0056	0.0053	1.0550	0.17	5
8	2.8	0.0102	0.0037	1.7150	0.28	6
9	5.6	0.01838	0.00445	2.5200	0.41	7
10	11.3	0.011	0.00445	1.7400	0.28	6

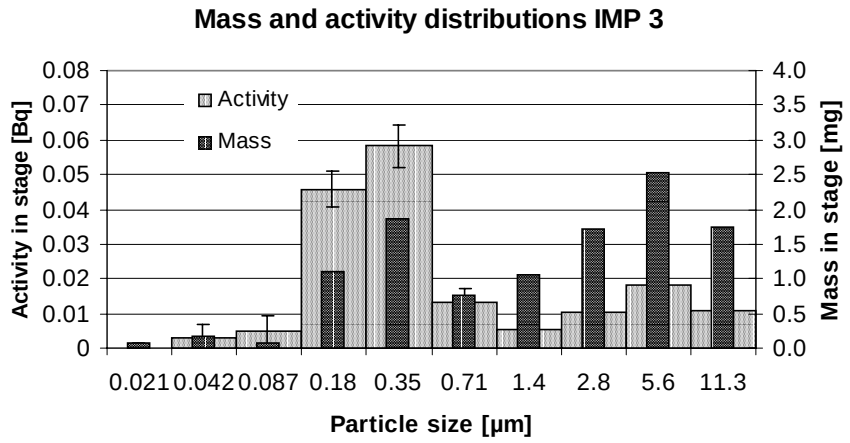

IMP4 Stage	Par. Size [µm]	Cs-137 [Bq]	s.d. [Bq]	Load [mg] [mg]	Mass load [mg/m3]	Specifi act. [Bq/g]
1	0,021	-0,0002	0,0052	0,0400	0,01	-5
2	0,042	0,0106	0,0052	0,1200	0,02	88
3	0,087	0,0074	0,0031	0,1700	0,03	44
4	0,18	0,021	0,0039	1,3750	0,22	15
5	0,35	0,0133	0,0042	1,2700	0,21	10
6	0,71	0,0135	0,0048	0,9000	0,15	15
7	1,4	0,006	0,0042	0,4950	0,08	12
8	2,8	0,0093	0,0045	0,5750	0,09	16
9	5,6	0,0077	0,0051	0,6800	0,11	11
10	11,3	0,011	0,0051	0,4100	0,07	27

Mass and activity distributions IMP 4

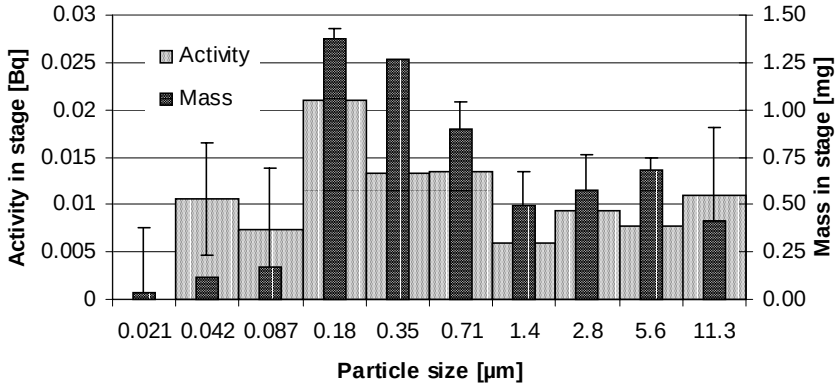

IMP 5 Stage	Par. Size [µm]	Cs-137 [Bq]	s.d. [Bq]	Load [mg] [g]	Mass load [mg/m3]	Specifi act. [Bq/g]
1	0.021	0.0174	0.006	0.12	0.02	145
2	0.042	0.0108	0.006	0.54	0.09	20
3	0.087	0.0283	0.0065	1.695	0.27	17
4	0.18	0.0654	0.0076	10.25	1.66	6
5	0.35	0.0375	0.0089	6.15	1.00	6
6	0.71	0.0199	0.0073	2.07	0.34	10
7	1.4	0.0081	0.0074	0.88	0.14	9
8	2.8	0.0146	0.006	0.39	0.06	37
9	5.6	0.0057	0.0072	0.23	0.04	25
10	11.3	0.011	0.0072	0.23	0.04	48

Mass and activity distributions IMP 5

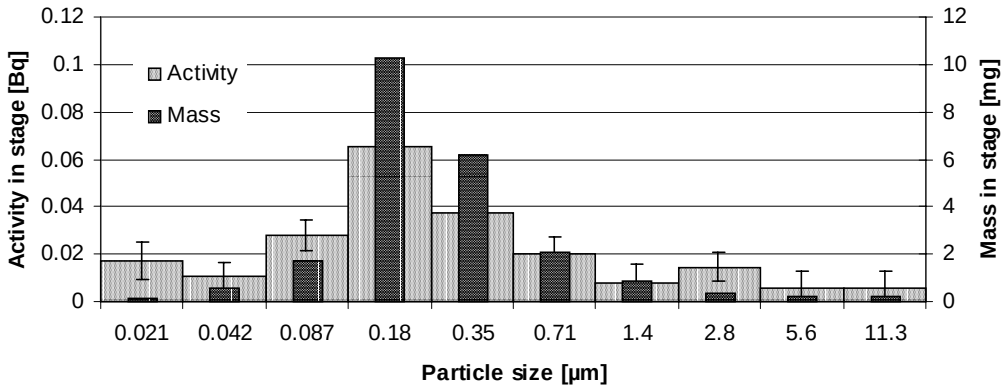

IMP 6 Stage	Par. Size [µm]	Cs-137 [Bq]	s.d. [Bq]	Load [mg]	Mass load [mg/m3]	Specifi act. [Bq/g]
1	0.021	0.0073	0.0071	0.0150	1.31	487
2	0.042	0.0073	0.0071	0.0750	1.46	97
3	0.087	0.0484	0.0084	0.3200	2.77	151
4	0.18	0.1075	0.009	1.4500	11.09	74
5	0.35	0.0683	0.0085	2.8550	3.79	24
6	0.71	0.0403	0.0082	1.9850	1.90	20
7	1.4	0.0368	0.0091	0.9100	3.50	40
8	2.8	0.0685	0.008	1.4850	5.98	46
9	5.6	0.0333	0.0069	3.2000	2.48	10
10	11.3	0.011	0.0069	1.1650	0.00	9

Mass and activity distributions IMP 6

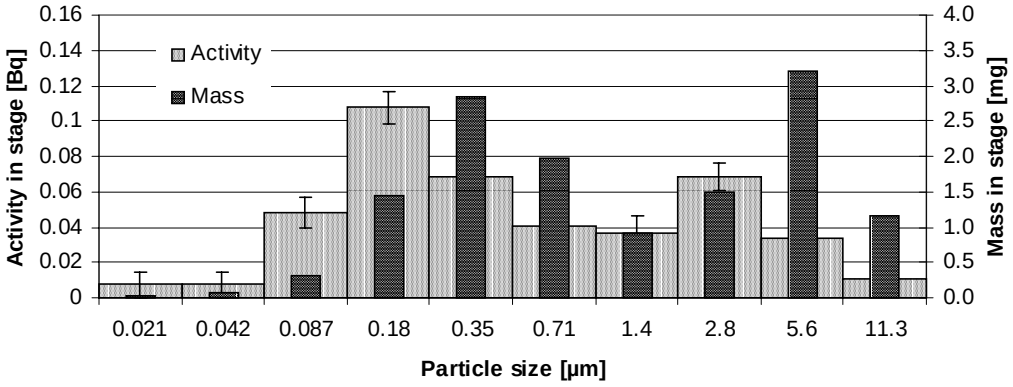

IMP 12 Stage	Par. Size [µm]	Cs-137 [Bq]	s.d. [Bq]	Load [mg] [g]	Mass load [mg/m3]	Specifi act. [Bq/g]
	0.021	0.0037	0.0059	0.14	5.51	27
1+2	0.042	0.0037	0.0059	0.19	7.48	20
3	0.087	0.0177	0.0050	0.46	18.11	39
4	0.18	0.0347	0.0084	1.39	54.53	25
5	0.35	0.0110	0.0061	0.79	30.91	14
6	0.71	0.0138	0.0058	0.21	8.07	67
7	1.4	0.0041	0.0049	0.20	7.87	20
8	2.8	0.0060	0.0054	0.32	12.40	19
9+10	5.6	0.0065	0.0070	0.30	11.81	22
	11.3	0.0065	0.0070	0.21	8.27	31

Mass and activity distributions IMP 12

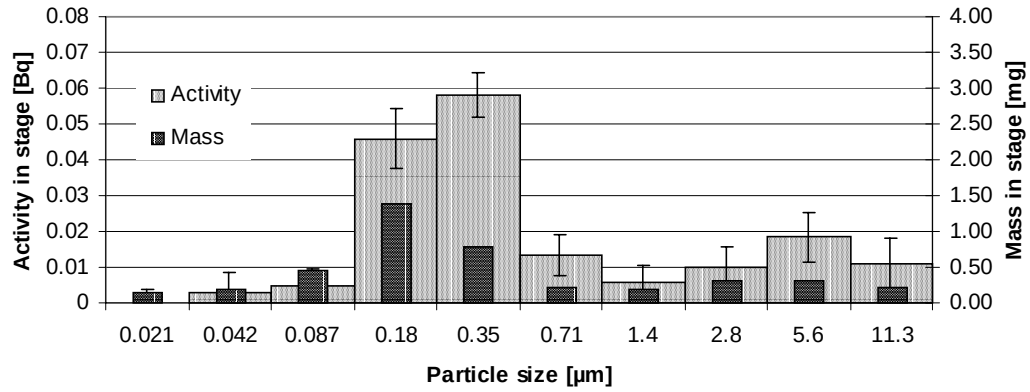

IMP 13 Stage	Par. Size [µm]	Cs-137 [Bq]	s.d. [Bq]	Load [mg] [g]	Mass load [mg/m3]	Specifi act. [Bq/g]
	0.021	-0.0012	0.0055	0.065	2.53	-18.2
1+2	0.042	-0.0012	0.0055	0.125	4.86	-9.5
3	0.087	0.0111	0.0060	0.505	19.65	21.9
4	0.18	0.0219	0.0074	1.225	47.67	17.9
5	0.35	0.0195	0.0071	0.695	27.04	28.0
6	0.71	0.0083	0.0038	0.295	11.48	28.2
7	1.4	0.0055	0.0054	0.16	6.23	34.4
8	2.8	0.0030	0.0050	0.195	7.59	15.5
9+10	5.6	0.0071	0.0063	0.165	6.42	42.7
	11.3	0.0071	0.0063	0.205	7.98	34.4

Mass and activity distributions IMP 13

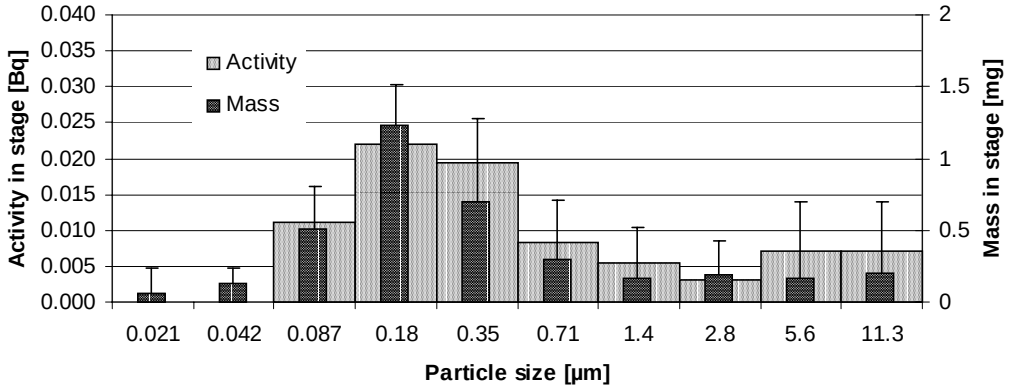

IMP 17 Stage	Par. Size [µm]	Cs-137 [Bq]	s.d. [Bq]	Load [mg] [g]	Mass load [mg/m3]	Specifi act. [Bq/g]
				0.095		
				0.21		
3	0.087	0.0000	0.0037	0.765		
4	0.18	0.0044	0.0026	3.575		1.22
5	0.35	0.0075	0.0020	4.905		1.53
6	0.71	0.0000	0.0037	1.12		
				0.51		
				0.195		
				0.065		
				-0.01		

Appendix D. Fuel Sample Measurements

Table D.1 Description of fuel samples

Time of sampling		***Log. # of sample: W1*** Type of fuel	Approximate weight, kg	Moisture content, %
16.06.99	15:30	Sawdust and shavings	1	35.7
17.06.99	9:35	Sawdust, shavings and chips	2	37.3
17.06.99	10:35	Sawdust, shavings and chips	2	40.6
17.06.99	11:35	Sawdust, shavings and chips	3	37.8
17.06.99	12:35	Sawdust, shavings and chips	2	35.5
17.06.99	13:35	Sawdust, shavings and chips	2	55.6
17.06.99	14:35	Chips	3	48.7
17.06.99	15:35	Chips	3	47.1
17.06.99	16:35	Chips	2	40.2
17.06.99	17:35	Chips	3	31.2
17.06.99	18:35	Chips	3	34.7
18.06.99	8:40	Shavings and chips	2.5	55.6
18.06.99	9:40	Shavings and chips	3	32.2
18.06.99	10:40	Shavings and chips	3	45.8
18.06.99	15:40	Shavings and chips	2	42.0
18.06.99	16:40	Shavings and chips	3	42.6

Table D.2 ^{137}Cs specific activity in the collected samples

Log #	Time of sampling	Activity of sample, kBq	Specific activity, Bq/kg	Total error, Bq/kg	Ratio error, %	Average value of specific activity, Bq/kg
17.06.99, Wood fuel samples						
W1	9:35	3.526242	154.0126	19.01092	12.34374	
		3.060448	134.475	19.04222	14.16042	154.2334
		4.023388	174.2126	18.93535	10.8691	
W1	10:35	3.97336	136.5576	15.09487	11.05386	
		4.677195	160.9695	14.36632	8.924868	144.6513
		3.99044	136.4267	15.02423	11.01267	
W1	11:35	2.38735	79.75698	14.47878	18.15362	
		1.856712	61.60783	14.31218	23.2311	77.87527
		2.824774	92.26101	14.13809	15.32401	
W1	12:35	2.152453	76.39287	15.3277	20.06431	
		2.352752	82.919	15.23253	18.37037	86.88519
		2.862128	101.3437	15.39125	15.18719	
18.06.99, Wood fuel samples						
W1	16:40	2.909738	94.86039	14.20572	14.9754	
		2.657956	88.90287	14.53174	16.34564	83.27103
		1.96742	66.04985	13.76341	20.83791	
17.06.99, Integrated ash samples from ash containers						
Z2(1)	19:30	193.9456	12206.59	99.94555	0.818784	
		194.4717	11863.02	96.99882	0.817657	12029.56
		188.0934	12019.06	100.2406	0.834014	
Z2(2)	19:30	149.0406	10622.39	102.1841	0.961969	
		145.301	10670.72	104.2791	0.977245	10671.13
		140.3393	10720.29	107.0576	0.998645	
Z1	19:30	188.9679	3052.936	26.00639	0.851849	
		191.4775	3040.29	25.70578	0.845504	3106.86
		196.4473	3227.353	26.83651	0.831533	
18.06.99, Integrated ash samples from ash containers						
Z2(1)	17:20	140.5509	10038.56	100.2032	0.998182	
		140.4934	10291.13	115.2985	1.120368	10154.34
		135.5475	10133.33	103.4692	1.021077	
Z2(2)	17:20	103.5323	8897.053	108.1458	1.215524	
		102.9445	8876.059	108.2977	1.22011	8919.375
		114.5706	8985.011	102.2217	1.137691	
Z1	17:20	274.4037	4083.783	27.93747	0.684108	
		270.5271	4022.218	27.74597	0.689818	4040.704
		264.3481	4016.112	27.70138	0.689756	

Table D.2 (continued)

Log #	Time of sampling	Activity of sample, kBq	Specific activity, Bq/kg	Total error, Bq/kg	Ratio error, %	Average value of specific activity, Bq/kg
20.06.99, Integrated bottom ash/slag samples						
Z0 (bottom ash)	entire test	369.0455	2144.742	12.98399	0.605387	
		344.7667	1986.645	12.5535	0.631895	2139.896
		389.4241	2288.301	13.44751	0.587663	
Z0 (slag)	entire test	422.7815	2701.961	13.82323	0.5116	
		414.2413	2667.974	13.79473	0.517049	2692.138
		411.4077	2706.48	14.0212	0.51806	
Z0 (slag)	entire test	379.8315	2458.798	13.33426	0.542308	
		378.524	2419.648	13.16188	0.543959	2440.328
		385.9617	2442.537	13.15497	0.538578	
17.06.99, Time-dependent ash samples						
Z2(1)	9:45	12.21338	10725.72	205.2852	1.913953	
Z2(2)	9:45	0.868946	2257.002	529.7599	23.47184	
Z1	11:15	0.649847	2008.801	550.027	27.38086	
Z2(1)	11:15	1.638177	6386.654	893.7692	13.99433	
Z2(1)	12:30	1.225071	7680.697	1354.46	17.63459	
Z2(2)	12:30	1.140318	9278.421	1032.783	11.13102	
Z2(1)	14:00	2.859481	10005.18	381.3261	3.811286	
Z2(1)	15:20	5.749388	10376.08	531.395	5.121344	
Z1	17:45	10.89116	4372.206	132.1397	3.022267	
Z2(1)	17:45	5.33275	10923.29	592.4054	5.423323	
18.06.99, Time-dependent ash samples						
Z1	8:50	0.315403	3879.492	398.0913	10.26143	
Z2(1)	8:50	2.764798	15637.99	1387.189	8.870631	
Z1	10:10	0.993884	2170.526	414.6168	19.10213	
Z2(1)	10:10	1.629808	12924.73	878.59	6.797746	
Z1	11:20	0.441726	3166.496	704.9007	22.26122	
Z1	12:35	1.312436	2850.644	434.9649	15.25848	
Z2(1)	12:35	1.777488	8603.524	1064.39	12.37156	
Z1	14:00	0.249144	4280.817	586.1751	13.69306	
Z2(1)	14:00	8.079776	7360.642	309.0678	4.198925	
Z2(1)	15:10	0.942915	8045.353	1605.246	19.95246	
Z1	15:20	5.952381	3266.411	193.5427	5.925241	
Z1	16:20	3.785104	3190.68	254.7268	7.983464	
Z2(1)	16:20	7.360032	6540.506	285.3875	4.363386	
Z2(2)	16:20	9.056656	7406.49	282.3111	3.811672	
17.06.99, Aerosols entrapped by “absolute” filters during the total dust measurements						
AD1	9:15	0.097591	966.2471	327.3552	33.87903	
AD2	9:15	0.123448	2864.223	878.2719	30.66353	
AD1	14:50	0.409205	15922.37	1649.297	10.35836	
AD2	15:04	0.102285	14612.16	5107.927	34.9567	
AD1	16:10	0.131036	4782.341	1399.768	29.2695	
AD4	12:28-18:00	0.250352	1093.717	212.7503	19.45205	
18.06.99, Aerosols entrapped by “absolute” filters during the total dust measurements						
AD1	10:25	0.140567	3872.367	1166.754	30.13025	
AD2	10:47	0.089846	6417.565	2993.34	46.64293	
AD1	14:41	0.087951	5143.329	2164.02	42.07431	
AD2	16:05	0.100193	12369.5	4858.472	39.27785	
AD4	10:00-16:45	0.153205	1758.958	542.567	30.84592	

Appendix E. Laser Measurements

Table E.1 Number of particulate of different fractions. The results of laser spectrometry of aerosols

17.06.99, Port S31, N_2 dilution ratio = 4.5; Volume of probe = 50 cm^3							
Time	**0,2-0,25 μm**	**0,25-0,3 μm**	**0,3-0,4 μm**	**0,4-0,5 μm**	**0,5-0,7 μm**	**0,7-1,0 μm**	**1,0-2,0 μm**
8:46	67298	19503	5139	4032	653	212	27
8:50	60570	19107	4752	3938	792	482	86
8:54	45662	14706	4964	5018	1481	1040	90
8:56	69561	19944	5157	5045	1211	761	77
8:59	32310	10112	3407	3182	950	644	54
9:00	19049	6737	1958	1611	320	171	23
9:03	17766	5940	1841	887	90	126	131
9:04	20651	6944	1881	1139	167	99	41
9:05	24570	8055	2300	1539	203	113	41
9:07	15089	5337	1467	788	99	50	5
9:08	15044	5247	1409	648	68	45	5
9:09	16844	5711	1818	833	68	59	27
9:10	22253	7992	2291	1436	270	230	68
9:11	47655	20457	5895	5148	1967	927	126
9:13	63927	29061	8766	8276	3366	1418	207
9:14	54729	25061	8159	6638	2534	1085	108
9:15	68711	34304	12182	8996	3245	1557	140
9:16	35105	15660	5207	3551	1247	657	59
9:18	20696	7596	2124	1377	333	171	27
9:19	36491	15111	4599	3915	1449	716	36
9:20	26703	10701	3281	2120	504	297	41
9:21	26451	10395	3429	2075	455	311	45
9:22	43061	18972	6206	3933	1130	581	50
9:24	45725	19143	6575	4203	788	410	144
9:25	25925	10008	3105	1769	486	279	77
9:27	17361	6048	1832	981	113	68	27
9:28	17564	5787	1778	891	108	68	27
9:29	40631	17937	5589	3812	761	369	77
MAX	69561	34304	12182	8996	3366	1557	207
MIN	15044	5247	1409	648	68	45	5
AVRG	35621,5	13627,71	4182,536	3135,036	887,7857	462,3571	66,64286
STDEV	18191,43	7812,718	2594,571	2271,721	921,6206	424,0264	48,27484

Table E-1 (continued)

17.06.99, Port S31, N_2 dilution ratio = 4.5; Volume of probe = 50 cm^3							
Time	**0,2-0,25 µm**	**0,25-0,3 µm**	**0,3-0,4 µm**	**0,4-0,5 µm**	**0,5-0,7 µm**	**0,7-1,0 µm**	**1,0-2,0 µm**
10:12	6935	2421	743	369	41	59	36
10:15	6597	1994	594	203	9	0	9
10:16	6512	2034	657	324	14	27	9
10:17	6804	2462	639	338	36	23	14
10:18	10130	3510	1008	513	72	90	9
10:23	26433	8924	2849	1719	135	153	41
10:24	23697	8442	2754	1269	144	176	68
10:25	22964	7844	2358	1166	104	135	68
10:26	23468	7907	2574	1256	86	140	41
MAX	26433	8924	2849	1719	144	176	68
MIN	6512	1994	594	203	9	0	9
AVRG	14837,78	5059,778	1575,111	795,2222	71,22222	89,22222	32,77778
STDEV	8943,146	3100,362	1019,749	555,7391	49,94692	64,61768	24,17529
17.06.99, Port S31, N_2 dilution ratio = 4.5; Volume of probe = 50 cm^3							
Time	**0,2-0,25 µm**	**0,25-0,3 µm**	**0,3-0,4 µm**	**0,4-0,5 µm**	**0,5-0,7 µm**	**0,7-1,0 µm**	**1,0-2,0 µm**
12:15	20075	6773	2565	977	72	59	18
12:16	20331	7169	2736	1238	167	108	41
1217	22662	7596	3096	1431	207	117	36
12:18	20115	6858	2750	1409	239	117	32
12:20	18167	5486	2345	1175	180	108	9
12:21	15143	4703	1962	806	90	50	23
12:23	15282	4604	1886	824	72	41	14
12:24	14459	4559	1832	743	45	18	14
12:25	13397	4262	1688	590	36	36	5
MAX	22662	7596	3096	1431	239	117	41
MIN	13397	4262	1688	590	36	18	5
AVRG	17736,78	5778,889	2317,778	1021,444	123,1111	72,66667	21,33333
STDEV	3252,446	1313,383	496,8432	304,0276	75,53219	39,47151	12,52996
17.06.99, Port S31, N_2 dilution ratio = 4.5; Volume of probe = 50 cm^3							
Time	**0,2-0,25 µm**	**0,25-0,3 µm**	**0,3-0,4 µm**	**0,4-0,5 µm**	**0,5-0,7 µm**	**0,7-1,0 µm**	**1,0-2,0 µm**
13:02	144000	8235	1773	1404	369	414	99
13:04	179703	8136	1782	1836	594	441	117
13:05	183483	8307	2079	1953	387	279	36
13:06	241857	9252	2223	2250	423	432	135
MAX	241857	9252	2223	2250	594	441	135
MIN	144000	8136	1773	1404	369	279	36
AVRG	187260,8	8482,5	1964,25	1860,75	443,25	391,5	96,75
STDEV	40511,87	517,7673	223,5403	350,8365	102,9769	75,83535	43,08422

Table E-1 (continued)

17.06.99, Port S31, N_2 dilution ratio = 4.5; Volume of probe = 50 cm^3							
Time	**0,2-0,25 µm**	**0,25-0,3 µm**	**0,3-0,4 µm**	**0,4-0,5 µm**	**0,5-0,7 µm**	**0,7-1,0 µm**	**1,0-2,0 µm**
15:14	2277	725	275	86	14	9	0
15:16	2075	531	176	90	14	0	0
15:17	3600	716	234	104	5	0	0
15:20	5675	2083	765	374	41	32	5
15:22	3024	1022	243	99	5	18	0
15:23	2867	837	270	104	18	14	0
15:26	2588	878	275	99	0	5	5
15:27	2831	774	216	144	14	5	0
15:30	3564	1062	293	117	5	0	0
15:31	3861	1166	351	99	14	14	5
15:33	3326	1026	293	117	0	5	14
15:34	3618	1080	261	162	9	23	5
MAX	5675	2083	765	374	41	32	14
MIN	2075	531	176	86	0	0	0
AVRG	3275,5	991,6667	304,3333	132,9167	11,58333	10,41667	2,833333
STDEV	941,3415	390,7786	151,4796	79,06437	11,01617	10,10363	4,26046
17.06.99, Port S31, N_2 dilution ratio = 4.5; Volume of probe = 50 cm^3							
Time	**0,2-0,25 µm**	**0,25-0,3 µm**	**0,3-0,4 µm**	**0,4-0,5 µm**	**0,5-0,7 µm**	**0,7-1,0 µm**	**1,0-2,0 µm**
18:20	1319	437	117	176	23	18	18
18:22	4712	860	230	135	14	5	0
18:23	3474	653	180	122	36	5	0
18:36	12011	2255	495	270	18	18	5
18:37	49464	8964	702	203	41	23	9
18:39	5670	1175	383	243	18	18	0
18:41	2408	801	302	126	18	9	0
18:43	2295	563	198	122	14	5	9
18:44	2075	603	216	144	36	23	0
MAX	49464	8964	702	270	41	23	18
MIN	1319	437	117	122	14	5	0
AVRG	9269,778	1812,333	313,6667	171,2222	24,22222	13,77778	4,555556
STDEV	15415,59	2737,178	185,4353	55,7736	10,52114	7,726218	6,366143

Table E-1 (continued)

17.06.99, Port S22, N_2 dilution ratio = 135; Volume of probe = 50 cm^3							
Time	**0,2-0,25 µm**	**0,25-0,3 µm**	**0,3-0,4 µm**	**0,4-0,5 µm**	**0,5-0,7 µm**	**0,7-1,0 µm**	**1,0-2,0 µm**
9:38	169155	61830	18900	13500	1080	270	0
9:39	356130	114750	39690	30240	3510	2160	270
9:41	312525	84240	36315	29160	4995	2430	945
9:43	218160	63045	27810	21330	4995	2295	405
9:44	142830	43875	18765	15930	1755	945	540
9:46	87750	32400	11475	6750	945	405	270
9:47	115830	39015	17415	8910	1215	1080	135
9:49	96660	34965	11475	7020	945	675	0
9:51	108405	38340	12555	7965	405	405	270
9:52	88560	31995	13905	8370	1215	675	270
9:53	110160	33075	13230	11475	1080	540	0
MAX	356130	114750	39690	30240	4995	2430	945
MIN	87750	31995	11475	6750	405	270	0
AVRG	164196,8	52502,73	20139,55	14604,55	2012,727	1080	282,2727
STDEV	93129,51	26545,71	10039,1	8654,083	1672,535	816,7221	279,6459
17.06.99, Port S22, N_2 dilution ratio = 135; Volume of probe = 50 cm^3							
Time	**0,2-0,25 µm**	**0,25-0,3 µm**	**0,3-0,4 µm**	**0,4-0,5 µm**	**0,5-0,7 µm**	**0,7-1,0 µm**	**1,0-2,0 µm**
11:33	251910	68175	16470	9315	405	675	0
11:34	110565	20385	6345	2970	135	405	135
11:35	70065	12420	6345	5940	270	405	135
11:37	84780	22275	6615	6480	945	540	0
11:51	357480	86130	19440	7155	540	945	405
11:53	68175	14310	6750	5535	1215	675	540
11:54	83295	19980	8370	5265	675	135	0
MAX	357480	86130	19440	9315	1215	945	540
MIN	68175	12420	6345	2970	135	135	0
AVRG	146610	34810,71	10047,86	6094,286	597,8571	540	173,5714
STDEV	113060,8	29590,72	5512,926	1933,579	380,6995	258,5053	216,4816
18.06.99, Port log. # S31, N_2 dilution ratio = 4.5; Volume of probe = 50 cm^3							
Time	**0,2-0,25 µm**	**0,25-0,3 µm**	**0,3-0,4 µm**	**0,4-0,5 µm**	**0,5-0,7 µm**	**0,7-1,0 µm**	**1,0-2,0 µm**
12:53	927	68	23	5	5	5	0
12:54	635	36	9	9	0	0	0
12:56	450	14	5	0	0	0	0
12:57	1040	131	18	14	5	0	0
MAX	1040	131	23	14	5	5	0
MIN	450	14	5	0	0	0	0
AVRG	763	62,25	13,75	7	2,5	1,25	0
STDEV	269,554	50,9141	8,22090	5,94418	2,88675	2,5	0

Table E-1 (continued)

18.06.99, Port log. # S31, N_2 dilution ratio = 4.5; Volume of probe = 50 cm^3							
Time	**0,2-0,25 µm**	**0,25-0,3 µm**	**0,3-0,4 µm**	**0,4-0,5 µm**	**0,5-0,7 µm**	**0,7-1,0 µm**	**1,0-2,0 µm**
15:57	20876	1103	113	77	32	14	14
15:58	74336	30092	8487	1445	54	50	9
16:00							
16:04	83795	21704	2781	374	27	9	9
16:06	3056	428	126	162	32	14	5
16:07	3632	248	99	95	23	14	0
16:09	9900	5333	135	113	14	5	0
MAX	83795	30092	8487	1445	54	50	14
MIN	3056	248	99	77	14	5	0
AVRG	32599,17	9818	1956,833	377,6667	30,33333	17,66667	6,166667
STDEV	36681,21	12869,62	3371,784	534,0553	13,39652	16,25628	5,56477
18.06.99, Port log. # S31, N_2 dilution ratio = 4.5; Volume of probe = 50 cm^3							
Time	**0,2-0,25 µm**	**0,25-0,3 µm**	**0,3-0,4 µm**	**0,4-0,5 µm**	**0,5-0,7 µm**	**0,7-1,0 µm**	**1,0-2,0 µm**
16:10	18036	1449	288	198	54	27	14
16:12	19593	1458	171	203	27	36	18
16:13	19103	1655	279	131	9	18	0
16:15	19125	1764	315	180	45	27	5
16:16	20084	1751	230	153	18	18	0
16:17	21740	1760	189	144	14	14	9
16:19	16722	1589	167	126	0	5	5
16:20	31338	2111	275	216	41	23	9
16:22	23400	1472	288	180	41	18	18
16:23	20619	842	149	99	32	9	0
16:24	21213	1188	144	122	23	27	9
16:26	30474	2097	216	126	18	14	0
16:27	18671	986	135	122	9	9	9
16:29	16754	1022	122	144	27	5	0
MAX	31338	2111	315	216	54	36	18
MIN	16722	842	122	99	0	5	0
AVRG	21205,14	1510,286	212	153,1429	25,57143	17,85714	6,857143
STDEV	4497,967	391,1156	66,68871	36,04881	15,60431	9,297288	6,561627
18.06.99, Port log. # S22, N_2 dilution ratio = 9; Volume of probe = 50 cm^3							
Time	**0,2-0,25 µm**	**0,25-0,3 µm**	**0,3-0,4 µm**	**0,4-0,5 µm**	**0,5-0,7 µm**	**0,7-1,0 µm**	**1,0-2,0 µm**
13:02	144000	8235	1773	1404	369	414	99
13:04	179703	8136	1782	1836	594	441	117
13:05	183483	8307	2079	1953	387	279	36
13:06	241857	9252	2223	2250	423	432	135
MAX	241857	9252	2223	2250	594	441	135
MIN	144000	8136	1773	1404	369	279	36
AVRG	187260,8	8482,5	1964,25	1860,75	443,25	391,5	96,75
STDEV	40511,87	517,7673	223,5403	350,8365	102,9769	75,83535	43,08422

Bibliographic Data Sheet **Risø-R-1146(EN)**

Title and authors

Power Production from Radioactively Contaminated Biomass and Forest Litter in Belarus – Phase 1b

Jørn Roed, Kasper G. Andersson, Christian L. Fogh, Svend K. Olsen, Henrik Prip, Helle Junker, Niels Kirkegaard, Jens-Martin Jensen, Alexandre J. Grebenkov, Vitalij N. Solovjev, Gregory G. Kolchanov, Leonid A. Bida, Peter M. Klepatzky, Igor G. Pleshchenkov, Arnold A. Gvozdev and Larry Baxter

ISBN
87-550-2619-2
87-550-2620-6 (Internet)

ISSN
0106-2840

Department or group
Nuclear Safety Research and Facilities Department

Date
March 2000

Groups own reg. number(s)

Project/contract No(s)
Chernobyl Bio-energy Project phase 1b

Pages	Tables	Illustrations	References
93	27	58	7

Abstract (max. 2000 characters)

The Chernobyl accident has led to radioactive contamination of vast Belarussian forest areas. A total scheme for remediation of contaminated forest areas and utilisation of the removed biomass in safe energy production is being investigated in a Belarussian-American-Danish collaborative project. Here the total radiological impact of the scheme is considered. This means that not only the dose reductive effect of the forest decontamination is taken into account, but also the possible adverse health effects in connection with the much needed bio-energy production. This report presents the results of an in-country, commercial-scale investigation of the effect of a baghouse filter in retaining contaminants so that they are not released to the atmosphere in the biomass energy production process. Approximately 99.5% of the activity of a commercially representative, dust-laden boiler flue gas was removed from the stream by using a combination of a cyclone and a baghouse filter.

Descriptors INIS/EDB

AEROSOLS; BAGHOUSES; BIOMASS; BOILERS; CESIUM 137; CONTAMINATION; CYCLONE SEPARATORS; DECONTAMINATION; EFFICIENCY; FABRIC FILTERS; FLUE GAS; FLY ASH; RADIOACTIVITY; WOOD WASTES

Available on request from Information Service Department, Risø National Laboratory,
(Information Service Department, Risø National Laboratory), P.O.Box 49, DK-4000 Roskilde, Denmark.
Telephone +45 46 77 40 04, Telefax +45 46 77 40 13.